SAFEWAY

GIS-Based Infrastructure Management System for Optimized Response to Extreme Events of Terrestrial Transport Networks

Data Acquisition Report (D3.1)

September 2019 (V1.0)

PUBLIC

This project has received funding from the European Union's Horizon 2020 research and innovation programme under grant agreement No. 769255.

SAFEWAY

GIS-BASED INFRASTRUCTURE MANAGEMENT SYSTEM FOR OPTIMIZED RESPONSE TO EXTREME EVENTS OF TERRESTRIAL TRANSPORT NETWORKS

Grant Agreement No. 769255

Data acquisition report

WP 3 MULTI-SCALE INFRASTRUCTURE MODELLING & MONITORING

Deliverable ID	**D3.1**
Deliverable name	**Data acquisition report**
Lead partner	Planetek Italia
Contributors	University of Vigo

PUBLIC

SAFEWAY Project Synopsis

According to European TEN-T guidelines, due consideration must be given to the risk assessments and adaptation measures during infrastructure planning, in order to improve resilience to disasters. SAFEWAY's aim is to design, validate and implement holistic methods, strategies, tools and technical interventions to significantly increase the resilience of inland transport infrastructure. SAFEWAY leads to significantly improved resilience of transport infrastructures, developing a holistic toolset with transversal application to anticipate and mitigate the effects extreme events at all modes of disaster cycle:

1. **"Preparation":** substantial improvement of risk prediction, monitoring and decision tools contributing to anticipate, prevent and prepare critical assets for the damage impacts;
2. **"Response and Recovery":** the incorporation of SAFEWAY IT solutions into emergency plans, and real-time optimal communication with operators and end users (via crowdsourcing and social media);
3. **"Mitigation":** improving precision in the adoption of mitigation actions (by impact analysis of different scenarios) together with new construction systems and materials, contributing to the resistance & absorption of the damage impact.

SAFEWAY consortium has 15 partners that cover multidisciplinary and multi-sectorial business fields associated with resilience of transport infrastructure in Europe: national transport infrastructure managers & operators, a main global infrastructure operator, partners able to provide various data sources with large coverage in real time, comprehensive ITC solutions, and leading experts in resilience, risk databases, remote sensing-based inspection, and decision systems based on predictive modelling.

SAFEWAY will carry-out 4 real case studies distributed through 4 countries, linked to 5 corridors of the TEN-T Core Network. SAFEWAY has as main expected impacts:

1. at least 20% improvement in mobility; and
2. at least 20% lower cost of infrastructure maintenance.

Document Information

Document Name	Data Acquisition Report
Version No.	V1.0
Due date Annex I	31/10/2019
Report date	05/09/2019
Number of pages	121
Lead Author	Angelo Amodio (Planetek), Vincenzo Massimi (Planetek), Belén Riveiro (UVIGO); Mario Soilán (UVIGO)
Other Authors	Anna Maria De Florio (PKI) Pablo del Rio (UVIGO) Ana Sánchez (UVIGO) Carlos Perez-Collazo (UVIGO)
Dissemination level	Public
Planetek's internal reference	pkm109-07-1.0_D3.1_Data_Acquisition_Report

Document History

Ver.	Date	Description	Authors	Checked by
0.1	26/04/2019	Creation of the document	V. Massimi	C. Perez-Collazo
0.2	03/05/2019	Structure and format	C. Perez-Collazo	
0.3	01/08/2019	Issue for internal review	V. Massimi; A. De Florio C. Perez-Collazo	A. Amodio
0.4	04/09/2019	Issue after internal review	M. Soilán	V. Massimi
1.0	06/09/2019	Quality Check	C. Perez-Collazo	M. Soilán

Document Approval

Ver.	Name	Position in project	Beneficiary	Date	Visa
1.0	Dr Belén Riveiro	Project Coordinator	UVIGO	06/09/2019	BR

Executive Summary

This document aims to offer a detailed description of the remote sensing platforms that will be used for the multiscale data acquisition of the transport networks within the case studies of SAFEWAY project.

The remote sensing technologies will be divided in the document into two groups:

- satellite technologies, equipped with radar and optical sensor, to monitor a wide area obtaining a synoptic view of the state of the infrastructures and of the surrounding area;
- terrestrial remote sensing technologies, to obtain geometric and radiometric data from the surveyed environments with high accuracy and resolution.

The decisions on which specific technologies will be used in SAFEWAY, and to what extent, should meet the necessities of the owners or operators of the infrastructures within the case studies defined at the beginning of the project. From these end user needs, a number of monitoring scenarios in the different case studies can be defined, and a clear data acquisition protocol can be addressed.

Table of Contents

Executive Summary **6**
Table of Contents **7**
Glossary of Terms **9**
1. Introduction **11**
2. SoA on Remote Monitoring of Transport Infrastructures **13**
2.1 Satellite technology 13
2.1.1 Optical satellite technology 13
2.1.2 Radar satellite technology 14
2.1.3 Roads and Railways monitoring 14
2.2 Terrestrial remote sensing technology 16
2.2.1 Road network monitoring 17
2.2.2 Railway network monitoring 26
3. Remote Monitoring Technologies/Systems **34**
3.1 Satellite monitoring technologies 34
3.1.1 Radar satellites 34
3.1.2 Performance of radar monitoring 35
3.2 Terrestrial monitoring technologies 36
3.2.1 Laser Scanner system components 36
3.2.2 Performance of laser scanning systems 40
3.2.3 Types of laser scanner systems 42
4. SAFEWAY Pilots and end-user needs for Remote Monitoring **45**
4.1 Pilot 1: Portugal 46
4.1.1 Adverse events 47
4.1.2 Evaluation of scenarios 48
4.1.3 Assets 48
4.2 Pilot 2: Spain 49
4.2.1 Adverse Events 50
4.2.2 Evaluation of scenarios 51
4.2.3 Assets 51
4.3 Pilot 3: United Kingdom 51
4.3.1 Adverse events 52
4.3.2 Evaluation of scenarios 52
4.3.3 List of assets 52
5. SAFEWAY Remote Monitoring data acquisition protocols **54**
5.1 Satellite technologies: Data acquisition protocols 54
5.1.1 This section contains the description of Sentinel-1 (radar) and Sentinel-2 (optical) data. Sentinel-1 data 54
5.1.2 Sentinel-2 data 56
5.2 Terrestrial technologies: Data acquisition protocols 57
5.2.1 Equipment 57
5.2.2 Hardware installation 60
5.2.3 Survey protocols 66
6. Performance Indicators for remote monitoring **68**
6.1 Performance indicators of satellite monitoring for infrastructures 69
6.2 Performance indicators for terrestrial remote sensing monitoring of infrastructures 70
Acknowledgements **75**

References **76**
Appendix 1. Tables **93**

Glossary of Terms

ALS	Aerial Laser Scanning
MLS	Mobile Laser Scanning
MMS	Mobile Mapping System
TLS	Terrestrial Laser Scanning
LiDAR	Light Detection and Ranging
OS	Optical satellite
RS	Radar satellite
Pilot	Near-life operational environment designed to test and validate the effectiveness and transferability of technologies and methodologies defined in the framework of the SAFEWAY project.
Demonstration site	A particular geographical location or transport network infrastructure section within a pilot, where one or more project technologies or methodologies are going be tested and validated in relation to one or more adverse events (natural or human-made).
Scenario	An outline of an event together with the assessment of the consequences that it may have on a transport infrastructure (i.e. affecting one or more critical assets and/or disrupting users) according to a set of predefined and measureable aspects or parameters. Scenarios are defined within the so called 'scenario-based risk analysis' which is the process of analysing a set of multiple scenarios with the aim of identifying potential risks and their linked hazards, to increase preparedness to handle them and minimize their impact.
Event	An event that may result in loss of life, health or stability, monetary losses or damage to the environment, DSB (2014). In SAFEWAY the focus is on adverse events in terms of malfunctioning of infrastructure - i.e., caused either by natural events (e.g., extreme weather events, earthquakes, landslides, etc.) and by human-made events (e.g., vehicle accidents, deficient maintenance, terrorism actions, etc.).

1. Introduction

This document aims to offer a detailed description of the remote sensing platforms that will be used for the multiscale data acquisition of the transport networks within the case studies of SAFEWAY project.

One of the main objectives of SAFEWAY project is to improve the resilience of transport infrastructures, anticipating and mitigating the effects of extreme events at all modes of the disaster cycle: (1) Preparation, (2) Mitigation and (3) Response and Recovery. As shown in Table 1, each dimension of resilience can be divided in a set of subdimensions and correspondent topics. This document is linked to infrastructure monitoring, that is, to the preparation dimension of resilience. Infrastructure monitoring can be thought of as the continual collection and review of meaningful data about the infrastructure. The interpretation of this data enables infrastructure management: Decisions about infrastructure capacity, availability, security or maintainability will be more accurate if the known data about the infrastructure is reliable and up to date; and a better decision making in this regard is directly related to one of the main and scientific technological objectives of SAFEWAY:

- To achieve 15% savings in maintenance costs, by improving structural health monitoring (specially ageing assets) and thus, propose retrofitting renewal of elements to reduce the current estimated expenditure in Europe.

In order to fulfil this objective, Working Package 3 of the project proposes to employ different remote sensing technologies to collect data from the infrastructure following a multi-scale and multi-resolution strategy, feeding the Infrastructure Information Models (IIM) to be developed in SAFEWAY.

These remote sensing technologies will be divided into two groups that allow the aforementioned multiscale analysis of the infrastructure: First, satellite technologies, equipped with radar and optical sensor, allow to monitor a wide area obtaining a synoptic view of the state of the infrastructures and of the surrounding area, both in term of stability and changes that may affect the infrastructure's resilience, without any installation on the ground. Then, terrestrial remote sensing technologies take advantage of the capabilities of LiDAR sensors to obtain geometric and radiometric data from the surveyed environments with high accuracy and resolution, which together with several other sensors (image, thermographic, meteorological), are mounted on static or mobile platforms that collect and synchronize data from the different sensors.

The decisions on which specific technologies will be used in SAFEWAY, and to what extent, should meet the necessities of the owners or operators of the infrastructures within the case studies defined at the beginning of the project. From these end user needs, a number of monitoring scenarios in the different case studies can be defined, and a clear data acquisition protocol can be addressed.

With this context, this document will contain the following information:

- A review regarding the state of the art on remote monitoring of transport infrastructures, with special emphasis on current remote sensing-based

solutions employed on the European infrastructure, and applications derived from the usage of remote sensing technologies (Section 2).
- A review regarding the state of the art on remote sensing technologies and systems that collect data for the applications seen in the previous section (Section 3).
- A description of the end-user needs for their study cases which justify the usage of the technologies that are proposed in this document (Section 4).
- A description of the specific scenarios that will be addressed within the case studies of the project, for the proposed technologies, and the data acquisition protocols (Section 5).
- The performance indicators / specifications of the data acquisition platforms (Section 6).

Table 1: Dimensions of resilience

Dimensions of resilience	Effect (time)	Subdimensions	Topics
Preparation	Short-Term and Long-Term	Prediction	Meteorological
			Structural
		Monitoring	RS – Satellite
			RS - Terrestrial
			Contact
		Decision	
Mitigation		Resistance	
		Absorption	
Response and recovery	Short-Term	Mobility	
		Communication	ICT
			Psychological
		Emergency	

2. SoA on Remote Monitoring of Transport Infrastructures

2.1 Satellite technology

Satellite technologies, both optical and radar, have been proved to be useful in different monitoring applications. A non-exhaustive list of examples includes the stability evaluation of infrastructures and the environment, the continuous monitoring of the urban/non-urban changes, risk assessment support related to the natural hazard like landslide, subsidence, flooding, etc. and as a consequence it can be considered as a powerful information source to support the improvement of the infrastructure resilience.

2.1.1 Optical satellite technology

The field of space-borne optical remote sensing has made significant progress since the launch of the first Landsat satellite in the early 1970s. Advances have been made in all aspects of optical remote sensing data, including improved spatial, temporal, spectral and radiometric resolutions, which have increased the uptake of these data by wider user communities.

The usefulness of optical remote sensing data in monitoring global and regional terrestrial ecosystems often depends on their spatial and temporal resolutions. In many applications, high spatial and temporal resolution is needed. However, due to limitations imposed by instrument field of view and swath width it is not always possible to achieve high spatial and temporal resolutions. Traditionally, sensors with high temporal resolutions (1–3 days) (e.g. NOAA AVHRR, Terra and Aqua Satellites) usually acquire data in coarse spatial resolutions (>250 m) owing to the wide field of view, while those with medium spatial resolutions (<100 m) with low field of view often acquire data at a coarse temporal resolution (e.g. 16-day revisit time for the Landsat series). To overcome this limitation, programmable/tasking satellites have been launched in the past decades that can acquire data at both high temporal (1–3 days revisit time) and high spatial resolutions (1–30 m), allowing focus on critical study areas.

Examples of optical sensors capable of acquiring both high temporal and spatial resolution data include satellite systems such as RapidEye, QuickBird, WorldView and Pleiades. Even though these sensors fulfil the requirement of high spatial and temporal resolution, to achieve high spatial resolution, satellites carrying these sensors tend to be in lower orbit, thereby reducing their swath width and requiring more imagery to cover regional to global scale studies. The launch of new satellite sensors in the last decade, like Landsat 8 and the European Copernicus Sentinel missions, represents a step forward in the availability and use of remote sensing data with an improved spatial resolution (10–60 m) combined with a high revisit time of five days and at a large swath (290 km for Sentinel-2).

Furthermore, in the recent past, many companies have developed even smaller optical satellites (micro- or nano-satellites, sometimes called cube-sats) that are relatively cheap to build and deploy on orbit, enabling mass production. Examples of these micro-satellites include the Skybox imaging Skysat satellites, Planet labs Dove satellites and UrtheCast satellites. Due to the relatively cheap cost of

assembling and deploying micro-satellites, these companies have launched or intend to launch swarms of them, which, thanks to their large numbers, will be able to revisit and photograph large regions of Earth several times per day, but in limited spectral bands (typically visible and broadband near-infrared capabilities only). Finally, as opposed to some of the conventional commercial imaging satellites that only collect images when tasked to do so, these microsatellites have the capacity to continuously collect data, ensuring global coverage.

2.1.2 Radar satellite technology

During the last decades radar satellite technologies have proven their usefulness to monitor the Earth thanks to the plenty of applications that can exploit their data. More and more application opportunities have emerged, thanks to the improved capabilities of the new space radar sensors in terms of both resolution and revisit time. Currently, different space-borne SAR data in L-, C- and X-band are available for monitoring applications.

Thanks to the all-weather, day-night capability to detect and quantify accurately small ground surface deformations, Synthetic Aperture Radar (SAR) Interferometry (InSAR) techniques are attractive for different areas of risk management such as monitoring of subsidence, volcanoes, tectonic movements, urban areas and infrastructure and slope instabilities. In particular, the technique allows detecting and monitoring millimetric displacements occurring on selected point targets exhibiting coherent radar backscattering properties. Successful applications to different geophysical phenomena have been already demonstrated in literature (Bovenga *et al.*, 2012; Nutricato *et al.*, 2017; Massimi, 2018; Massimi, Forenza and Alisiconi, 2018).

Furthermore, the available archive data from the European Space Agency (ESA) missions ERS-1/2 and ENVISAT (ENV), allows performing ground instability analysis back in time almost all over the Earth, complementing the currently running Sentinel-1 mission available since 2014 on almost all the world.

Throughout this section, the state of the art regarding the monitoring of both road and railway network using optical and radar technologies is being described, focusing on the most recent trends, applications, and processing methodologies.

2.1.3 Roads and Railways monitoring

Data from optical remote sensing can have a great value for monitoring different natural or anthropic phenomena that can have potential impacts on transport networks maintenance and safeness.

In general, a change detection application could support in different ways the identification of specific locations that need maintenance and/or where safeness issues may arise due to some variations from the standard situation.

Change detection algorithms applied to the optical data may be of different nature according to the targeted objects, and of course the spatial and temporal resolution of the input data determines the size of what can be "detected" and the phenomenon that can be "monitored".

If we refer to the Sentinel-2 data, which represent today a great opportunity for their provision at no cost and for their revisit time of 3-5 days (depending of the

latitude) and a spatial resolution up to 10 meters in the visible and near infrared spectral range, the change detection applications may target different phenomena potentially impacting the transport network.

Sentinel-2 opens a large scale of new applications allowing to continuously monitor changes on the ground over huge area of interest (regional to national scale) highlighting hot spots of changes that, once detected, could be further inspected, if deemed necessary, with greater detail using very high resolution satellite images and visual inspection.

Digital Change Detection algorithms can provide binary land cover "change/no-change" information by automatically detecting the spatial regions within a bi-temporal image pair where meaningful change is likely to have occurred, then a human operator (or another process) can analyse the changes using his/her knowledge.

For change detection, using a pair of images, three main categories of methods could be used:

- Simple Detection: use Mean Difference, Ratio Of Means or Root Mean Square Differences of the relevant bands (typically visible and near infrared bands).
- Normalized index change detections: produce normalized indicators related to the targeted change to be detected (e.g. built-in areas) and compare them.
- Post Classification Comparison: make supervised classification of the pairs and compare results (e.g. land cover comparison, Built-up Areas comparison).

Monitoring examples using optical remote sensing for specific thematic applications potentially impacting the transport networks maintenance and safeness are:

Monitoring the evolution of artificial surfaces

The automatic detections can generate alerts, that can activate further inspections with other techniques.

Monitoring the coastal erosion

Optical satellite data can be a precious source of information for monitoring coastal erosion and potential connected impacts on transport network infrastructures. Using comparative analysis of more optical images over time, coastal trends in terms of erosion, stability, and advancements can be identified and represented through geospatial indicators which can support decision making for new interventions and works.

Monitoring wildfires

Optical satellite data can be used to map the boundaries of fires occurring in many areas. Once this information has been achieved, time series of images are used to monitor -through vegetation or other spectral indexes- the vegetation regeneration process and, in general, the burnt area evolution over time after forest fires.

Monitoring examples using radar remote sensing for specific thematic applications potentially impacting the transport networks maintenance and safeness are:

Displacement monitoring of roads and railways infrastructures

The historical and continuous acquisition of radar data by means of MTI algorithms makes it possible to continuously monitor both the structural motion of roads and railways and the third-party induced displacement that may negatively impact the infrastructures.

Flood mapping

Data acquired from satellite based Synthetic Aperture Radar systems, such as Sentinel-1, with their ability to penetrate cloud coverage are also very useful to evaluate the extent of flooding events especially during or soon after the storms, when cloud coverage usually doesn't allow the use of optical data. SAR sensors have very low return from water bodies making them an ideal tool for mapping flood extents. In a radar image, the delineation between water and non-water can be clearly delineated.

In order to produce flood extents, the raw SAR data must first be pre-processed. The processing techniques include calibrating the pixel values and speckle filtering the data. The dataset must also undergo terrain correction to correct for effects such as foreshortening, layover, and shadow. Following this it can be transformed from ground range geometry to a specific coordinate reference system (e.g. WGS84).

After the pre-processing stage a histogram of backscatter coefficients can be generated and is used to help determine a value which most accurately reflects the threshold between water and non-water. Finally, the resulting binary raster image can be converted into a vector dataset for analysis with other existing datasets.

Mapping of this nature has obvious applications in flood risk management and planning. It can assist engineers and planners make more informed decisions and so help reduce the risk from future floods. In addition, the fast turnaround possible between the data being acquired to the flood extents being produced means these maps could assist emergency services during a flood event.

2.2 Terrestrial remote sensing technology

Even though LiDAR technology popularity has significantly increased during this decade, this has been in development since the second half of the past century. Its development started in the 1960s with several applications in geosciences. Years later, land surveying applications appeared in the picture thanks to the use of airborne profilometers. This equipment resulted to be useful for deriving the vegetation height, by evaluating the returned signal (Link and Collins, 1981). During the 1980s and 1990s, the use of laser scanning for environmental and land surveying applications increased. In the second part of the 1990s, civil engineering related applications started to arise, but it was not until the last part of the century and the beginning of the new one when the first terrestrial devices for 3D digitalization performance appeared. From this point, numerous applications for different fields quickly raised (B Riveiro *et al.*, 2016), and Terrestrial Laser

Scanning (TLS) proved to be the appropriate technology to use when detailed 3D models were required. With the evolution of technology, the resolution and quality of data given by laser scanning devices have been improved. And so, in these final years, mobile mapping systems are arising in order to perform high resolution surveys of large infrastructures (tunnels, roads, urban modelling…) in a short period of time.

Nowadays, the main bottleneck for LiDAR technology is processing the large amount of data acquired with laser scanning devices. Throughout the years, many tools have been developed for point-cloud data processing. Most of these depend on manual or semi-automatic operations that have to be performed by a specialist in the field of geomatics. The current challenge is to develop tools for an efficient automation of data processing, using information provided by ALS, MLS or TLS.

Many companies and research groups investing in this technology have allowed its fast development. With the appearance of machine learning algorithms, the tedious and hard processing tasks tend to disappear or be minimized. These tools allow, not only the development of advanced, efficient and intelligent processing, but also interpretation of data. One of the main objectives exploited is obtaining inventories for road, railway or urban management. Now, this has evolved and the trend is to obtain spatial models of infrastructures based on the fusion of geometric and radiometric data and monitoring the infrastructure behaviour and changes through the years. These models have a notorious potential for BIM (building information modelling) and AIM (asset information model) applications, allowing to have not only as-design representations of the asset but also as-built and as-operate models which can be updated over time.

Throughout this section, the state of the art regarding the monitoring of both road and railway network using LiDAR-based technologies is described, focusing on the most recent trends, applications, and processing methodologies.

2.2.1 Road network monitoring

The successful integration of laser scanners, navigation sensors and imagery acquisition sensors on mobile platforms has led to the commercialization of Mobile Laser Scanning systems meant to be mounted on vehicles such as regular vans or passenger cars, as it can be seen in Section 5.2. As these vehicles naturally operate along the road network, a large part of the existing research regarding the processing and understanding of the data collected by these systems has revolved around applications related with the monitoring of the road network.

This section of the review will focus on those applications, which will be divided in two main groups: Road surface monitoring, and off-road surface monitoring. This conceptual division, which is considered by similar reviews of the field (Guan, Li, *et al.*, 2016; Ma *et al.*, 2018) will allow the reader to focus separately on different elements and features of the road network.

2.2.1.1 Road surface monitoring

The automatic definition of the ground has been one of the most common processes that are carried out using data from LiDAR-based sources. Although this application has been on the literature since the beginning of the century (Lohr, 1998; Sithole, 2001) there has been a continuous research and improvement

motivated by two main factors: The remarkable improvement of the LiDAR-based systems, and the increased computational power available for research. Nowadays, LiDAR-based data has been used for automatically detecting and extracting not only the road surface but also different elements and features on the road such as road markings and driving lanes, cracks, or manholes. Furthermore, an efficient extraction of the road surface is typically a preliminary processing step that allows the separation of ground and off-ground elements when using 3D point clouds as main data source. Hence it is a process that can be found in a large proportion of works focused on object detection and extraction from 3D point cloud data.

Road surface extraction

Within the literature, different ways of organizing the existing knowledge on road surface extraction can be found. Ma *et al.* (2018) define three main methodological groups based on the data structure: (1) 3D-point driven, (2) 2D Geo-reference feature image-driven, and (3) Other data (ALS/TLS) driven. Differently, Guan, Li, *et al.* (2016) define four groups based on the processing strategy, which can be summarized in two larger groups: (1) Processes based on previous knowledge of the road structure and (2) Processes based on the extraction of features for identification or classification of the road surface. For the following analysis of the state of the art, the approach of Guan, Li, *et al.* (2016) will be taken as reference. In **¡Error! No se encuentra el origen de la referencia.**, a summary that has into account both approaches (based on the data structure and on the processing strategy) can be found.

- *Road surface extraction based on its structure:* A common approach for road surface extraction relies on the definition of road edges that delineate its limits. This approach has been evolving since the beginning of this decade. Ibrahim and Lichti (2012) propose a sequential analysis that segments the ground based on the point density and then a Gaussian filtering to detect curbs and extract the road surface afterwards (Figure 1a). These steps are analogous in similar works, changing the curb detection method: Some works perform a rasterization (projection of the 3D point cloud in a gridded XY plane, generating two dimensional geo-referenced feature (2D GRF) images) and detect curbs using image processing methods such as the parametric active contour or snake model (Kumar *et al.*, 2013; Kumar, Lewis and McCarthy, 2017) or image morphology (Rodríguez-Cuenca *et al.*, 2015a, 2016). Guan, Li, *et al.* (2014) generate pseudo scan lines in the plane perpendicular to the trajectory of the vehicle to detect curbs by measuring slope differences. Differently, a number of approaches have been developed for curb detection directly in 3D data, using point cloud geometric properties such as density and elevation (Yang, Fang and Li, 2013), or derived properties such as the saliency, which measures the orientation of a point normal vector with respect to the ground plane normal vector (Wang, Luo, *et al.*, 2015) and has been successfully used to extract curbs or salient points in different works (Sánchez-Rodríguez *et al.*, 2018; Soilán *et al.*, 2018). Xu, Wang and Zheng (2017) use an energy function based on the elevation gradient of previously generated voxels (3D equivalent of pixels) to extract curbs, and a least cost path model to refine them. Using voxels

allows to define local information by defining parameters within each voxel, and to reduce the computational load, so they are commonly used for road extraction (Douillard *et al.*, 2011; Zai *et al.*, 2018). Hata, Osorio and Wolf, (2014) propose a robust regression method named Least Trimmed Squares (LTS) to deal with occlusions that may cause discontinuities on the road edge detection. A different approach can be found in (Cabo *et al.*, 2016), where the point cloud is transformed into a structured line cloud, and lines are grouped to detect the edges (Figure 1b). Although good results can be found among these works, most of them rely on curbs to define road edges, hence the extraction of the road surface will not be robust when it is not delimited by curbs, as it is the case of most non-urban roads.

- *Road surface extraction based on feature calculation*: A different approach for road surface extraction is based on previous knowledge about its geometry and contextual features, which can be identified on the 3D point cloud data. Guo, Tsai and Han (2015) filter points based on their height with respect to the ground and then extract the road surface via TIN (Triangulated Irregular Network) filter refinement. Generally, the elevation coordinate of the point cloud is the key feature that is employed for road surface extraction: Serna and Marcotegui (2013, 2014) defined the λ-flat zones algorithm, which analyses the local height difference of the point cloud projected on the XY plane. Also, Fan, Yao and Tang (2014) employ a height histogram for detecting ground points as a pre-processing step on an object detection application. Another feature that is commonly used is the roughness of the road surface. Díaz-Vilariño *et al.* (2016) present an analysis of roughness descriptors that are able to classify different types of road pavements (stone, asphalt) with accuracy. Similarly, Yadav, Singh and Lohani (2017) employ roughness together with radiometric features (assuming uniform intensity as a property of the road) and 2D point density to delineate road surfaces from non-road surfaces. As it was the case for curb detection methods, there are scan-line based methods that rely on the point topology (Ying Zhou *et al.*, 2014) or density (Che and Olsen, 2017) across the scan line for extracting the road surface.

From this analysis, it can be seen that there exist a large number of works focused on the extraction of the ground or the road surface, but there is still not an established standard for this process, and it is typically designed *ad hoc* for a more complex final application.

Table 2: Summary of state-of-the-art works for road surface extraction

		PROCESSING STRATEGY	
		Based on road structure (road edge delineation)	**Based on feature calculation**
Data structure	2D GRF	(Kumar *et al.*, 2013; Rodríguez-Cuenca *et al.*, 2015a, 2016; Kumar, Lewis and McCarthy, 2017)	(Serna and Marcotegui, 2013, 2014)
	3D point cloud	(Douillard et al., 2011; Ibrahim and Lichti, 2012; Yang, Fang and Li, 2013; Hata, Osorio and Wolf, 2014; Wang, Luo, et al., 2015; Xu, Wang and Zheng, 2017; Sánchez-Rodríguez et al., 2018; Soilán et al., 2018; Zai et al., 2018)	(Fan, Yao and Tang, 2014; Guo, Tsai and Han, 2015; Díaz-Vilariño *et al.*, 2016; Che and Olsen, 2017; Yadav, Singh and Lohani, 2017)
	Scan lines	(Cabo *et al.*, 2016)	(Ying Zhou *et al.*, 2014)

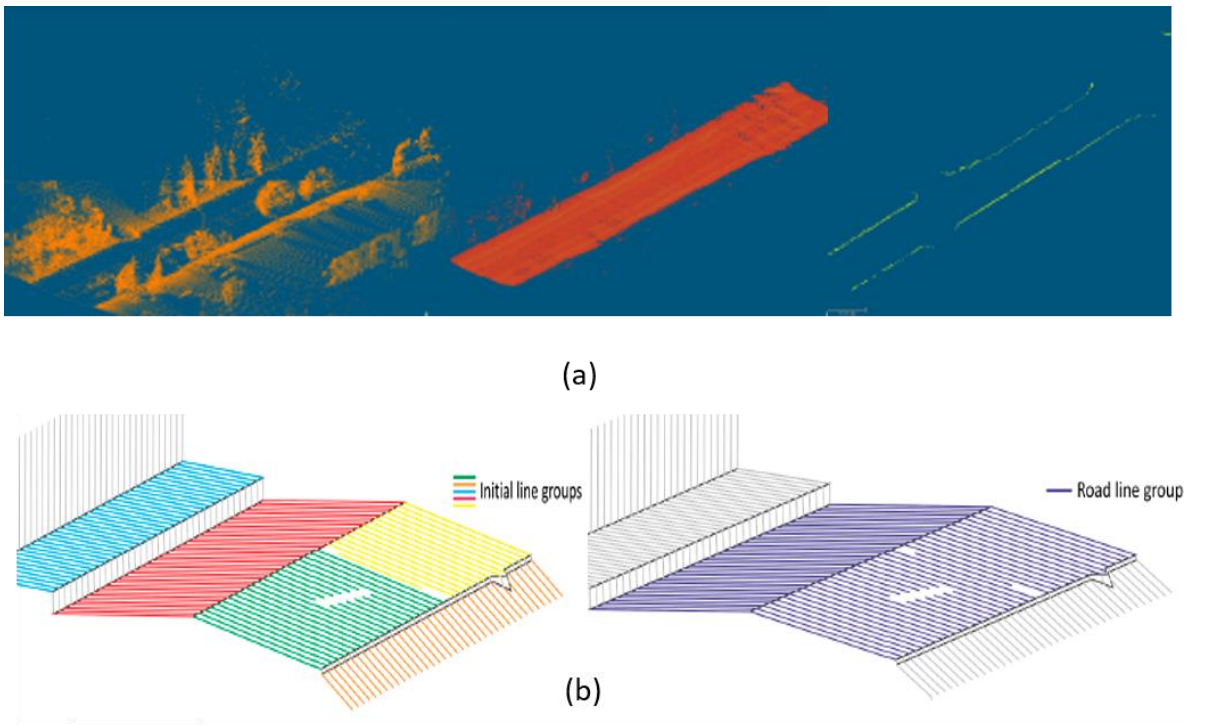

Figure 1: Road surface extraction. (a) Ibrahim and Lichti (2012) segment non-ground (left) and ground (centre) using a density-based filter. Then, a 3D edge detection algorithm based on local morphology and Gaussian filtering extracts road edges (right). (b) Cabo *et al.* (2016) scan lines are grouped based on length, tilt angle and azimuth, and the initial groups (left) are joined following predefined rules using the vehicle trajectory to define the road surface (right)

Road markings and driving lanes

Derived from road extraction methods, there exists a vast literature focused on the automatic detection of road markings, which are highly important road elements as they are one of the main information sources for drivers and pedestrians. This automation may assist maintenance and inventory tasks, reducing both the cost of the process and the subjectivity of the inspection activities (Soilán *et al.*, 2017). The main feature that allows the detection of road markings using 3D point clouds as data source is its reflectivity, which is translated into larger radiometric attributes of the 3D data. Most road marking detection works exploit this feature once the road pavement is extracted. For example Guo, Tsai and Han (2015) generate raster binary images based on the intensity of the road points and extract different classes of road markings. As it can be seen in Figure 2, the generation of binary images based on point cloud intensity is a common approach (Arias *et al.*, 2015; Guan, Li, Member, *et al.*, 2015; Riveiro *et al.*, 2015; Yan *et al.*, 2016; Soilán *et al.*, 2017; Ma *et al.*, 2019), being the principal differences among these works the features employed for road marking detection, and the classification methods employed: Some works rely on previous knowledge and heuristics to classify different road markings (Yu, Li, Guan, Jia, *et al.*, 2015; Jung *et al.*, 2019) while others follow a more recent trend based on machine learning (Soilán *et al.*, 2017) or deep learning (Wen *et al.*, 2019). A comprehensive summary of these methodological differences is shown in Table 3. As it can be seen, automatic road marking detection and classification using data from LiDAR scanners is more than feasible, and may be a standard data source not only for road marking inspection but for applications such as driving line generation (Zhao, 2017; Ma *et al.*, 2019; Ye *et al.*, 2019). For other applications such as autonomous driving where real-time information is required, road marking recognition is carried out using RGB images analysed by machine learning or deep learning classification models (Li *et al.*, 2017; Jia *et al.*, 2018; Tian *et al.*, 2018; Ding *et al.*, 2019).

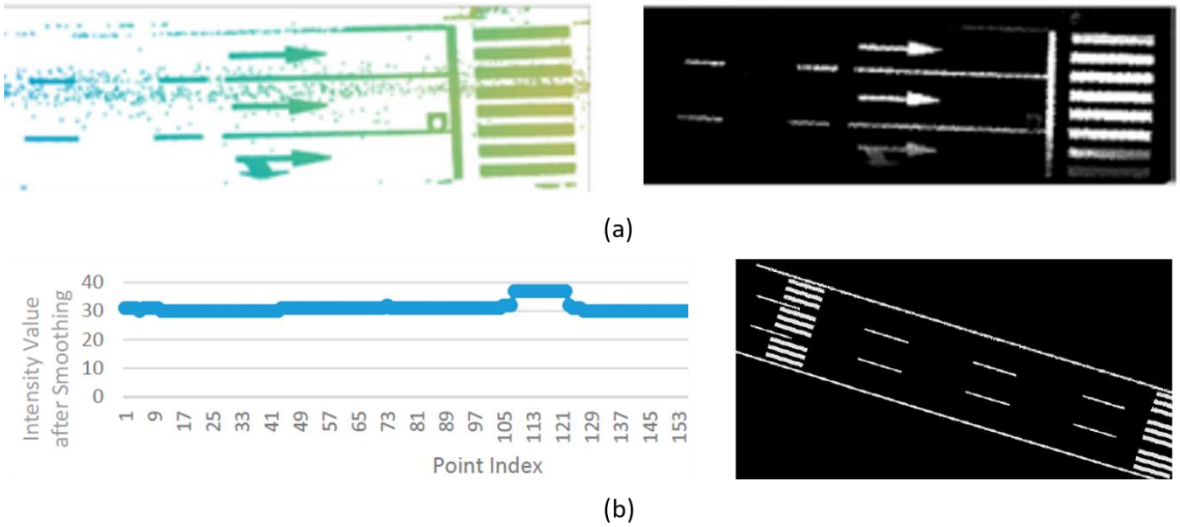

Figure 2: Road markings and driving lanes. (a) Soilán *et al.* (2017) apply an intensity filter on the point cloud (left) and generate a 2D GRF image representing the road markings (right). (b) Yan *et al.* (2016) propose a scan line based method using the gradient of point intensity to detect road marking points on each scan line (left) and generate a 2D GRF image representing the road markings (right)

Table 3: Summary of state-of-the-art works for road marking extraction

		PROCESSING STRATEGY		
		Detection process		**Classification process**
Data structure	2D GRF	Morphology	Adaptive thresholding	- Template matching (Guo, Tsai and Han, 2015; Soilán *et al.*, 2017) - Neural Networks (Soilán *et al.*, 2017) - Deep Learning (Wen *et al.*, 2019)
		(Arias *et al.*, 2015; Guo, Tsai and Han, 2015; Riveiro *et al.*, 2015; Jung *et al.*, 2019)	(Guan, Li, Member, *et al.*, 2015; Kim, Liu and Myung, 2017; Soilán *et al.*, 2017)	
	3D point cloud	- Spatial density filter: (Yu, Li, Guan, Jia, *et al.*, 2015) - Scan line separation: (Yan *et al.*, 2016)		- Deep Boltzmann Machines (Yu, Li, Guan, Jia, *et al.*, 2015)
	Photogra mmetry			- Deep Learning (CNNs) (Li *et al.*, 2017; Tian *et al.*, 2018)

Road cracks and manhole covers

Detecting and positioning road cracks is another relevant application that has been addressed by researchers using LiDAR-based technologies. Using 3D point clouds, Yu *et al.* (2014) extract 3D crack skeletons using a sequential approach based on a preliminary intensity based filtering, followed by a spatial density filtering, a Euclidean clustering, and a L_1-median-based crack skeleton extraction method. However, 3D methods are not the most common approaches for crack detection, as the 3D point clouds are typically projected into 2D GRF images based on different features such as intensity (Guan, Li, Yu, *et al.*, 2015) or minimum height (Chen *et al.*, 2016), in order to detect road cracks. Guan, Li, Yu, *et al.* (2015) define an Iterative Tensor Voting, while Chen *et al.* (2016) perform convolutions with predefined kernels over their GRF images. Cracks can be also detected with other sensors that are typically mounted on MLS systems. There exist computer vision approaches that analyse images, as done by Gavilán *et al.* (2011) using line scan cameras; and there exist also approaches using Ground Penetrating Radar (GPR) (Venmans, Van De Ven and Kollen, 2016) and thermal imaging (Aparna *et al.*, 2019). Another relevant road surface element, especially in urban environments, are manhole covers, which can also be automatically detected using 3D point clouds. Guan, Yu, *et al.* (2014) use an analogous approach than for detecting cracks in (Guan, Li, Yu, *et al.*, 2015), that is, generating a GRF image and applying a multi-scale tensor voting and morphological operations to extract manhole covers. Yu, Guan and Ji (2015) generate GRF images as well, but detect manhole covers based on a multilayer feature generation model and a random forest model for classification.

2.2.1.2 Off-Road surface monitoring

In a number of infrastructure monitoring applications, the elements of interest are not the road surface or its elements, but different objects or infrastructure assets that play a relevant role on the correct performance of the network. This section will analyse the state of the art regarding the monitoring of those elements and assets, namely**¡Error! No se encuentra el origen de la referencia.**: traffic signs, pole-like objects and roadside trees.

Traffic signs

Traffic signs play a clearly important role in the transportation network as one of the main information sources for drivers, together with road markings. Their standardized geometry and reflective properties have encouraged researchers to develop different methods for the automatic detection and recognition of road markings from MLS systems data. Pu *et al.* (2011) shown that based on a collection of characteristics such as size, shape or orientation, it is possible to recognize different objects, provided previous knowledge on their geometry. Not only geometry but the radiometric properties (high reflectance) of traffic sign panels have been recurrently used for traffic sign detection. Ai and Tsai propose a traffic sign detection process which filters a 3D point cloud based on intensity, elevation and lateral offset (Ai and Tsai, 2016). The method is able to evaluate the retroreflectivity condition of the traffic sign panels, which is directly related to the wear and tear of the material and is a relevant feature for traffic sign monitoring (Ai and Tsai, 2014). Unlike road markings, there are only a few works that rely on 2D GRF images for traffic sign detection. Riveiro *et al.* (2016) filter the point cloud by generating a 2D raster based on point intensity values, simplifying the detection of traffic sign panels using a Gaussian Mixture Model afterwards. Furthermore, they generate raster images on the plane of the detected traffic signs to recognize their shape. However, 3D point cloud data resolution is still not enough to extract semantic information of the traffic signs (Soilán *et al.*, 2016b), hence that recognition is typically performed on RGB images from the cameras of the MLS system. Traffic sign panel detection primarily relies on an intensity-based filter of the 3D point clouds, followed by different filtering strategies, based on geometric and dimensionality features (Wen *et al.*, 2015; Soilán *et al.*, 2016a, 2016b; Huang *et al.*, 2017; Guan *et al.*, 2018) (Figure 3a). A different approach for traffic sign detection can be found in (Yu, Li, Wen, *et al.*, 2016), where a supervoxel based bag-of-visual-phrases is defined, and traffic signs are detected based on their feature region description. Given that the 3D point clouds are spatio-temporally synchronized with 2D images in a MLS system, it is straightforward to extract images of the traffic sign panels and perform computer vision processes on them to extract semantic information: Some works rely on machine learning strategies such as Support Vector Machines using custom descriptors (Soilán *et al.*, 2016b) or existing features such as Histogram of Oriented Gradients (HOG) (Tan *et al.*, 2016), while others rely on the more recent trend of Deep Learning, approaching to an end-to-end recognition process, using Deep Bolztmann Machines (Yu, Li, Wen, *et al.*, 2016; Guan *et al.*, 2018) or convolutional neural networks (Arcos-García *et al.*, 2017) (Figure 3b). These techniques are also employed using only imagery data (Gudigar *et al.*, 2019; Jain *et al.*, 2019). All the mentioned work is summarized in Table 4.

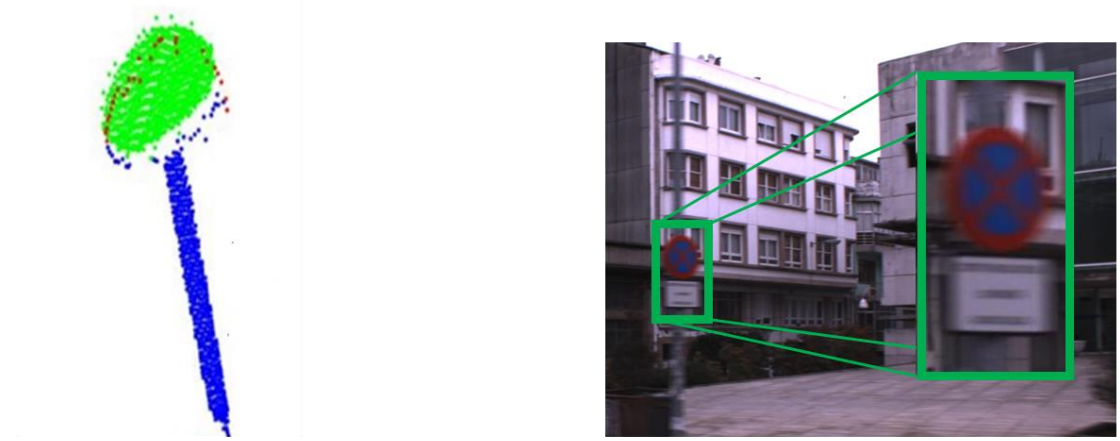

(a)

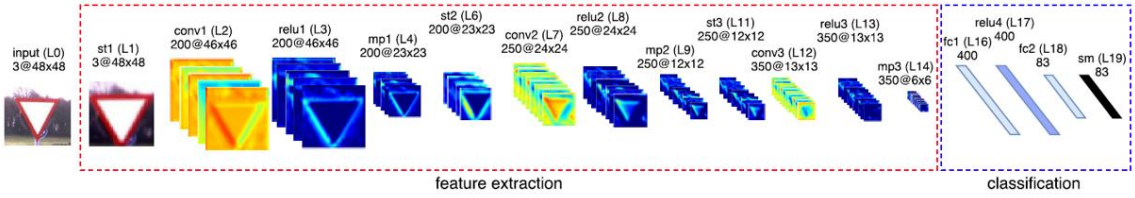

(b)

Figure 3: Traffic signs. (a) Soilán *et al.* (2016b) detect traffic sign panels applying intensity filters on a previously segmented point cloud (left), define geometric parameters for each traffic sign and project the panel on georeferenced RGB images (right). (b) Arcos-García *et al.* (2017) classifies those RGB images applying a Deep Neural Network that comprises convolutional and spatial transformer layers

Table 4: Summary of state-of-the-art works for traffic sign detection

		PROCESSING STRATEGY	
		Detection process	**Classification process**
Data structure	2D GRF	Intensity-based raster (Belén Riveiro *et al.*, 2016)	
	3D point cloud	- Intensity-based filtering (Wen *et al.*, 2015; Soilán *et al.*, 2016a, 2016b; Huang *et al.*, 2017; Guan *et al.*, 2018) - Bag-of-visual-phrases (Yu, Li, Wen, *et al.*, 2016)	
	Photogrammetry		- SVM (Soilán *et al.*, 2016b; Tan *et al.*, 2016) - Deep Boltzmann Machines (Yu, Li, Wen, *et al.*, 2016; Guan *et al.*, 2018) - CNN (Arcos-García *et al.*, 2017; Gudigar *et al.*, 2019; Jain *et al.*, 2019)

Pole-like objects

Detecting pole-like objects is a common objective in 3D point cloud processing works, as their geometry is well defined and easily recognizable when monitored by a LiDAR-based system. They are typically used to detect street lights or power line poles (Cheng *et al.*, 2014). Ground segmentation is usually a pre-processing step, as ground removal leads to an isolation of off-road objects. From that point, there is a large number of processing strategies to detect pole-like objects. Yu, Li, Guan, Wang, *et al.* (2015) group 3D points with an Euclidean cluster, refine them with a Normalized Cut segmentation and then construct a Pairwise 3-D shape context to detect pole-like objects with a similarity measurement. A 3-D shape feature is also developed by Guan, Yu, *et al.* (2016), and each object is compared against a bag of contextual-visual words (Yu, Li, Guan, *et al.*, 2016). Similarly, Wang, Lindenbergh and Menenti (2017) develop a 3D descriptor (SigVox) using an Octree and principal component analysis (PCA) to get dimensional information at different levels of detail (Figure 4a). Other notable approaches include the application of anomaly detection algorithms (Rodríguez-Cuenca *et al.*, 2015b), or the development of classification models such as Random Forests (Yan *et al.*, 2017) or Support Vector Machines (Wu *et al.*, 2017) for shape features. In a second group of approaches, those that do not rely on ground segmentation as a preliminary step use to perform a voxelization of the 3D data, and pole-like objects are detected based on the voxelized structure. Cabo *et al.* (2014) perform a relatively simple study of the local structure of occupied voxels to define pole-like objects, and Li, Li and Li (2016) define an adaptive radius cylinder model given previously knowledge regarding the geometrical structure of a pole-like object. Supervoxels are also exploited for detecting pole-like objects, obtaining structure, shape or reflectance descriptors (Teo and Chiu, 2015; Wang, Wang, *et al.*, 2015).

Roadside trees

With a LiDAR-based mobile system it is possible to map the presence of trees alongside the road network. As there is a correlation between vegetation and fire risk in a road environment, roadside tree detection processes are clearly beneficial in road network monitoring applications. As seen for traffic sings and pole-like objects, ground segmentation is usually the first pre-processing step, isolating above ground objects. Xu *et al.* (2018) propose an hierarchical clustering to extract trees' nonphotosynthetic components (trunks and tree branches), formulating a proximity matrix to calculate cluster dissimilarity, and solving the optimal combination to merge clusters (Figure 4b). Other clustering algorithms employed for tree extraction are the Euclidean Cluster (Guan, Yu, Ji, *et al.*, 2015; Huang *et al.*, 2015), or, as in Li *et al.* (2016) work, a region growing based clustering in a voxelized space to distinguish between trunk and crown in a tree. Machine and Deep Learning models are also developed for tree classification. Zou *et al.* (2017) employ a Deep Belief Net (DBN) to classify different tree species from images obtained after a voxelization-rasterization process. Guan, Yu, Ji, *et al.* (2015) classify up to 10 tree species using waveform representations and Deep Boltzmann Machines. Dimensional features obtained from PCA analysis are also used for classification, with SVM (Huang *et al.*, 2015) or Random Forests (Weinmann *et al.*, 2017) as classification models.

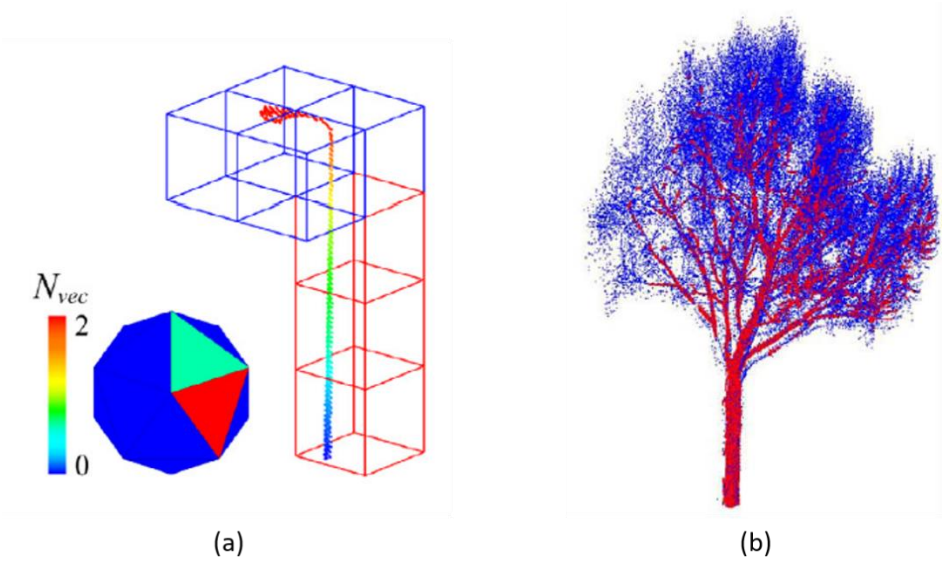

Figure 4. Pole-like objects and roadside trees. (a) Wang, Lindenbergh and Menenti (2017) recognize street objects using a voxel-based shape descriptor determined by the orientation of the significant eigenvectors of the object at several levels of an octree. (b) Xu *et al.* (2018) recognize trunks and tree branches by optimally merging clusters of points

2.2.1.3 Current and future trends

Throughout this section, different applications of LiDAR-based systems for road network monitoring have been reviewed. Most of the mentioned works have been developed in the last five years, and the number of publications is still increasing yearly. As LiDAR technology continues its evolution, there are more robust solutions for specific road monitoring applications, however, there is a lack of standards, in the industry, to apply when LiDAR data is automatically processed. In the last couple of years, the performance of Deep Learning in 2D images has led researchers to develop Deep Learning models for 3D data (Qi *et al.*, 2016, 2017; Tatarchenko, Dosovitskiy and Brox, 2017; Su *et al.*, 2018), which are being developed to solve classification problems using 3D data acquired by MLS systems (Kumar *et al.*, 2019; Luo *et al.*, 2019; Wen *et al.*, 2019). This paper presents an extensive literature review that describes different methods and applications for the monitoring of terrestrial transportation networks using data collected from Mobile Mapping Systems equipped with LiDAR sensors.

2.2.2 Railway network monitoring

Most of the works regarding railway infrastructure are developed using Mobile Laser Scanners, as previously presented at the introduction of this section. These are large infrastructures and the applications in which their point-clouds are employed usually require a high resolution. This is why MLS is the most appropriate technology to be used for railway networks, although there are some works developed using ALS or TLS data (Soni, Robson and Gleeson, 2014; Collin, Carreaud and Lançon, 2016; Arastounia, 2017).

In this section, a summary of the most relevant applications of LiDAR data concerning the railway network is shown. One way of classifying the existing works in relation to railway infrastructure recognition and inspection may be attending to

the collection methods used to obtain the 3D point clouds. Likewise, Lou *et al.* (2018) proposed a classification based on the methods followed for classifying points. On this basis, three main categories were proposed: (i) data-driven and model-driven methods, using point features and geometrical relationships; (ii) learning-based methods, which use imagery data and/or MLS point data; and (iii) multi-source data fusion methods (Beger *et al.*, 2011; Arastounia, 2012; Neubert *et al.*, 2012; Yang, Fang and Li, 2013; Zhu and Hyyppa, 2014; Ma *et al.*, 2018). Although other classification proposals can be also considered, the classification in this paper is made attending to the main goal, or application of each work (Figure 5), as proposed in Che, Jung and Olsen (2019), where a review about object recognition, segmentation and classification using MLS point clouds in different environments, such as forest, railway and urban areas is presented. In addition, several figures (Figure 6 - Figure 10) provide extra context to some of the works cited throughout the subsequent sections.

Figure 5: Classification of the railway network monitoring based on the application

2.2.2.1 Railway inventory and 3D modelling

The automatic classification of points forming specific objects is one of the first tasks that need to be developed in any area of study. Che, Jung and Olsen (2019) made a review to this end presenting different and broadly known techniques for object recognition and features extraction from MLS 3D point clouds. Al-Bayari (2019) has also presented a series of case studies in civil engineering projects using a mobile mapping system, but with specific programs for the post-processing of the extracted point clouds. And so Leslar, Perry and McNease (2010) in the railway field. They performed some preliminary classification of points in terms of the number of return of each point, and the remaining ones were manually selected and classified, using external programs and semi-automatic methods.

In the railway network, the works from Arastounia are relevant when applying heuristic methods to classify points from MLS point-clouds. His algorithms follow a data-driven and model-driven approach (Lou *et al.*, 2018), grouping points into railway objects' classes (Arastounia, 2012, 2015; Arastounia and Elberink, 2016). Later on, he published a specific work regarding the automatic recognition of rail tracks and power line cables using TLS and ALS data, with better performance than the previous methodologies presented by the author (Arastounia, 2017). Following these advances, Sánchez-Rodríguez *et al.* (2018) developed an algorithm for MLS tunnel point cloud classification. They used not only heuristic methods but also SVMs (Géron, no date) for the classification of possible rails in the track. The results obtained in these two latter works are depicted in Figure 6. Regarding the use of classifiers, Luo, Jwa and Sohn (2014) used the Conditional Random Field (CRF) classifier to make a prediction with local coherence, resulting also in a context based classification of points into different railway objects.

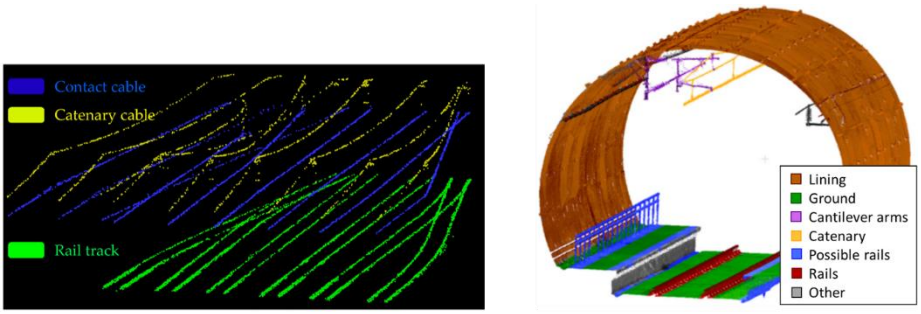

Figure 6: Inventory and 3D modelling.(a) Arastounia (2017) classified rail tracks and contact cables using an improved region growing algorithm. Then, the catenary cables' points are classified as they are placed in the neighbourhood of the contact cables. (b) Sánchez-Rodríguez *et al.* (2018) classified MLS data using dimensional analysis and RANSAC methods, and validated the rails' classification with SVM algorithms

Another option for LiDAR point cloud processing is converting them into 2D images. Zhu and Hyyppa (2014) directly made this conversion and classified data using image processing techniques. And mixing images with point clouds, Neubert *et al.* (2012) extracted of railroad objects from very high resolution helicopter-borne LiDAR and ortho-image data. They also used LiDAR data fusion methods to classify rails. This opens up a new idea for the process of laser scanning data using deep learning techniques to classify points, and so, Rizaldy *et al.* (2018) made a multi-class classification of aerial point clouds using Fully Convolutional Networks (FCN), which is a Convolutional Neural Network (CNN) designed for pixel-wise classification.

Next step should be the conversion of the classified points into 3D models. In this relation, there is not much work in the last years, but with the appearance of BIM and Digital Twin, it will soon become a need. Some authors have been using specific programs for that conversion (Kwoczynska, Sagan and Dziura, 2016), while others directly convert the LiDAR point-cloud data into 3D models. This application within the railway network still need to be developed. Most authors in this field based their research in specific elements of the infrastructure, and automatically detecting damage or pathologies in them. In the subsequent sections, a summary of the most critical works concerning this matter is shown.

2.2.2.2 Rails

One of the most extended practices when working with point-clouds in railway environments is the extraction of the tracks' centreline. Beger *et al.* (2011) used data fusion of extremely high resolution ortho-imagery with ALS data to reconstruct railroad track centrelines. The images were used to obtain a first railroad track mask and laser points classified, and then, rail track centreline was approximated using an adapted RANdom SAmple Consensus (RANSAC) algorithm (Fischler and Bolles, 1981). Continuing with centre lines' estimation, Elberink and Khoshelham (2015) proposed two different data-driven approaches in order to automate this process. First, they extracted the tracks from MLS point clouds. Then, centre lines were directly generated using the detected rail track points, or generating fitted 3D models and implicitly determining the mentioned centreline.

Railway tracks' point-clouds may be extracted automatically from MLS data. Sánchez-Rodríguez *et al.* (2018) found possible rails according to the curvature of ground-points neighbourhood and then, they used SVM classifiers to verify the results obtained (Figure 7a). Also, Lou *et al.* (2018) developed a method to this end which processes data in real time. They exposed the validity of using a low cost LiDAR sensor (Velodyne) for performing mobile mapping surveys (Figure 7b). Stein (2018) also used low cost sensors, contributing with his thesis to the improvement of track-selective localization. He determined the railway network topology and branching direction on turnouts applying a multistage approach. More specifically, Stein, Spindler and Lauer (2016) proposed a model-based rail detection in 2D MLS data. They developed a spatial clustering to distinguish rails and tracks from other captured elements.

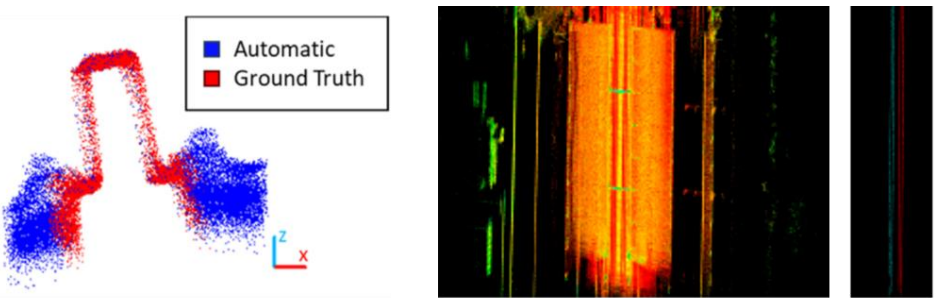

(a) (b)

Figure 7: Rails. (a) Sánchez-Rodríguez *et al.* (2018) classified them analysing also the point cloud curvature (elevation difference) and validated the results applying SVM classifiers. (b) Lou *et al.* (2018) detected rails based on their elevation difference together with their reflection characteristics

For the creation of 3D models from rails' point-clouds, Soni, Robson and Gleeson (2014) first extracted rail track geometry from TLS point clouds. Then, models were created for monitoring purposes. Later on, Yang and Fang (Yang and Fang, 2014) also created railway tracks 3D models but from MLS point clouds. Which first, detect railway bed areas, then follow patterns and intensity data of rails to find tracks. Similarly, Hackel *et al.* (2015) detected rails and other parts of the track applying template matching algorithms (model-based) as well as support vector machines (feature based). The results show that this methodology can be used for data from any laser scanner system.

Some authors go beyond railway tracks' detection, and propose methods not only for classification but also for the inspection of these elements, as described in Section 2.2.2.5.

2.2.2.3 Power line

Most of the railway network uses aerial contact lines to provide energy supply to trains during operation. Therefore, monitoring of their composing elements it is essential for railway companies. To this respect, Jeon and Choi (2013) proposed a method based on RANSAC algorithms to automatically detect railroad power lines in LiDAR data. Then, iterative RANSAC and least square adjustment were used to estimate the line parameters and build the 3D model of railroad wires. As exposed in Section 3.2.1, the work from Arastounia (2015) stands out since he proposed an heuristic methodology for classifying points in the railway environment. This

calculates points' neighbourhoods and recognises objects by their geometrical properties and topological relationships. Specifically, the recognition of overhead contact cables was developed applying PCA and region growing algorithms. Catenary and return cables are detected attending to their distribution in the 3D space with respect to the contact cable. In relation to this method, Pastucha (2016) used the MMS (Mobile Mapping System) trajectory to limit the search area vertically and horizontally for extracting the catenaries. Then, the method classifies points applying also RANSAC algorithms and geometrical and topological relationships. This also provides the location of cantilevers and poles or structural beams supporting the wires. Zhang *et al.* (2016) also used information from the MLS trajectory to extract significant data from it. They apply self-adaptive region growing methods to extract power lines, and PCA combined with information entropy theory method to detect junctions.

A different concept is presented by Guo *et al.* (2016). Working with ALS point clouds, they presented a method for power line reconstruction, analysing the distribution properties of power-lines for helping the RANSAC algorithms in the wires' reconstruction (Figure 8a). Using both laser scanning and imaging data, Fu, Chang and Liu (2018) automatically extracted the geometric parameters of the aerial power line without manual aiming. This could later be used as input information for the 3D modelling of the power line infrastructure.

The unsupervised classification of points is still under development. Like in any other field, for the railway network there is not a standard to follow when developing and applying these algorithms. Since the distribution of the electrification system in the space is quite regular, Jung *et al.* (2016) proposed a classifier based on CRF. It takes into account both short and long range homogeneity of the cloud. For locally classifying points, SVM are used and ten target classes are obtained, representing overhead wires, movable brackets and poles, as shown in Figure 8b. Wang *et al.* (2018) presented also a power line classification method for detecting power line points and the power line corridor direction. They have based their investigation on the Hough transform, connectivity analyses and simplification algorithms.

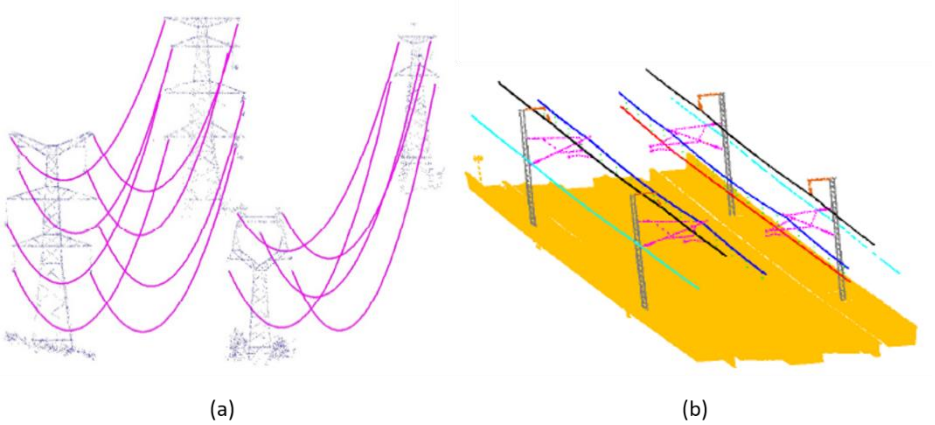

Figure 8: Power line. (a) Guo *et al.* (2016) classified ALS point clouds into power line cables using a JointBoost classifier and then used RANSAC to reconstruct the cables' shape . (b) Jung *et al.* (2016) grouped points in MLS data using SVM classification results as inputs for the multi-range CRF model

2.2.2.4 Signalization

Although the detection and classification of signals has been deeply and successfully developed in the roadway network (Section 2.2.1.2), not so much in the railway field. Presumably, the same techniques can be used for detecting rail signage. As will be presented in 2020 by Karagiannis, Olsen and Pedersen (2020), methods for detecting railway signs working with RGB or video images are being developed. They use image processing techniques and features extraction (Marmo, Lombardi and Gagliardi, 2008; Agudo *et al.*, 2016) to locate the signage. Beyond these state-of-the-art results, they have implemented the Faster R-CNN (Convolutional Neural Network for object detection) for sign detection also in RGB images (Figure 9).

Figure 9: Signalization. Karagiannis, Olsen and Pedersen (2020) implemented a R-CNN for sign detection using RGB images

2.2.2.5 Inspection

In the railway environment, as in many other fields, inspections should be carried out using non-destructive techniques (NDT). These do not intervene with the structural condition of the elements being inspected, and allow to repeat the tests as many times as necessary without causing any damage. Nowadays, different techniques are used, as presented in (Falamarzi, Moridpour and Nazem, 2019). Falamarzi, Moridpour and Nazem (2019) made a review concerning the main sensors and techniques used in the railway environment to detect damage. Some sensors categorized as NDT are ultrasonic testing (UT), eddy current (EC), magnetic flux leakage (MFL), acoustic emission (AE), electromagnetic acoustic transducers (EMATs), alternate current field measurement (ACFM), radiography, microphone and thermal sensors, among others. These detect defects from the surface to the internal part of the element being studied. High resolution and thermographic cameras are also good examples of NDT. They are widely used when performing visual inspections and applying image processing techniques for damage detection (Minbashi *et al.*, 2016; Falamarzi, Moridpour and Nazem, 2019). Although, laser scanning is also a non-destructive technology that may be used for damage detection, there is not a defined technique for the inspection of the railway network.

The most common inspection developed in railway's point clouds is the inspection of rail tracks and gauge clearance between them and the power line. In 2004, Blug *et al.* (2004) had already developed a method for using laser scanning data from the CPS 201 scanner for clearance measurements. Years later, Mikrut *et al.* (2016) determined the clearance gauge using MLS point clouds applying the 2D contours method. They use cross sections of the point clouds to create a 2D image and an operator reviews them to obtain suspicious areas. When using TLS data, Collin, Carreaud and Lançon (2016) proposed the use of the Infra-Red information in order to extract distortions. They compared information from different campaigns and then visually extract cracks, wear seepages and humid areas, among others. Continuing with this and together with points' classification, Niina *et al.* (2018) performed a clearance check after the automatic extraction of rails matching their shape with and ideal rail head using the iterative closest point (ICP) algorithm (Besl and McKay, 1992). The objects inside the clearance and related to a contact line are detected by visual confirmation, as explained in Figure 10a.

Concerning rails inspection, Chen *et al.* (2017) developed a methodology for comparing laser scanning data with a point cloud reconstructed from CAD models, in order to measure the existing rail wear. In relation with this part of the infrastructure, the railway ballast is also an important asset to take into account. The recent work from Sadeghi *et al.* (2019) showed a method for the development of a geometry index for ballast inspection using automated measurement systems (Figure 10b).

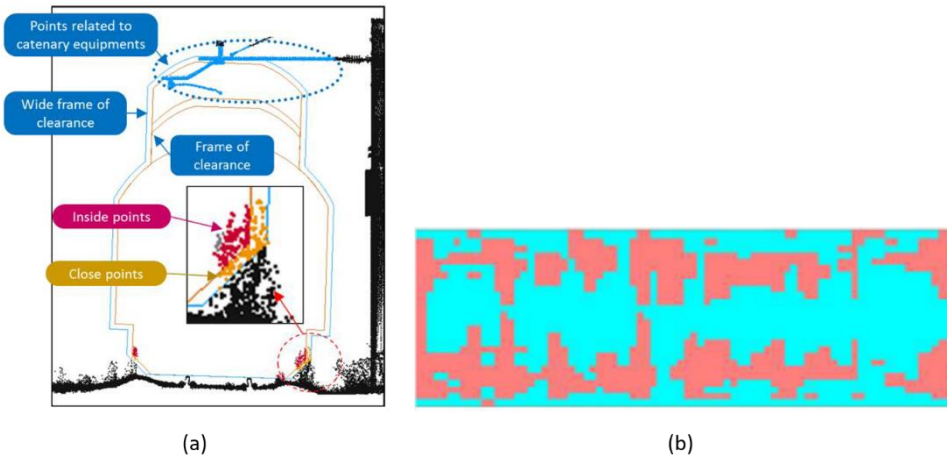

Figure 10: Inspection. (a) Niina *et al.* (2018) extracted the rails' top head in order visually inspect the clearance gauge. (b) Sadeghi *et al.* (2019) performed a ballast inspection based on a geometry index developed to this respect

In the railway environment, as in many other fields, inspections should be carried out using non-destructive techniques (NDT). These do not intervene with the structural condition of the elements being inspected, and allow to repeat the tests as many times as necessary without causing any damage. Nowadays, different techniques are used, as presented in (Falamarzi, Moridpour and Nazem, 2019). Falamarzi et al. made a review concerning the main sensors and techniques used in the railway environment to detect damage. Some sensors categorized as NDT

are Ultrasonic Testing (UT), Eddy Current (EC), Magnetic Flux Leakage (MFL), Acoustic Emission (AE), Electro Magnetic Acoustic Transducers (EMATs), Alternate Current Field Measurement (ACFM), radiography, microphone and thermal sensors, among others. These detect defects from the surface to the internal part of the element being studied. High resolution and thermographic cameras are also good examples of NDT. They are widely used when performing visual inspections or applying image processing techniques for damage detection (Minbashi *et al.*, 2016; Falamarzi, Moridpour and Nazem, 2019). Although laser scanning is also a non-destructive technology that may be used for damage detection, there is not a defined technique for the inspection of the railway network.

The most common inspection developed in railway's point clouds is the inspection of rail tracks and gauge clearance between them and the power line. Blug *et al.* (2004) had already developed a method for using laser scanning data from the CPS 201 scanner for clearance measurements. Years later, Mikrut *et al.* (2016) determined the clearance gauge using MLS point clouds applying the 2D contours method. They use cross sections of the point clouds to create a 2D image and an operator reviews them to obtain suspicious areas. When using TLS data, Collin, Carreaud and Lançon (2016) proposed the use of the IR information in order to extract distortions. They compared information from different campaigns and then visually extract cracks, wear seepages and humid areas, among others. Continuing with this and together with points' classification, Niina *et al.* (2018) performed a clearance check after the automatic extraction of rails matching their shape with and ideal rail head using the Iterative Closest Point (ICP) algorithm (Besl and McKay, 1992). The objects inside the clearance and related to a contact line are detected by visual confirmation.

Concerning rails inspection, Chen *et al.* (2017) developed a methodology for comparing laser scanning data with a point cloud reconstructed from CAD models, in order to measure the existing rail wear. In relation with this part of the infrastructure, the railway ballast is also an important asset to take into account. The recent work from Sadeghi *et al.* (2019) showed a method for the development of a geometry index using automated measurement systems.

3. Remote Monitoring Technologies/Systems

3.1 Satellite monitoring technologies

3.1.1 Radar satellites

Synthetic Aperture Radar (SAR) satellites provide continuous all-weather, day-and-night worldwide imagery with high revisiting time acquired in a double orbit, ascending and descending. An InSAR system measures the phase difference between synthetic aperture radar (SAR) echoes backscattered from targets on the ground and received by two antennae located at slightly different positions (with a relative distance known as the spatial baseline). Through the processing of a time series of SAR images with Multi-Temporal Interferometry (MTI) algorithms, it is possible to measure the millimetre displacements of ground targets called persistent scatterers – PS or Distributed Scatterers- DS that correspond to human-made objects (buildings and other engineered structures like roads and railways) and rock outcrops measuring the distance between the satellite and the objects itself with millimetre precision. These elements are characterized by the coherent backscattering of the phase signal in time. MTI algorithms make a distinction between Persistent Scatterers (PS) associated with a single pixel of the radar image and the Distributed Scatterers (DS) that are associated with a group of statistically homogenous pixels of the radar image.

In short, the PS and the DS represent points (PS) or areas (DS) with high phase stability (or equivalently high coherence) of the signal reflected by the target objects on the ground, thanks to which it is possible to monitor a zone (in which they are present) even for a long period of time according to the availability of the images.

To make distance measurements between the satellite sensor and the target on the ground, phase difference images (interferograms) are generated by exploiting radar images acquired over the same area during successive satellite passes.

SAR acquisitions are in fact shifted over time and knowing a priori the topography, the ground and infrastructure displacements are measured with millimetre precision. When a series of SAR acquisitions is available over the area of interest, the MTI algorithms combine them into several differential interferograms.

MTI is only little affected by bad weather and can provide long-term (years), regular (weekly-monthly), precise (mm) measurements of ground and infrastructures displacements over large areas (thousands of km^2) obtaining spatially dense PS/DS (from hundreds to thousands measured points per km^2).

The standard output of a MTI application is typically provided as radar targets (PS/DS) positions (lat., long., height) and their average yearly displacement rates overlapped to a map or optical image.

The strengths of MTI include:

-the wide area coverage (regional-global) combined with high spatial resolution (meters) and excellent precision (mm-cm) in the measurement of the displacement;

-the provision of regular, long term (years) and frequent (weeks/days) information thanks to the availability of the radar acquisitions, some of which (e.g. ESA's data) are now free of charge.

Thus, MTI extends the applicability of radar interferometry to monitor the ground and infrastructure stability from regional to local scale.

The displacements are measured along the satellite line of sight (LOS), with incidence angles being between 20-50° and with the current satellites operating on polar orbits, mainly two independent measurements on opposite pass directions (ascending or descending) are possible with interferometry techniques, limiting the displacement vector measurement to the plane orthogonal to the south–north directionand it is also nearly impossible to retrieve movements in the satellite flight direction (azimuth), which is approximately north-south. Neverthless by combining LOS displacements from ascending and descending CSK datasets, it is possible to derive horizontal and vertical displacement maps.

Nowadays, several satellite missions are available, providing interferometric SAR data at different wavelengths, spatial resolutions, and revisit times. In Table 10 (see Appendix), the principal satellite missions are listed with those parameters which are relevant for the ground and infrastructures monitoring.

3.1.2 Performance of radar monitoring

The SAR satellite parameters, which impact on the quality of the MTI products, are the wavelength of the SAR signal (decreasing from L, ~23 cm, to C, ~5.5 cm, to X band, ~3.1 cm), the revisit time, the spatial resolution, and the orbital tube. The main figures that allow to select the optimal SAR sensor to be used for the ground and infrastructure monitoring are: the number of measurable coherent targets (CT) on the grounds (e.g. the PS/DS density), the maximum detectable displacement velocity, the revisiting time and a reliable and constant image acquisition plan.

The density of detectable targets depends heavily on the ground cover, being in general highest over urban areas, thanks to the abundance of artificial structures with coherent backscattering. Both wavelength and spatial resolution can impact on the CT density. Several studies have proven that high-resolution data from CSK, TSX, and RSAT2 lead to a significant increase in the number of potential CT with respect to the data from medium resolution missions, such as ERS1/2, ENV, and RSAT1. There is limited information in the literature on the PS densities obtainable from L-band MTI, due to the few datasets available over Europe and suitable for MTI.

Commercial high-resolution X-Band SAR sensors, such as the COSMO-SkyMed (CSK) and TerraSAR-X (TSX) constellations, acquire data with spatial resolution reaching metric values, and provide revisit times of up to a few days leading to an increase in the density of the measurable targets, as well as to improvements in the detection of nonlinear displacements.

Medium resolution C-band SAR data have been thoroughly exploited for the ground displacement monitoring in the last two decades, thanks to the ERS-1/2 and ENVISAT-ASAR (ENV) missions, and RADARSAT-1/2 (RSAT1/2).

Considering the Sentinel-1 sensor that will be used in this project, the ground deformation is measured with a precision of 1.5 mm/year along the satellite's line of sight. Horizontal localization of PS is provided with a precision of ± 10 m. The accuracy of the measures are guaranteed by a high level of error compensation of the MTI that allows the generation of time series analysis highlighting displacement trends over time. The major sources of errors for the MTI are the atmospheric disturbance and the topography influence that are removed using 25 or more multitemporal SAR images.

Optical satellites

In Figure 11, the principal satellite missions with main performances are listed with those parameters which are relevant for the ground and infrastructures monitoring.

Year of launch	Satellite	Sensor on-board	Spatial resolution	Temporal resolution (revisit time)	Spectral range
2011	Pleiades-1A	VHR	50 cm–2 m	1 day	0.48–0.95 μm
2011	ResourceSat2	LISS-3&LISS-4	LISS-3: 56 m; LISS-4: 5.8 m	24 days	0.52–0.86 μm
2012	SPOT-6	New AstroSat Optical Modular Instrument (NAOMI)	2.2–8.8 m	1–5 days	0.45–0.89 μm
2012	Pleiades-1B	VHR	50 cm–2 m	1 day	0.48–0.95 μm
2012	KOMPSAT-3	Advanced Earth Imaging Sensor-AEISS	0.7–2.8 m	28 days	0.45–0.9 μm
2013	Landsat-8/LDCM	OLI, TIRS	15–30 m	16 days	0.43–12.51 μm
2013	Skysat-1	Skybox Image Sensor	0.9–2 m	1.8 per day	0.45–0.9 μm
2014	Skysat-2	Skybox Image Sensor	0.9–2 m	1.8 per day	0.45–0.9 μm
2014	SPOT-7	NAOMI	2.2–8.8 m	1–5 days	0.45–0.89 μm
2014	WorldView-3	WV-3	~0.3 m	1–4.5 days	0.45–2.245 μm
2015	KOMPSAT-3A	AEISS	0.7–2.8 m	28 days	0.45–0.9 μm
2015	Sentinel-2A	MultiSpectral Instrument (MSI)	10–60 m	10 days	0.443–2.19 μm

Figure 11: Some of the main optical sensors available in the last years

3.2 Terrestrial monitoring technologies

Laser scanner is a survey and monitoring technology based on obtaining measurements of distance between a LiDAR sensor and its surroundings, that is, every object detected by the laser beams emitted by the sensor. The result of this process is a dataset in the form of a point cloud containing the position of every detection point on those objects relative to the sensor. To further reference point positions in a global frame, other positioning sensors can be included into the laser scanner platform, either if this is static or mobile. The contribution of each component of the platform to the data acquisition process is explained through this section.

3.2.1 Laser Scanner system components

In order to determine the position of the points of the cloud acquired with a laser scanner at a global level, it is necessary to reference them within an appropriate coordinate system. First, the points are referenced to the local coordinate system of the LiDAR. Then, the location of the platform in a global coordinate system, for instance WGS84, is determined using navigation and positioning systems (Tao,

2000). Finally, the relative position and orientation of the LiDAR in the platform with regard to the navigation and positioning system is determined for the correct geo-referencing of the point cloud. This distance between the centre of the navigation system and the centre of other systems is known as lever arm or offset.

3.2.1.1 LiDAR

LiDAR (Light Detection And Ranging) technology is based on illuminating points of objects surrounding the scanner with a laser beam. The backscattered laser light is collected with a receiver and the distance to the point is calculated using one of the techniques explained later in this section. In order to correctly do so, the light returned by the object must be within the FoV (Field of View) of the receiver. Therefore, both the receiver and the emitter must be mounted and have apertures such that they share the same optical path (Wehr and Lohr, 1999). In the cited article, it is also described the Instantaneous Field of View (IFoV) as the narrow divergence of the laser beam, whose physical limit is determined by divergence of light. Due to this factor, the IFoV of the receiver must be bigger than that of the emitter. Photodiodes are used as receivers, recording the backscattered signal and deriving the ranging distance between the scanner and the target object as well as the remaining power of the signal, designated as intensity (Wujanz *et al.*, 2017). PIN and APD (Avalanche Photo-Diode) are usually employed for this task, although there are other types of photo-detectors, like PMT (Photomultiplier Tube) (Kashani *et al.*, 2015).

Two range measurement techniques are used by laser scanners: Time-of-Flight (ToF) and Continuous Wave (CW) modulation. For Time-of-Flight (or pulse ranging), the distance between the laser emitter and the scanned object is calculated based on the time that it takes to the laser beam since it is emitted until the backscattered pulse is received. Ranging resolution achieved by this type of scanner is directly proportional to time counter resolution, with a maximum range that is determined, primarily, by the time counter maximum measurable time interval and the laser energy losses during flight. In a CW scanner (also known as phase difference ranging), a continuous signal is emitted, and its travel time can be inferred considering the phase difference between the emitted and the received signal and the period of that signal. The range resolution in this case is directly proportional to the phase difference resolution. It also depends on the signal's frequency; an increasing frequency reduces the minimum range interval that can be measured, so the resolution is higher. The maximum range (maximum measurable range (Wehr and Lohr, 1999)) is determined by the maximum measurable phase difference, equal to 360º (2π radians).

To express the position of the points obtained during a scan in a local coordinate system, laser scanners use opto-mechanical assemblies with two rotating mirrors that head the laser beam, measuring their rotation speeds. Combining these two angular measurements with ranging data, it is possible to express the location of the point in a spherical coordinate system (Armesto-González *et al.*, 2010). Another point-cloud acquisition method, slightly varying compared to the explained above, is that used by some Velodyne laser scanners models. These scanners use a column of laser diodes (from 16 to 128, depending on the model) that covers a Vertical Field of View of up to 40° pitch angle. This column rotates around the central axis of the scanner, determining the angle with a rotation

encoder and producing rings of point range measurements for each one of the diodes (Moosmann and Stiller, 2011). Both methodologies are employed by 3D scanners, but it is possible to obtain a 3D representation of a scene using a 2D scanner too. In such case, the 2D scans are combined with data of the path followed by the vehicle during the surveying process, monitored with a GPS/INS/odometer navigation system. This solution is presented in Abuhadrous *et al.* (2016) as a cheaper alternative to 3D systems, and it is demonstrated that it allows for the identification and segmentation of urban scene features (road, building fronts and trees).

In addition to geometric measurements of a scene, laser scanner can provide further information. Intensity data of the backscattered light, for instance, provides information about the surface of scanned objects (Kashani *et al.*, 2015). It is calculated based to the amplitude of the returned signal and depends primarily on the surficial properties of the object that reflects the laser pulse. The main superficial properties affecting how the laser pulse is backscattered are reflectance and roughness. Armesto-González *et al.* (2010) a method for the detection of damage on the surface of historical buildings (e.g. superficial detachment and black crust development) based on intensity data provided by laser scanners is presented.

Some laser scanner systems are able to record several echoes produced by the same emitted laser pulse when its path is interrupted by more than one target. According to Wagner et al., the number and timing of the recorded trigger-pulses are critically dependent on the employed detection algorithms (Wagner *et al.*, 2004). Thus, the optimal solution would be to record the full-waveform, as it is formed by the sum of all echoes produced by distinct targets within the travel path of the laser pulse (Wagner *et al.*, 2006).

Bathymetric laser systems are also a representative case of additional features provided by laser technology. The energy received by the sensors of these systems is divided in two parts: the energy reflected by the surface of the water and the energy that crossed it (Hickman and Hogg, 1969). Kashani *et al.* (2015) indicated that the power of the returned pulse decays exponentially with water depth. The relation between decrease of returned energy and water depth is described by an attenuation coefficient, which is diffuse as it is in turn related to an absorption coefficient and a backward scattering coefficient.

3.2.1.2 Positioning and navigation systems

The components or subsystems of the positioning and navigation system can be classified in two different groups. The first group is for systems with exteroceptive perception, meaning that they provide position and orientation with respect to a reference frame (Kais *et al.*, 2005). GNSS (Global Navigation Satellite System) belongs to this group. The second one is for those systems having proprioceptive perception and providing time derivative information of the position and orientation of the mobile. In this case, an initial state of the system must be defined, and subsequent states are calculated upon it. This group includes INS (Inertial Navigation System) and DMI (Distance Measurement Unit).

- GNSS is a technology for positioning and navigation that uses a constellation of satellites as a reference. In such systems, position is estimated based on

the distances between a receiver and the set of satellites, calculating them by estimating the propagation time that transmitted signals take from each satellite to the receiver (Closas, Fernández-Prades and Fernández-Rubio, 2009). The most widespread GNSS technology is the GPS, operated by the US Air Force. It is capable of providing precise position and time, traceable to global time standards (Dana, 1997). The broadest UTC (Universal Time Coordinated) time dissemination is, in fact, provided by GNSS (Petit, Arias and Panfilo, 2015). GNSS are employed for geo-referencing of the data in both static and mobile laser scanner platforms.

Receivers of a GNSS can be adapted to various operational modes, fundamentally DGPS (Differential GPS), RTK (Real-Time Kinematic) and PPK (Post-Processed Kinematic) (I. Puente, González-Jorge, Martínez-Sánchez, *et al.*, 2013). DGPS and RTK are similar, but there are some differences between them. The first one is the type of receivers used: single-frequency for DGPS and dual-frequency for RPK. The minimum number of satellite signals needed by DGPS is 3, while RPK mode needs at least 4, and 5 during initialization. This process takes around one minute, operating in RTK, but it is immediate in DGPS. However, an advantage of RPK over DGPS is the achieved accuracy, of just a few centimetres, while DGPS is only capable of reaching sub-meter accuracy, although it needs at least 4 satellite signals in that case. Lastly, in PPK mode, position data are stored for later correction using a reference station. The advantages offered by this mode are higher accuracy (usually) and absence of data latency, signal obstruction or coverage problems.

Some of the drawbacks of GNSS technology are outages, multipath propagation and dilution of precision. An outage occurs when the visual line between the satellites and the GNSS receiver is blocked (e.g. when vehicle enters a tunnel or, in general, when the receiver is placed in interiors). The signal is then interrupted and positioning is not possible. Because of this, systems relying on GNSS use additional navigation and positioning systems for assistance. Multipath is another main source of error for GNSS navigation systems (Closas, Fernández-Prades and Fernández-Rubio, 2009) caused by tall obstacles, like buildings and trees (Ma *et al.*, 2018). Part of the emitted energy bounces against these obstacles before going back to the receiver, so the measured ToF corresponds to a distance longer than intended. Finally, the geometrical disposition of the emitter and the transmitters (e.g. position of the satellites of a GNSS constellation relative to the receiver to be positioned) also affect the position estimation uncertainty, an issue that is known as dilution of precision (Langley, 1999).

- INS use internal accelerometers and gyroscopes to calculate the position and attitude (tilt and heading) of a mobile laser scanner platform by the dead reckoning technique. These sensors measure displacement vectors of the system in a recursive manner to determine its situation (Kao, 2010). The error from every calculation step is accumulated, so accuracy in the position estimation increasingly degrades. Accelerometers calculate the acceleration of the system in Cartesian axes, and then it is integrated into velocity and subsequently into position (Advanced Navigation, 2017). Both the measurement and integration processes introduce certain noise in the results and it increases exponentially over time, which is consistent with the previous

statement about dead reckoning operation. Gyroscopes measure the angular velocity of the system, so its attitude can be evaluated. If the system is moving in a horizontal plane (e.g. a vehicle on a road) the angular speeds are proportional to the system heading. There are various types of gyroscopes: mechanical, micro-electromechanical (MEMS) (Seshia, Howe and Montaguet, 2002) and optical, which in turn are either Ring Laser Gyroscopes (RLG) or Fiber Optic Gyroscopes (FOG), according to their operating principles (Kavanagh, 2007).

- A DMI can be included as well to obtain additional information in the case of using a mobile platform, and to contrast and complete the one provided by GNSS and INS systems. This device calculates travelling distances as a function of wheel rotation (Kao, 2010). Similar to the INS case, it tends to drift, because its functioning is also based on dead reckoning. Additionally, the difference between distance measurements obtained from the left and right wheels is proportional to the relative heading of the mobile (if the difference is small) so a differential DMI is capable of estimating heading.

Combination of GNSS long-term accuracy and INS (as well as DMI) short-term accuracy makes it possible to improve position and velocity estimations. To integrate the data gathered by these components and estimate position and attitude of the system, a Kalman filter is applied. This filter consists on a set of mathematical equations and provides an efficient computational (recursive) solution of least-square method to the discrete-data linear filtering problem (Welch, Bishop and Hill, 1995). It was introduced in 1960 by R.E. Kalman and supports estimations of past, present and even future states.

3.2.2 Performance of laser scanning systems

There are various factors regarding the quality of the point-cloud data acquired by a laser scanner. In Yoo *et al.* (2010), a methodology for establishing comparative analysis was developed, being valid for both static and mobile systems. The factors evaluated according to this methodology are accuracy (and precision), resolution and completeness of the data.

- *Accuracy* decreases with the scanning distance, as the footprint area of the laser beam (i.e. the area illuminated by the beam) increases with the range (Wagner *et al.*, 2006). Regarding differences between ranging measurement principles, and according to (Wehr and Lohr, 1999), pulse ranging accuracy is influenced by pulse length or rise time. Phase difference ranging depends on laser signal wavelength. Furthermore, ranging accuracy is inversely proportional to signal-to-noise ratio, a function of the power of the received signal, input bandwidth, the signal receiver sensitivity and other parameters. Also, when Pulse Repetition Frequency (PRF) increases, the laser pulse energy decreases and the resulting beam is wider, so standard deviation grows (Chasmer *et al.*, 2006).
- *Resolution* of a system is related to the density and homogeneity of the point cloud. Point density is defined as the number of neighbour points whose distance is inferior to a reference distance from each reference point (Yoo *et al.*, 2010), calculating the mean density as the mean of all point densities. Point density decreases with distance, when the angle between an emitted

laser beam and the next one (i.e. angular resolution) is kept constant, depending on the angular speed of the rotating mirror (opto-mechanical system) or the number of diodes in a column (laser array system). Homogeneity of the point cloud indicates how homogeneous is the distribution of points in the cloud. Generally, ranging allows to reach higher ranges, while phase difference ranging offers higher resolution.

- *Completeness* of the acquired data is affected by nonvisible zones, areas that are out of the scanner FoV. Nevertheless, information about the scanned scene may be missed too because of shadow zones. These are areas occluded due to any object in the line of sight of the scanner that would hinder capturing the point clouds of an object of interest (Kiziltas *et al.*, 2008).

Additional factors related to laser scanner performance are reflectivity, which can lead to measurement errors on objects with reflective surfaces; and scanner warm-up, which is a necessary step before starting data collection or drifting out of calibration (Kiziltas *et al.*, 2008). Correct positioning and geo-referencing of points of the cloud is influenced as well by the accuracy achieved by the navigation system, as well as the accuracy of the lever arms measurements.

3.2.2.1 Comparison of monitoring technologies

Laser scanning technology has certain characteristics that make it more suitable for some tasks than other MMS technology. For instance, in the case of defect detection or alignment tasks (Golparvar-Fard *et al.*, 2011), more accurate measurements are possible with laser scanner compared to image-based solutions. It has also been proved to be suitable for 3D displacement measurement of particular points of a structure and to obtain its static deformed shape better than with Linear Variable Displacement Gauges (LVDTs), electric strain gauges and fibre optic sensors (Park *et al.*, 2007). Moreover, it has the advantage that no direct contact is needed.

The mentioned MMS technologies have however certain advantages over laser scanner. Image-based 3D reconstruction equipment has a lower cost, higher portability and allows a fast data acquisition process. Image-based 3D reconstruction is based on triangulation, by which "a target point in space is reconstructed from two mathematically converging lines from two-dimensional (2D) locations of the target point in different images" (Dai *et al.*, 2012). Thus, it is necessary to take images from different perspectives of the object. This could be considered a drawback when comparing with laser scanning, as the later obtains directly a 3D point cloud with one single setup (Ingensand, 2006), but there are already existing systems like the Biris camera that are capable of simultaneously obtaining two images on the same CCD camera (Beraldin *et al.*, 2000). Another advantage of images is the "visual value in understanding large amounts of information" (Golparvar-Fard, Peña-Mora and Savarese, 2009). In the cited study, daily progress images of a construction site are used to produce a 3D geometric representation of the site over time ("4D model").

Nevertheless, and in addition to the aforementioned higher accuracy reached by laser scanners, these systems are not dependent on the illumination, as it is the case for cameras. However, imaged-based and laser scanning technologies can be combined to obtain a richly detailed representation of a scene by fusion of the

acquired datasets. For example, in (Zhu *et al.*, 2011) MLS point clouds were used for geometric reconstruction of buildings and classification of the scanned points, while images of the buildings served for photorealistic texture mapping.

3.2.3 Types of laser scanner systems

There are, basically, three types of laser scanner system arrangements, namely TLS (Terrestrial Laser Scanner), ALS (Aerial Laser Scanner) and MLS (Mobile Laser Scanner). This classification is based on the platform type that is employed to install the system. In this section, each type of laser scanner is detailed.

TLS are stationary systems, typically consisting on a LiDAR device mounted on a tripod or other type of stand, capable of obtaining high-resolution scans of complex environments, but with data acquisition times in the order of minutes for a single scan (Olsen *et al.*, 2010). In the case of ALS, the laser scanner is installed on an aircraft (typically an airplane) combining the periodical oscillation of the laser emitting direction with the forward movement of the aircraft to obtain a dense point-cloud. Due to the small scanning footprint achieved by the laser, spatial resolution is higher than that provided by a radar (Kobler *et al.*, 2007). ALS is employed, for instance, to obtain virtual city models or Digital Terrain Models (DTM). Finally, an MLS is defined as a "vehicle-mounted mobile mapping system that is integrated with multiple on-board sensors, including light detection and ranging (LiDAR) sensors" (Ma *et al.*, 2018). MLS allows for safer inspection routines, as operators can execute their job from the interior of the vehicle, instead of manually moving and placing the equipment as in the TLS case. This is translated in a faster and safer data acquisition process. At the same time, MLS still allows for production of dense point clouds. However, data processing methods used in stationary terrestrial or airborne laser scanning cannot be directly applied in some cases to MLS, due to differences in how the data is acquired, mainly the geometry of the scanning and point density (Jaakkola *et al.*, 2008). Another benefit of MLS is the capability to capture discrete objects from various angles, or to be merged with images of the same scene to add more information to the data (I. Puente, González-Jorge, Martínez-Sánchez, *et al.*, 2013). The combination of laser scanner and image-based data is commented later in this document.

A Mobile Laser Scanner system can be adapted to various configurations, depending on the specific requirements of a certain survey process or where the scanning is going to take place. In (Kukko *et al.*, 2012), the most usual configurations for MLS (in this particular case, for a ROAMER single-scanner Mobile Mapping System using a FARO Photon 120 scanner) are detailed. The most broadly used is the vehicle configuration. This offers a fast surveying method, being possible to scan urban areas at normal traffic speed. To obtain road surface points, the scanner is adapted to a tilted position, which also produces scans that provide more information about the objects along the track direction than vertical scanning (Kukko *et al.*, 2012) as narrow structures along the survey path are hit multiple times by sequential scans, and vertical and horizontal edges are captured with equal angular resolution. Automated procedures for structure recognition can be applied on MLS point clouds, such as the introduced in (Pu *et al.*, 2011) for ground and scene objects segmentation.

Another option is to install the equipment on top of a trolley for applications that are not suitable for a vehicle. In the ROAMER case (Kukko *et al.*, 2012) , this configuration was adopted to obtain a pedestrian point of view and point cloud data detailed enough to be used for personal navigation applications. When a certain scenario restricts the use of other solutions due to irregular terrain, difficult access, etc., a valid alternative is to use a backpack configuration, like the Akhka solution introduced in (Kukko *et al.*, 2012). This solution was proved as a low-cost, compact and versatile alternative for Mobile Mapping Systems by (Ellum and El-sheimy, 2000), although in this case the employed mapping sensor was a megapixel digital camera instead of a laser scanner. Kukko et al. also presented a MLS installed on a boat to obtain river topographical data.

3.2.3.1 Comparison of commercial laser scanners

There are numerous laser scanners currently available in the market, offering different characteristics in terms of performance and possible applications. Regarding MLS, the most notable features to establish a comparison between models are the maximum acquisition range, accuracy and data acquisition rate. The specifications of representative models used for MLS platforms from the main laser scanner manufacturers are detailed in Table 5. In Figure 12, those models are displayed.

Table 5: Comparison of different commercial laser scanners

Manufacturer	RIEGL	Teledyne Optech	FARO	SICK	Velodyne
LiDAR Model	VUX-1HA	Lynx HS300	Focus 350	LMS511	Alpha Puck
Measurement principle	ToF	ToF	Phase difference	ToF	ToF
Minimum range	1.2 m		0.6 m		
Maximum range	420 m @ 300 kHz	250 m	350 m	80 m	300 m
Range accuracy	5 mm		0.30 mm @ 25 m		Up to 3 cm
Range precision	3 mm	5 mm			
PRF (Pulse Repetition Frequency)	300 –1000 kHz	75 – 800 kHz	122 – 976 kHz		2400 kHz
Scan frequency	10 – 250 Hz	300 Hz	97 Hz (V)	25 – 100 Hz	
Laser wavelength	Near infrared		1550 nm	905 nm	903 nm
Field of View	360º	360º	300º (V) 360º (H)	190º	40º (V) 360º (H)
Angular resolution	0.001º		0.01º	0.167º	0.11º (V) 0.1 - 0.4º (H)

Figure 12: Commercial laser scanners: (a) RIEGL VUX-1HA; (b) Optech Lynx HS300; (c) FARO Focus 350; (d) SICK LMS511; (e) Velodyne Alpha Puck

4. SAFEWAY Pilots and end-user needs for Remote Monitoring

This section describes the different Pilot areas where data is going to be acquired for the upcoming activities of WP3: Pilot 1 (Portugal, *Infrastructures of Portugal – IP* -), Pilot 2 (Spain, *Ferrovial*) and Pilot 3 (United Kingdom, *Network Rail – NR*-). The most relevant information needed for the definition of scenarios is shown for each Pilot (most relevant adverse events and assets as well as the main strategic lines for evaluating the scenarios). Definitions for the groups of critical assets that are considered in this section can be seen in Table 6. Other key concepts (Pilot, demonstration site, scenario, adverse event) can be found in the Glossary.

Table 6: General groups of critical assets

Asset	Short definition
Bridge	Infrastructure built over a water course so that road or rail traffic can cross from one side of it to the other. This comprises all types of bridges available in the transport network of study (e.g.: Overline, underline, masonry arch, girder, etc.).
Culvert	Draining element under a roadway, railway or similar.
Embankment	Wall of soil used to raise a terrain level facilitating the pass of a road or to contain a flooding area.
Pavement	Asphalted path for road traffic.
Retaining wall	Rigid walls used for the soil's lateral support.
Track	Group of two parallel rails passed by the train.
Tunnel	Underground passageway built for road or rail traffic.
Viaduct	Infrastructure built over a valley so that road or rail traffic can cross from one side of it to the other.

For each Pilot, the information shared by end-users in terms of inspection procedures and remote monitoring needs is organized in a number of tables that summarize the capabilities of the technologies defined in Section 2 and Section 3. A summary of that information is shown in Table 11. It is based on the inspection

needs of Network Rail, although it can be extrapolated to all the Pilots of the project.

In Table 11 (see Appendix), for every asset considered (left column), the technologies with a potential usefulness are remarked (middle column), and a general description of the information that can be measured is presented (right column). The available technologies are presented using the following acronyms:

- RS (Radar Satellites)
- OS (Optical Satellites)
- LS (Laser Scanning, including Terrestrial Laser Scanning, Mobile Laser Scanning, and Aerial Laser Scanning)
- TLS (Terrestrial Laser Scanning)
- MLS (Mobile Laser Scanning)
- ALS (Aerial Laser Scanning)
- PHTGRM (Photogrammetry)
- THRMGR (Thermography)

Other relevant remarks for the understanding of **¡Error! No se encuentra el origen de la referencia.**:

- Whenever the usage of a certain technology is unlikely to lead to fully automated processes regarding the extraction of information, a '~Semi' note is added to the technology acronym.
- Whenever the extraction of information is unlikely or uncertain when using the proposed technologies, it is also remarked (as 'Uncertain').

Table 13-Table 21 in the Appendix (which have been elaborated for each Pilot and will be mentioned throughout this section) specify, for each technology, to which extent it is possible to detect or extract information from different assets, using the legend in Table 12 (see Appendix).

4.1 Pilot 1: Portugal

The first Pilot will take place in Portugal in two demonstration sites: one in the region of Santarém (Demonstration Site 1.A, Figure 13) and another in Leiría (Demonstration Site 1.B, Figure 14). They include both railway and road sections of the Atlantic corridor.

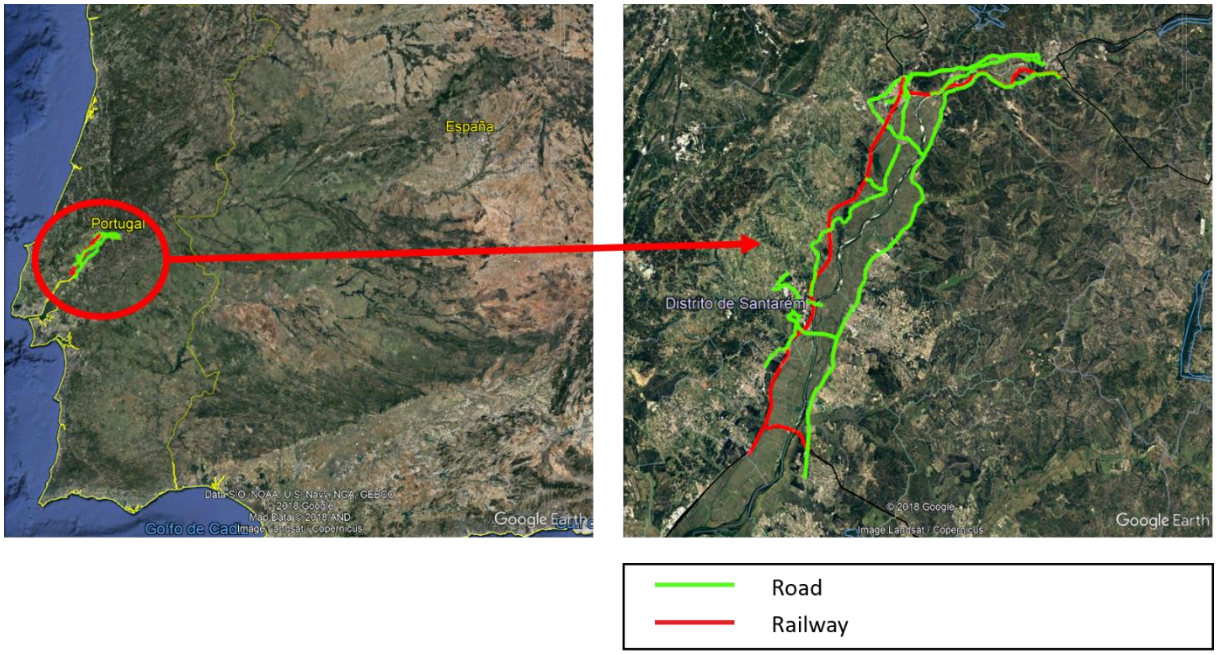

Figure 13: Demonstration Site 1.A: Santarém (Source: Data provided by *Infraestruturas de Portugal* on Google Earth)

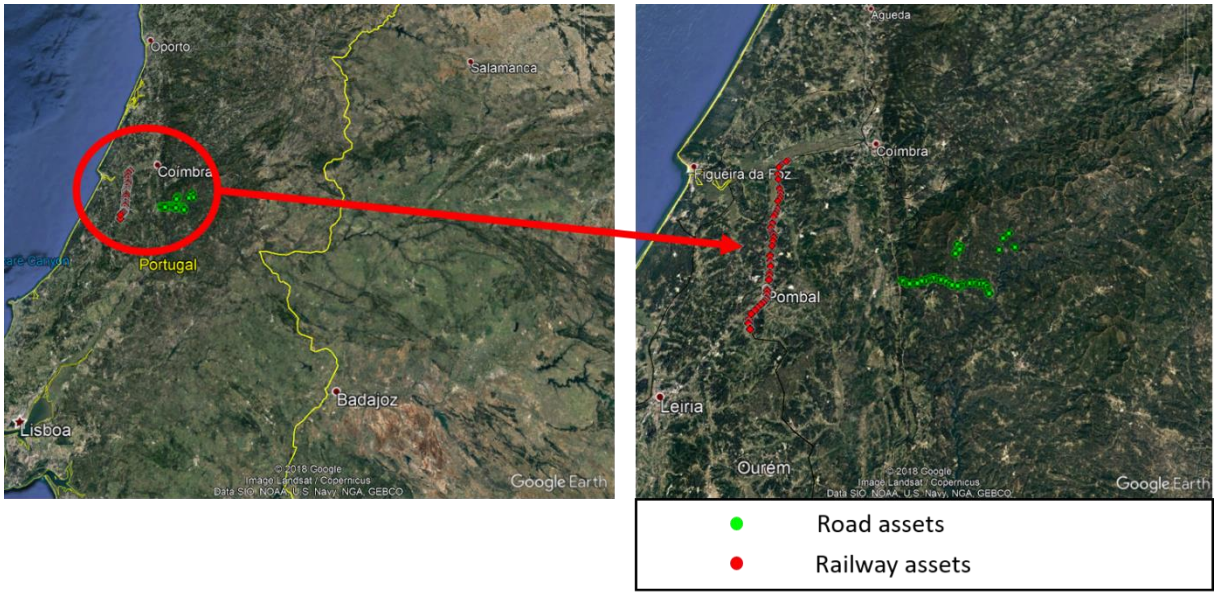

Figure 14: Demonstration Site 1.B: Leiría (Source: Source: Data provided by *Infraestruturas de Portugal* on Google Earth)

4.1.1 Adverse events

Various types of adverse events will be considered for the definition of scenarios in the Portuguese pilot. The natural hazards taken into account depend on the selected demonstration site; floods in the case of Santarém and both floods and wildfires in Leiría. The human-made hazards are related to the condition of the

infrastructures, but accidents and intentional events (e.g. provoked fires in Leiría) are considered as well.

The events to investigate in the Santarém demonstration site are:

- Natural hazards (NH): Floods are considered a major risk because roads and railway included in this site are placed along the basin of the Tagus River.
- Human-made hazards (HMH): Events related with structural condition and accidents affecting the infrastructures.

In the Leiría demonstration site, there will be considered:

- Natural hazards (NH): The area is affected by wildfires, events that are closely related with heatwaves occurrence. The number, duration and amplitude of heatwaves is expected to increase in the future according to climate change projections. Flooding is also an event to be considered in this demonstration site.
- Human-made hazards (HMH): Fires can also be provoked by humans. Other human related risks are those regarding the structural condition of the assets and accidents.

4.1.2 Evaluation of scenarios

The focus of this pilot is to enhance emergency responses, inter-modality and behavioural and psychological issues of users (as a short-term decision-making) since it will be checked the ability of IMS to deliver information to the users through information panels and setting gateways in certain real or simulated events.

- Emergency response
- Inter-modality
- Behavioural and psychological aspects of users
    - Short-term decision making
        - Information methods
        - Setting gateways

4.1.3 Assets

The Demonstration Site 1.A (Santarém) includes both road and railway transportation modes, so it can be validated in a multimodal context. Regarding the road section, the available information includes 49 pavement sections that cover a total of 311 km (both directions considered separately in highway sections) as shown in Figure 15. Similarly, the railway area is subdivided in 31 sections from four different railway lines, covering a total of approximately 92 Km.

Apart from the pavement and rail sections, there is information available regarding bridges and viaducts. There are data from more than 150 assets in road sections, and a similar number for the rail sections

For the Demonstration Site 1.B (Leiría), the available information is divided in road and railway assets (similarly than for Demonstration Site 1.A, bridges and viaducts), with approximately 40 assets for each transportation mode (Figure 14).

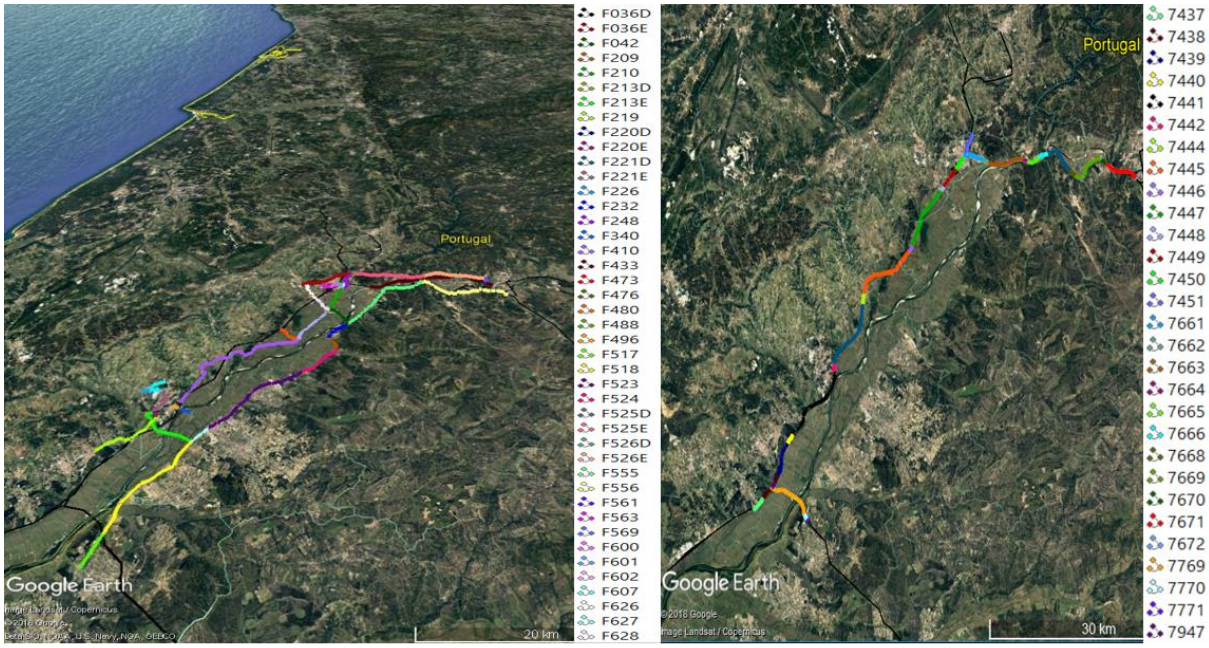

(a) (b)

Figure 15: Demonstration Site 1.A – Santarém: (a) Road sections (b) Railway sections. In both cases, each section has a randomly selected colour. (Source: Data provided by *Infraestruturas de Portugal* on Google Earth)

As bridges are the most relevant assets for this Pilot, the capabilities of the proposed data acquisition technologies for extracting information from bridges are summarized in Table 13 (see Appendix). These tables consider exclusively the data provided for inventory and inspection of road networks. For railway network assets, the information is summarized in Table 15-Table 21, which summarize data from Network Rail (Section 4.3) that can be extrapolated for all Pilots.

4.2 Pilot 2: Spain

This Pilot will take place in Spain, along the Mediterranean Corridor, and considers two demonstration sites: Demonstration site 2.A, in Málaga, includes a section of high-speed railway (154km of length) including four stations (Figure 16). The Demonstration Site 2.B in Murcia (Figure 17) includes conventional railway, comprising older infrastructure whose conservation may be worse than the high-speed infrastructure of Demonstration Site 2.A.

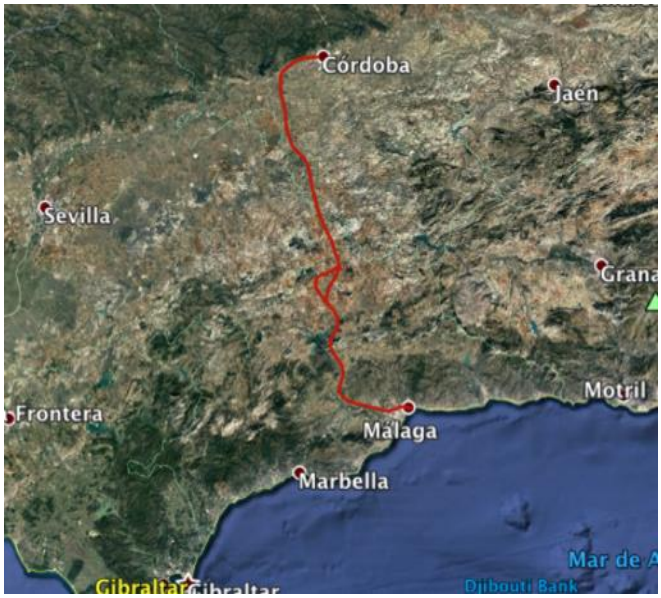

Figure 16: Demonstration Site 2.A: Málaga. (Source: Data drawn in Google Earth, not directly provided by Ferrovial)

Figure 17 : Demonstration Site 2.B: Murcia. The railway section has been manually drawn (Source: Data drawn in Google Earth, not directly provided by Ferrovial)

4.2.1 Adverse Events

For this pilot, there are both natural and human-made hazards that have to be considered:

- Natural events:
  - Earthquakes
  - Flooding
  - Storms / Heavy Rain
  - Hot / Cold waves
  - Landslides
- Human-made events
  - Car accidents
  - Other accidents / vandalism

- Provoked fires

4.2.2 Evaluation of scenarios

Based on installed weather stations (measures of rain, temperature, humidity and noise) accelerometers that feed the National Geologic Institute database and already deployed IoT (Internet of Things) sensors, it will be possible to assess risks related to natural hazards such as floods, storms, landslide, earthquake, hot/cold waves; and risks from man-made induced hazards such as terrorist attacks, fires and train crashes.

Adaptive structures should be evaluated to reduce the impact of certain risks in the long-term (elastomeric solution in seismic areas, low degradation materials, etc.). It will be necessary to adapt existing infrastructures.

New self-healing materials could be evaluated after the introduction of new constructions and retrofitting solutions.

4.2.3 Assets

The assets for Pilot 2 are summarized in the following list:

- Tunnels
- Underpasses and overpasses
- Viaducts
- Slope of Embankments
- Culverts
- Protection elements
- Fencing
- Surrounding vegetation
- Rail track
  - Fish plate joint
  - Railway sleeper
  - Ballast
  - Railroad switch
  - Expansion joints

According to the information provided by Ferrovial, Table 14 (see Appendix) summarizes the critical assets for the Spanish pilot. It also summarizes the technologies available and considered relevant for the inspection of each asset.

It is important to highlight that the requirements presented by Ferrovial concerning inspection, are not expected to be performed using monitoring technologies (neither satellite nor terrestrial) within SAFEWAY's WP9.

4.3 Pilot 3: United Kingdom

The only demonstration site for this Pilot (Demonstration Site 3.A) is placed in Stoke-On-Trent, covering a 10-mile section of the London-Manchester railway line, which is the most frequented train line in the United Kingdom (Figure 18). This line is part of the London North Western rout, the biggest in the country, running the railways in the North West and West Midlands and, thus, a critical component of the North Sea-Mediterranean corridor of the TEN-T network.

Figure 18: Demonstration Site 3.A: Stoke-on-Trent (Source: Data drawn in Google Earth, not directly provided by Network Rail)

4.3.1 Adverse events

The events considered in the scenarios evaluated in this demonstration site are the following:

- Natural hazards (NH): Sudden weather events are frequent in the area, especially heavy rain causing floods.
- Human-made hazards (HMH): Structural failures are expected because of the advanced age of the assets, some of them between 100 and 150 years. Human provoked events like bridge strikes are also considered. Also, human activities like mining (a cause of subsidence) involving geotechnical movements may be related to structural failures.

4.3.2 Evaluation of scenarios

The aim of the scenario evaluation is to gain insight into the current situation of the network, regarding infrastructure assets and the environment, to develop solutions that can be used to anticipate extreme events occurrence, reduce the cost of inspections and improve safety, both for network users and operators.

4.3.3 List of assets

A total of 158 individual assets belonging to 8 types of structures are described along the 10-mile line section as shown in Table 7**¡Error! No se encuentra el origen de la referencia.**.

Table 7: Assets of Demonstration Site 3.A: Stoke-on-Trent

Asset type	Number of assets
Tunnel	1
Underbridges	15
Overbridges	20
Footbridges	5
Retaining walls	34
Culverts	52
Pipe bridges	26
Side of line bridges	5

Table 15-Table 21 (see Appendix) have been completed using data from Network Rail as reference. The aspects reflected in those tables are used to assess the state of the infrastructure at component level. In addition, they provide information about the capability of the available technologies to perform the damage assessment and the subsequent definition of Performance Indicators (Section 6). Each of these tables reflect the characteristics to be studied depending on the type of structure and/or element considered.

5. SAFEWAY Remote Monitoring data acquisition protocols

This section describes the data acquisition protocols for the different technologies that have been introduced in Section 3. First, the protocols and relevant acquisition information for satellite technologies are defined, and then a similar approach is followed for terrestrial technologies.

5.1 Satellite technologies: Data acquisition protocols

The satellite monitoring activity in the SAFEWAY project will be mainly based on the Copernicus Sentinel data. The data acquisition will be performed through the Copernicus Open Access Hub that provides complete, free and open access to Sentinel-1, Sentinel-2, Sentinel-3 and Sentinel-5P images, starting from the In-Orbit Commissioning Review (IOCR).

5.1.1 This section contains the description of Sentinel-1 (radar) and Sentinel-2 (optical) data. Sentinel-1 data

A new and interesting opportunity for the continuous monitoring of roads and railways infrastructures stability is provided by the Sentinel-1 satellite constellation, the last imaging radar mission of the European Space Agency (ESA) within the framework of Copernicus European programme for Earth Observation. Considering the cost/benefit of the obtainable information by processing these data with the Multi-Temporal Interferometry algorithms, Sentinel-1 satellite can be considered the optimal SAR satellite sensor to monitor the ground and infrastructures like roads and railways on wide areas.

Sentinel-1 by offering regular global-scale coverage, free imagery, improved revisit time (up to 6 days) and long wavelengths (5.6 mm) can now guarantee wider and more efficient application of MTI for the global infrastructure monitoring. The two-satellites Sentinel-1A and 1B provides high reliability data with a short revisit time, global coverage and rapid data dissemination to support operational applications in the priority areas of marine and land monitoring and emergency services. To accomplish the above, the satellites carry the Synthetic Aperture Radar (SAR) instrument that offers medium-to high-resolution radar imagery at C-band. Sentinel-1A has been acquiring data since 2014, whilst Sentinel-1B has been acquiring data since 2016.

The use of Sentinel-1 with respect to the other C-Band constellations, have the following advantages:

- It is possible to detect signals from targets with short de-correlation time such as Distributed Scatterers. Indeed, using the Sentinel-1 images it is possible to monitor the ground displacements also on soil characterized by a mean decorrelation time of about 10 days (like pasture) improving the number of measurable targets.
- Higher maximum measurable velocity that responds to the specific requirements of ground and infrastructures monitoring.
- The lowest velocity standard deviation.

Sentinel-1 is acquired in 4 modes (Figure 19):

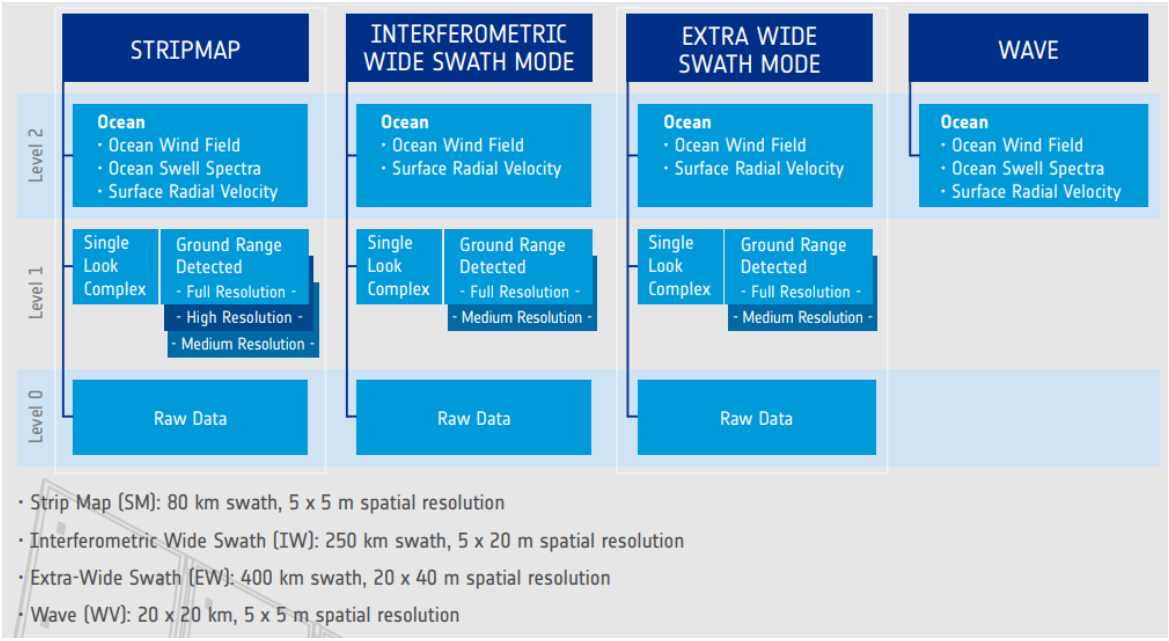

Figure 19: Sentinel-1 acquisition modes

The acquisition schema is represented in Figure 20:

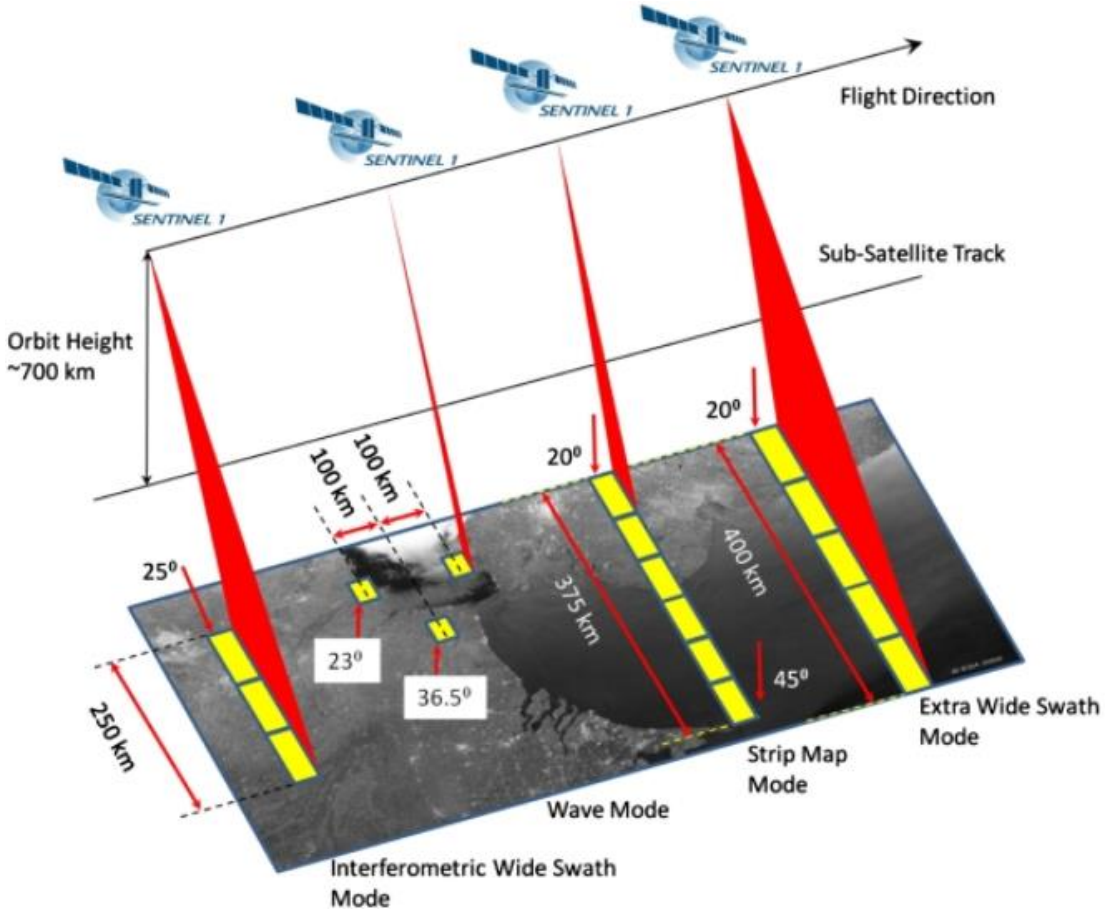

Figure 20: Sentinel-1 acquisition schema

Each mode can potentially produce products at:

- Raw Level-0 data (for specific usage) (typical size 1GB/product)
- Level-1 Single Look Complex data comprising complex imagery with amplitude and phase (systematic distribution limited to specific relevant areas) (typical size 8GB/product)
- Level-1 Ground Range Detected data with multilook intensity only (systematically distributed) (typical size 1GB/product)
- Level-2 Ocean data for retrieved geophysical parameters of the ocean (systematically distributed).

Within the SAFEWAY project the Sentinel-1 IW – Level 1 Single Look Complex data will be processed by means of MTI algorithm in order to continuous monitor the roads and railways infrastructures stability.

5.1.2 Sentinel-2 data

Sentinel-2 carries an innovative wide swath high-resolution multispectral imager with 13 spectral bands, (443 nm–2190 nm) with a swath width of 290 km and spatial resolutions of 10 m (4 visible and near-infrared bands), 20 m (6 red-edge/shortwave-infrared bands) and 60 m (3 atmospheric correction bands) for a new perspective of our land and vegetation.

The combination of high resolution, novel spectral capabilities, a swath width of 290 km and frequent revisit times provides unprecedented views of Earth.

The mission is based on a constellation of two identical satellites in the same orbit, 180° apart for optimal coverage and data delivery. Together they cover all Earth's land surfaces, large islands, inland and coastal waters every five days at the equator.

Sentinel-2A was launched on 23 June 2015 and Sentinel-2B followed on 7 March 2017.

Sentinel-2's multispectral imager undertakes systematic acquisition in a single observation mode.

The following 3 levels are available for Sentinel-2 images:

- Level-1B: Top of atmosphere radiances in sensor geometry. Level-1B is composed of granules, one granule represents the sub-image one of the 12 detectors in the across track direction (25 km), and contains a given number of lines along track (approximately 23 km). Each Level-1B granule has a data volume of approximately 27 MB. Level-1B products require expert knowledge of orthorectification techniques.
- Level-1C: Top of atmosphere reflectances in fixed cartographic geometry (combined UTM projection and WGS84 ellipsoid). Level-1C images are a set of tiles of 100 sq km, each of which is approximately 500 MB. These products contain applied radiometric and geometric corrections (including orthorectification and spatial registration).
- Level-2A: Bottom of atmosphere reflectances in cartographic geometry. This product is currently processed by on the user side by using a processor running on ESA's Sentinel-2 Toolbox. The possibility of making a standard

core product systematically available from the Sentinels core ground segment is currently being assessed as part of the CSC evolution activities.

Within the SAFEWAY project the Sentinel-2 Level-2A will be used.

5.2 Terrestrial technologies: Data acquisition protocols

This section exposes the necessary equipment to perform the survey in the railway environment with a Mobile Mapping System (MMS). Moreover, the main installation and survey needs are described.

> ***Note:*** *Part of the information of this document comes from the datasheets of the products involved.*

5.2.1 Equipment

The Mobile Mapping System (MMS) used in this project to generate survey-grade LiDAR data is a Lynx mobile mapper (Lynx M1). It was manufactured by Optech and released in 2007 (*Teledyne Optech*, 2019). According to the application, the LiDAR system can be combined with any number of sensors in order to obtain extended results. Usually, the monitoring of the position of the scanning system is possible thanks to the use of a Global Navigation Satellite System (GNSS), together with an Inertial Measurement Unit (IMU), and Distance Measurement Indicators (DMI). The positioning system was designed by APPLANIX (POS LV 520) and the GNSS receivers belong to TRIMBLE. As a result, the LiDAR system provides information about the relative position of objects with respect to the MMS in a local coordinate system, while positioning devices give the absolute location of the vehicle with respect to a global coordinate system (e.g. WGS84).

The platform used for supporting the sensors on top of the vehicle has been developed by Optech in collaboration with the University of Vigo. The weight of the whole set is about 100 kg (~220 lb), and may be mounted on a van, a wagon or a draisine. Whichever the vehicle, it moves along a predefined trajectory while the laser scanner is continuously working. With this, the so called trajectory followed by the platform is registered into a global coordinate system. The result is an extremely dense 3D point cloud, created when the laser scanner is synchronized with the navigation system.

5.2.1.1 LiDAR system and associated sensors

The Mobile Laser Scanning (MLS) system uses the LiDAR technology to obtain a three dimensional (3D) representation of the environment. The collected data are points distributed in the 3D space forming what is called a 'point cloud'. The laser scanner works directing a beam of laser light to any object in the space, and computing the distance between the LiDAR system and the target object. The distance is calculated through the time delay between the emission and return of the light beam. When the distance measurement device is combined with optomechanical systems or mirrors, which deflect the laser beam and measure the deflection angle, the mentioned point cloud is obtained.

The LYNX scanner available obtains a maximum of 500,000 points per second, with a frequency up to 200 Hz. The maximum working range is about 200 m in a

full circle with 360º of angular coverage, being 1 m the minimum range of operation between the LiDAR sensor and the object. The different characteristics of the returned laser signal are recorded, as well as the intensity reflected by the objects. A short description of the equipment's specifications can be found in Figure 21.

Parameter	V200	M1
Number of lidar sensors	1-2	1-2
Camera support	Up to 2 cameras Individually scalable frame areas	Up to 4 cameras Individually scalable frame areas
Maximum range	200 m, 20%	200 m, 20%
Range precision	8 mm, 1 σ[1]	8 mm, 1 σ[1]
Absolute accuracy	±5 cm, (1 σ)[1]	±5 cm, (1 σ)[1]
Laser measurement rate	75-200 kHz programmable	75-500 kHz programmable
Measurement per laser pulse	Up to 4 simultaneous	Up to 4 simultaneous
Scan frequency	80-200 Hz programmable	80-200 Hz programmable
Scanner field of view	360° without obscurations	360° without obscurations
Power requirements	12 VDC, 30 A max. draw	12 VDC, 30 A max. draw
Operating temperature	-10°C to +40°C (extended range available)	-10°C to +40°C (extended range available)
Storage temperature	-40°C to + 60°C	-40°C to + 60°C
Laser classification	IEC/CDRH Class 1 eye-safe	IEC/CDRH Class 1 eye-safe
Vehicle	Fully adaptable to any vehicle	Fully adaptable to any vehicle

1 Under test conditions. Contact Optech for details.

Figure 21: Lynx system specifications

Optech gives some general recommendations when using the Lynx system: The selected vehicle carrying the sensors must not be too big, since it could find difficulties when performing the survey in certain areas. Although it has to be strong enough in order to support the weight of the necessary equipment, and also provide enough power to the Lynx.

In the railway environment, it is recommended to use a draisine in order to avoid dimensional problems.

- **Global Navigation Satellite System (GNSS) and Inertial Measurement Unit (IMU)**

The navigation system allows the georeferencing in geographical coordinates of the whole survey. The GNSS receiver is used to evaluate the location of the MMS, while the IMU acts as its origin of coordinates. Lynx uses GPS data collected by the receptor in real time, and GPS data collected independently by a base receptor in order to create a differential GPS solution post-processed.

However, the vehicle's location may vary a few metres when interferences with satellites appear (e.g. multiple signals, tunnels, dense vegetation…). The IMU is then used as a complement to the GNSS since it does not depend on external sources of information. It gives real time position, orientation and velocity measurements of the moving platform by integrating the accelerometer and gyroscope readings over time, and every sensor must be calibrated to its respect. In order to maintain the quality of the measurements, the IMU needs to be recalibrated periodically.

The GNSS used in this project is the APPLANIX POS LV 520, which integrates an IMU with two Trimble R4 GPS antennas. They provide the absolute accuracies (RMS) presented in Table 8 (Puente *et al.*, 2012; Iván Puente *et al.*, 2013).

Table 8: Absolute Accuracies (RMS)

	Heading	Roll	Pitch	X	Y	Z
RMS	0.015º	0.005º	0.005º	0.02 m	0.02 m	0.05 m

The vehicle where these devices will be installed has to be long enough to place the two GPS antennas. The distance between them must be of at least 1.5 m, preferably between 2 and 5 m, being 2 m the standardised distance. This separation will condition the precision of the direction measurements obtained through the IMU.

- **Distance Measurement Indicator (DMI)**

The DMI is an encoder used to measure linear distances. The APPLANIX system employed in this project provides accurate vehicle velocity updates. It is formed by the DMI itself, a control-stick and a cable. This device needs to be mounted on one of the back wheels of the vehicle (Conforti and Zampa, 2012; I. Puente, González-Jorge, Riveiro, *et al.*, 2013).

The data provided by this unit is useful for reducing the error induced by the GNSS and IMU measurements. After the survey, these data and the LiDAR ones are processed together with the ones from the navigation systems in order to reference the laser positioning points to the ellipsoid WGS84. The DMI and IMU also allow the navigation when the GPS connexion is lost (Puente *et al.*, 2012; Meng, Wang and Liu, 2017).

5.2.1.2 Spherical camera (Ladybug5)

This project will use the Spherical Camera Ladybug5, which has fully integrated multiple cameras to obtain 360º panoramic images. It is composed by a set of six Sony® ICX655 CCD sensors arranged in a circular five-camera configuration plus a single vertical camera.

The camera has to be placed in a pole in the front-top part of the vehicle, so that no equipment from the MMS is captured. Moreover, in order to improve the results in closed environments (tunnels), a new structure has been developed. The camera was provided with four artificial light bulbs at its basis, obtaining with this useful RGB images during the laser survey.

5.2.1.3 Control Rack

There are four different racks in the system: acquisition, control, LiDAR and power supply. All four need to be installed inside the moving vehicle, and are connected and managed by an expert operator using only the control rack. In addition, to remotely operate the equipment from the control position, a line of communication between the vehicle itself and the equipment is needed. The ideal would be an

Ethernet network connexion or even a screen directly connected to the control rack.

The acquisition and synchronization of data from the different sensors in the MMS is made using the control rack. It has a server that allows the download of data in a rapid and reliable manner. The acquisition system is in charge of synchronizing and shooting the cameras when needed, but it is run using the control rack. As said before, the LiDAR system also has its own rack, which controls the LiDAR heads, IMU, GNSS antennas and DMI.

The power rack provides electric supply to all these systems, as well as the spherical camera's lighting system. A connection of 220V of alternating current is necessary in order to give the electric power needed. If the moving vehicle used had no power generator that may be used, an electric generator will be installed. Two Uninterruptible Power Supply (UPS) systems will also be installed to ensure the continuous electrical supply in the storage and control rack, and the LiDAR and DMI system. These should also be placed inside the vehicle.

> ***Note:*** *Modifications to the moving platform, if required, would always be consulted, approved and authorised beforehand.*

5.2.2 Hardware installation

5.2.2.1 Installation procedure

- **LYNX Mount Structure Platform**

It can be placed on the roof of the vehicle.

The **base plates** and **vertical stands** for mounting the laser scanners are attached to the platform with nuts and bolts.

Axial fans can be installed on the base plate under laser scanners to refrigerate them when operating under hot weather conditions.

- **LiDAR sensors**

The sensors are placed in the vertical stands inserting the pins on their sides inside the slots of the stands, and must aim outside from the rear of the vehicle.

Adjusting the nuts of the **stand mechanism**, the sensors are fixed to their scanning position.

The area around the LiDAR sensors must be free of obstructions that could interrupt the laser beam trajectory.

Silent-blocks can be used to reduce the effect of vehicle vibrations on the sensors.

The necessary wiring consists on power and communication cables connected to the control rack inside the vehicle.

The maximum length of the cables connecting the sensors and the control rack is 5 metres. Hence, the separation between them must be inferior to this distance.

- **GNSS and IMU**

An A-shaped stand is employed to install the primary GNSS antenna on top of the array box.

- The primary antenna must be placed directly over the IMU of the array box.
- GNSS primary antenna-IMU lever arm must be measured with centimetre precision.

The secondary GNSS antenna is placed directly on the roof of the vehicle.

- Longer distances between primary-secondary antennas improve precision of azimuth and vehicle heading determination (1,5 m minimum / 5 m maximum; 2.0 m recommended by Optech).

The roof of the vehicle must be free of obstructions that could interrupt the line of sight between the GNSS satellites and the receivers.

GNSS antennas connections must be protected against moisture and dust with tape.

The necessary wiring consists on RF cables connected to the control rack inside the vehicle.

IMU

The array box must be attached and aligned to the structure platform using the available slots.

- **DMI**

It must be placed close to the optic encoder.

The device must be installed in a wheel that does not turn (i.e. it cannot be installed on the directional axis of the vehicle), as that could produce incorrect measurements or damage the device.

The DMI is attached to the vehicle using either a **temporary or permanent mount** (clamp).

- Permanent: Inserting metal bolts in holes drilled on the fender of the vehicle.
- Temporary: Using either suction pads or a magnetic band fixed with nylon bolts to attach the clamp to the fender of the vehicle.

The **encoder** is attached to the wheel of the vehicle using an adapter for the wheel hub. This adapter has different slots to place rings that are connected to the wheel hub bolts. The slots to be used depend on the number of bolts of the hub.

- The hub adapter must be correctly centred to avoid data signal noise and excessive vibrations.

Once the hub adapter is installed, the temporary/permanent clamp is slid over the **control rod**.

- The control rod must be placed perpendicular with respect to the road.

The **power/data cable** is connected to the DMI encoder and covered with tape to protect it against dust and moisture. The cable is guided along the control rod and fixed with tie-wraps. Then, it is connected to the **control unit**.

- **Thermographic Camera (if required)**

The thermographic camera should be installed on a platform that allows to modify its orientation, so it could be adapted to different inspection situations.

The necessary wiring consists on a power cable, an Ethernet cable and one for the TTL signal. It is introduced inside the vehicle through its superior side.

- **Spherical Camera (Ladybug5)**

An illumination system could be necessary to make possible to operate the camera under low-light conditions (e.g. inside a tunnel).

The necessary wiring consists on a power cable, USB 3.0 cable and one for the TTL signal.

- **Control rack**

Each sensor is connected to one of the racks:

  - Acquisition rack
    - 360º camera
    - Thermographic camera
    - LiDAR rack
  - LiDAR rack
    - LiDAR sensors
    - IMU
    - GNSS antennas
    - DMI
  - Control rack
    - Controls data gathering
    - Runs the acquisition and control software
    - Stores the information
    - It must be placed on a level surface.
    - There must be enough space behind the unit to correctly connect the wires and not obstruct its vents.
    - The power supply, the HDD bay and the power switch must be easily accessible.
  - Power rack
    - 220V AC for the illumination system
    - 220V AC for the control system
    - 12V DC for the LiDAR system

5.2.2.2 Required parameters and sensors' calibration

Installation key parameters:

- **LiDAR lever arm:** Distance between the LiDAR sensor centre and the IMU centre. The orientation of the LiDAR (roll, pitch and azimuth) with respect to the IMU must be measured and defined as well.
- **DMI** (Figure 22)**:**
  - **DMI lever arm:** Distance between DMI centre and IMU centre.
  - Determination of the DMI point of reference origin in X, Y and Z axis:
  - Diameter of the wheel where the DMI is installed.
  - DMI scale factor. It is necessary for the correct conversion from DMI pulse per revolution measurements to meters. It is calculated using the next equation:

$$s = \frac{n}{d\pi}$$

n = pulses per wheel revolution

d = Wheel diameter

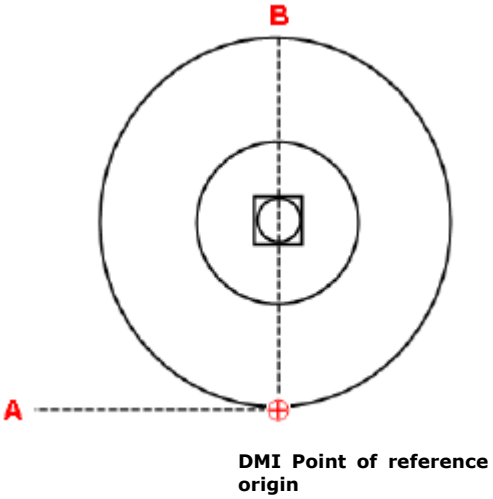

Figure 22: DMI Point of reference determination. (Source: Optech manual)

- **Primary antenna lever arm 2:** Distance between the primary antenna centre and the IMU centre. Provided by Optech.
- **Distance between GNSS antennas:** Used by the GAMS (GNSS Azimuth Measurement Sub-system) to calculate heading. To do so, the vector between the primary and secondary GNSS antennas phase centres must be precisely measured.
- **Ladybug5 Spherical Camera lever arm:** Distance between camera and IMU respective centres.
- **Thermographic camera lever arm:** distance between camera and IMU respective centres. The angular orientation of the camera with respect to the IMU must be defined as well, using a calibration support.

Lever arms and initial aiming angles (roll, pitch, azimuth) must be introduced in the LV-POSView software after installation or position modification of the instruments.

Precise measurements of the parameters above minimize the error presumption during data processing.

5.2.2.3 Survey plan

LiDAR parameters can be edited in the "LiDAR configuration" menu of the software. For each LiDAR sensor, it is possible to set up minimum and maximum data **acquisition ranges**. All results out of these thresholds will be rejected.

For these LiDAR sensors, the minimum valid range for data acquisition is 1 meter around the longitudinal axis of the LiDAR sensor (Figure 23). The maximum dimensions of the Lynx system (when the case is mounted) are:

1474 mm (Length) – 827 mm (Width) – 575 mm (Height)

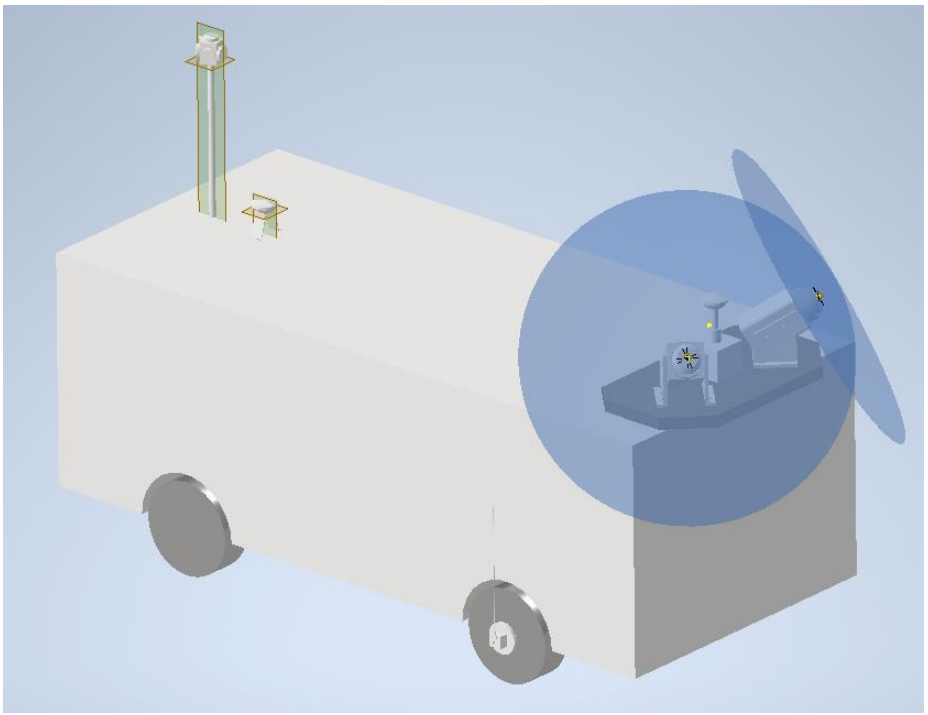

Figure 23: Inspection vehicle with Optech Lynx attached. The minimum scanning ranges are represented by blue circular surfaces

5.2.2.4 Security

In this section, a list of preventive measures from the Optech manual necessary to take into account to operate correctly and safely the system are presented.

- **Laser safety**
  - Lynx is a "Class 1 Laser Product" and complies with IEC 60825-1 rules, so radiation emitted through the windows of the sensor is completely sight-safe (Figure 24).

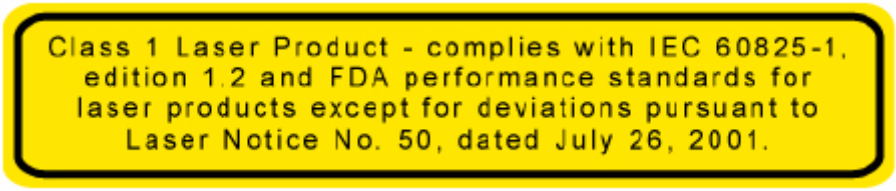

Figure 24: Class 1 Laser compliance label (Source: Optech manual)

- A "Class 3b Laser" is inside the sensor, so its case must be open **only** if the sensor is turned off to avoid exposure to the beam, as radiation levels are over sight-safe thresholds (Figure 25).

Figure 25: Class 3B Laser case opening label (Source: Optech manual)

Laser specifications can be seen in Table 9:

Table 9: Laser specifications (Source: Optech manual)

Parameter	Specifications
Wavelength	1550 nm
Pulse repetition frequency	100 kHz
Pulse width	<5 ns
Pulse energy	<3μJ
Average power	<200 mW
Peak pulse power	1 kW

- **LiDAR sensor**
  - Manipulate the sensor carefully, as it is heavy-weighting.
  - Maintain protection covers when not operating.
  - Do not touch the window of the sensor.
  - Do not open the sensor case (except for replacing the dryers).
  - Do not place the sensor perpendicular to the floor when initialising it, because bearings of the motor could be damaged.
  - Check the correct operation of each LiDAR fan when using the system with temperatures > 10ºC (50ºF).

- Wait while the sensor warms up if there is condensation on its window due to changes in environmental temperature.

- **GNSS antenna**
  - Do not attach metal labels to the antenna.
  - Maintain ceramic parts of the antenna clean and free from scratches.
- **DMI**
  - Do not bend the control rod nor use it to hold the DMI.
  - Do not install the DMI on a directional wheel.
  - Avoid collisions of the DMI with road elements.
  - Verify the joints of the DMI hub adapter before its use.
  - Be careful when opening the doors of the vehicle (specially with sliding doors).
- **Cameras**
  - Always remove the case of the camera in a clean and protected environment and maintain both cameras and lenses clean.

5.2.3 Survey protocols

In this section, general requirements for performing a MLS survey are described. Every survey requires planning before performance in order to achieve the better results possible considering the needs in each case. This planning involves: selection of suitable equipment; definition of the suitable trajectory; preparation and calibration of the equipment; definition of the working parameters.

5.2.3.1 Weather conditions

Laser scanners are an active remote sensing technology, so surveys can be performed at night. Nevertheless, most of the surveys are planned during the day due to navigation issues and to obtain useful RGB images. In any case, it is important to consider this as well as the benefits that could provide to the survey (less pedestrian and/or roadway traffic, less impact if interrupting the service of any infrastructure…).

Since the majority of the LiDAR systems work with laser in the visible light range, dust and vapour can severely affect the results of the measurements. Moreover, some sensors are sensitive to direct sunlight as well as bad reflectivity surfaces. All these factors should be taken into account when picking a date for performing the survey, since the weather conditions need to be specific.

It is also important to take into account the vegetation in the survey area. This could be both a good or a bad issue when performing a survey. In some cases, vegetation would provoke occlusions of important areas in the infrastructure, so it would be better to acquire the data in leaf-off conditions (Riveiro, Conde and Arias, 2015; Filgueira *et al.*, 2017).

5.2.3.2 Accuracy improvement

After the installation of the equipment in the moving platform, it must be calibrated. In the railway environment, at least 200-300 m of outdoors' rail track is necessary for calibrating the sensors. The vehicle will move operated by an expert and the calibration will be verified.

To improve the trajectory's accuracy, it is necessary to perform stops in a place with good GNSS coverage. These stops will last at least 10 minutes at the beginning and ending of each itinerary.

It is important to highlight that accuracy depends not only on the equipment, but also on the geometry of the 3D scenario under study and the speed of the moving platform over the tracks. It must be constant and a maximum of 30-40 km/h.

6. Performance Indicators for remote monitoring

This section serves as starting point for the search of Key Performance Indicators (KPIs). KPIs are number of performance measurements that will evaluate the success of the project activities.

RAMSSHEEP approach was proposed for defining KPIs (Kick-off meeting, Parallel Session WP3-4-6):

RAMSSHEEP:

Reliability

Availability

Maintainability

Safety

Security

Health

Economy

Environment

Politics

Measuring KPIs depends on several aspects. In specific **scenarios**, **KPIs** will depend on a specific **set of aspects**. These aspects are defined with a number of parameters or **Performance Indicators (PIs)**.

Performance Indicators of the infrastructures will be defined at different levels, depending on the monitoring techniques:

- **PIs at the component level** (Pavement, curbs, sidewalks, drainage, lighting, signage...)
- **PIs at the system level** (structural safety, traffic safety, durability of the whole system)
- **PIs at the network level** (structure condition assessment + structure importance on the network).

A Scenario is defined as an outline of a possible future event that assess the outcomes that an extreme event may have on a transport infrastructure – i.e., affecting one or more critical assets and/or disrupting users. Scenarios are defined within the so called "scenario-based risk analysis", which is the process of analysing a set of multiple scenarios or "alternative worlds" with the aim of identifying potential risk and their linked hazards, to increase preparedness to handle them and minimize their impact. \A methodologic approach to the definition of Performance Indicators for RS-Satellite and RS-Terrestrial as baseline is proposed, based on the needs provided through the different scenario that will be exploited in the SAFEWAY pilot.

6.1 Performance indicators of satellite monitoring for infrastructures

Within the dimensions of resilience, satellite remote sensing technology it's very useful to support the preparation phase. This means that by means of satellite sensors it is possible to extract parameters related to the infrastructure conditions which allow the definition of the Performance Indicators.

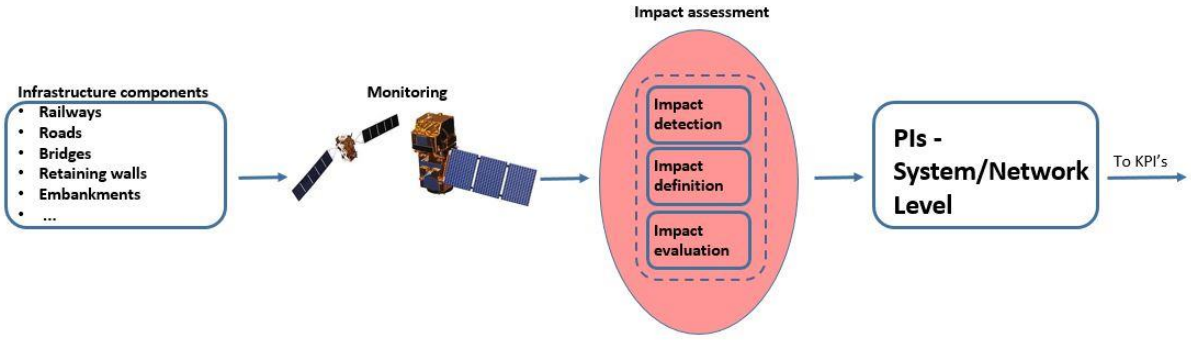

Figure 26. Satellite remote sensing monitoring of infrastructures to obtain PIs at a component level

From Figure 26. it can be inferred the necessity of:

- Define which aspects are the most relevant to assess in each scenario.
- Define which aspects can be assessed with the RS-Satellite technology.

Define how to translate the assessment to an objective Performance Indicator that allow its subsequent contribution to the infrastructure KPIs.

For satellite monitoring technologies, the extracted PIs are at the System/Network level and the Performance Indicator can be built according to a rating index in terms of impacts of the infrastructures/surrounding stability and changes:

- Rating Index 1: No or very slight impact of infrastructures/surrounding area changes.
- Rating Index 2: Slight impact of infrastructures/surrounding area changes. If no measures are taken, the risk of negative impact on the infrastructure will increase.
- Rating Index 3: Moderate to severe impact of infrastructures/surrounding area changes with no decrease in serviceability. Medium-term damages on the infrastructures may be expected.
- Rating Index 4: Severe impact of infrastructures/surrounding area changes. The level of the damages of the infrastructure have to be instigated.
- Rating Index 5: Extreme impact of infrastructures/surrounding area changes with possible consequences on the capacity of the infrastructure. The field inspection to detect the level of the damages/impact of the measured phenomena is suggested with priority.

As seen in Figure 26, impact assessment has three different stages:

1- *Impact detection*: Localization of infrastructures/surrounding change. E.g.: infrastructures movements, illegal buildings, etc.

2- *Impact definition:* Definition of the impacts nature. E.g.: subsidence due to natural phenomena and/or third party activities, new buildings constructions etc.

3- *Impact evaluation:* Quantification/Qualification of the impact based on a set of threshold values. E.g.: Magnitude of the infrastructures/surrounding changes.

These stages allow the categorization of the impacts as primary performance indicators at the network/system level. These indicators will be employed to define the infrastructure inspection priorities (rating indices defined above) and carry the results to the definition of KPIs.

In (Stenström, Parida and Galar, 2012) several parameters and performance indicators are defined for railway infrastructures. Few of them are actually measurable with RS-Satellite technology, and in particular those related to the technical and condition indicators at the network/system level such as:

- Embankments
    - Slope movements
- Railways/Roads movements with millimetre precisions
- Railways/Roads surrounding movements with millimetre precisions
- New artificial structures detection and monitoring in the area surrounding the railways/roads
- Marine erosion assessment to evaluate the impact on the railways/roads over the coastal zones
- Identification of flood-prone areas along the railway/road networks.
- Identification of third-party activity along the railways/roads that may negatively impact the infrastructure.

Each infrastructure is measured with some parameters (e.g. ground/infrastructure displacement, surrounding area changes), and that measurements are translated to PIs (e.g. Potential roads/railways impact of the detected phenomena) specified with a rating index and with a location.

Summarizing, Performance Indicators for RS-satellite will be defined at the system/network level, following the information in the Appendix.

6.2 Performance indicators for terrestrial remote sensing monitoring of infrastructures

Attending to (*Quality specifications for roadway bridges, standardization at a European level*, no date), inspection and monitoring, which are the activities that can be carried out by the terrestrial technologies presented in this report, aim at the evaluation and assessment of structural safety and reliability.

These monitoring activities are associated with performance indicators:

- Results of individual monitoring tasks can be **transferred into a general and objectified evaluation system** e.g. via an evaluation matrix, with the objective of assessing any reductions of functionality.
- Depending on the measurement task, different physical values can be collected at discrete time intervals. This information may enable **predictions on the future behaviour** of the physical values. Also, any change may be observed over time.

The concept of *Performance Indicator* (PI) is really broad. Different infrastructure owners have their own performance indicators, but they can be clustered in different items such as PIs related to material properties, related to equipment and protection, related to geometry changes, etc.

Performance indicators can also be categorized according to different levels, being PIs of a level an aspect or parameter of a higher level. For bridges, the following categorization has been made:

- **PIs at the component level** (Pavement, curbs, sidewalks, drainage, lighting, signage...)
- **PIs at the system level** (structural safety, traffic safety, durability of the whole system)
- **PIs at the network level** (structure condition assessment + structure importance on the network).

For terrestrial monitoring technologies, the extracted PIs should be at the component level, where a Performance Indicator can be built according to a rating index in terms of damage:

- Rating Index 1: No or very slight damage. No measures required.
- Rating Index 2: Slight damage, defects with no further deterioration. If no measures are taken, the predicted life time will decrease.
- Rating Index 3: Moderate to severe damage with no decrease in serviceability. Medium-term maintenance and repair actions are necessary.
- Rating Index 4: Severe damage. Maintenance measures are to be instigated as soon as possible.
- Rating Index 5: Extreme damage with impact on the capacity of the structure. Repair must be performed immediately.

As seen in Figure 27, damage assessment has three different stages:

4- *Damage detection*: Localization of damage in the structure component. E.g.: Traffic sign damaged.

5- *Damage identification:* Definition of the damage nature. E.g.: Loss of reflectivity properties.

6- *Damage evaluation:* Quantification/Qualification of the damage based on a set threshold value. E.g.: Reflectivity approaching the lower limit.

These stages allow the categorization of the damage as a primary performance indicator. These indicators will be employed to define the structure component

functionality (rating indices defined above) and carry these results to the definition of KPIs (note that these PIs may be intermediate indicators of the infrastructure performance that are used to define PIs on higher levels that have more direct influence on the KPIs).

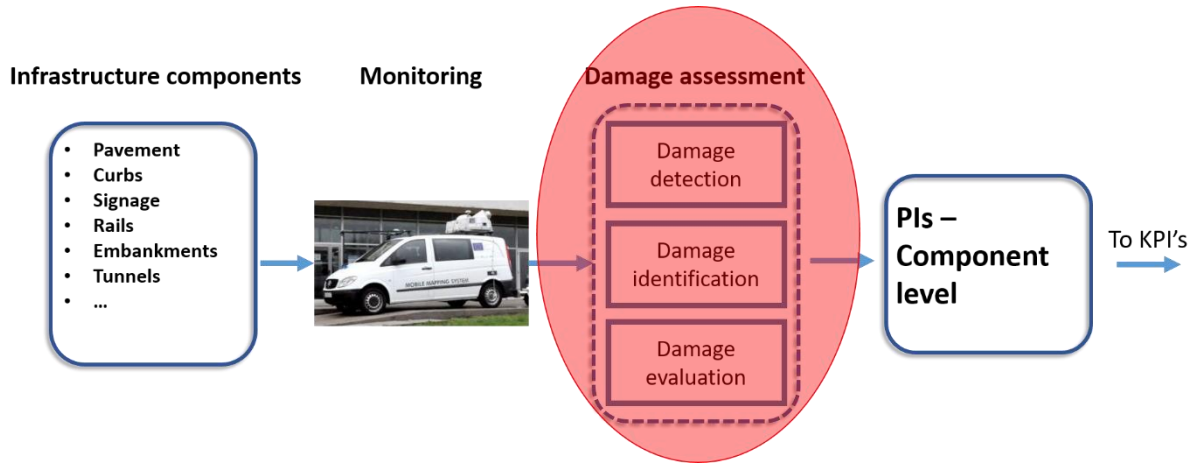

Figure 27: Terrestrial remote sensing monitoring of infrastructures to obtain PIs at a component level

In Stenström, Parida and Galar (2012) several parameters and performance indicators are defined for railway infrastructures. Few of them are actually measurable with RS-Terrestrial technology (most of the PIs are managerial indicators which are related with parameters such as punctuality, speed restrictions or traffic volume), but some of them refer to the structure components such as:

- Embankments
  - Ballast composition
  - Track stiffness
  - Ballast contamination
  - Moisture content
- Track geometry
- Track surroundings
- Rail
  - Rail integrity
  - Rail profile, surface and fasteners
- Switches and crossings
- Electrification
- Signalling

Each component is measured with some parameters (e.g. rail integrity with temperature and longitudinal stress), and that measurements are translated to PIs (e.g. Potential rail breaks, buckling, actual rail breaks, specified with a rating index and with a location).

Regarding road infrastructure, an enumeration of PIs is found in (Haas *et al.*, 2009), which define measurable PIs in roads following Canadian and International Practice. However, these PIs are in a higher level than the component level, some examples are:

- Number of accidents per million vehicle km
- Number of restricted / closed lines
- Emissions of GHGs, NOx, Sox, VOC
- Vehicle noise
- Vehicle operating costs
- Response time to incidents

These data cannot be gathered with remote sensing equipment, but with statistical analysis and specific sensors.

In Hakkert, A.S, Gitelman, V. and Vis (2007), a study that is specifically focused on road safety PIs calculates the performance of road segments based on EuroRAP's Road Protection Score. They extract some road characteristics that are relevant for this score:

- Speed
- Barrier (right, left, middle)
- Median (width)
- Side area cut (placement)
- Side area embankment (placement)
- Junctions (not signalized)
- Junctions (signalized or roundabouts)
- Intersection merging
- Intersection access

Summarizing, Performance Indicators will be defined at component level, following the information in the Appendix.

Acknowledgements

This deliverable was carried out in the framework of the GIS-Based Infrastructure Management System for Optimized Response to Extreme Events of Terrestrial Transport Networks (SAFEWAY) project, which has received funding from the European Union's Horizon 2020 research and innovation programme under grant agreement No 769255.

References

Abuhadrous, I. *et al.* (2016) 'Digitizing and 3D Modeling of Urban Environments and Roads using Vehicle-Borne Laser Scanner System To cite this version : Digitizing and 3D Modeling of Urban Environments and Roads using Vehicle-Borne Laser Scanner System'.

Advanced Navigation (2017) 'Spatial Reference Manual'.

Agudo, D. *et al.* (2016) 'Real-time railway speed limit sign recognition from video sequences', in *International Conference on Systems, Signals, and Image Processing*. doi: 10.1109/IWSSIP.2016.7502716.

Ai, C. and Tsai, Y.-C. J. (2014) 'Critical Assessment of an Enhanced Traffic Sign Detection Method Using Mobile LiDAR and INS Technologies', *Journal of Transportation Engineering*. doi: 10.1061/(asce)te.1943-5436.0000760.

Ai, C. and Tsai, Y. J. (2016) 'An automated sign retroreflectivity condition evaluation methodology using mobile LIDAR and computer vision', *Transportation Research Part C: Emerging Technologies*. doi: 10.1016/j.trc.2015.12.002.

Al-Bayari, O. (2019) 'Mobile mapping systems in civil engineering projects (case studies)', *Applied Geomatics*. Springer Berlin Heidelberg, 11(1), pp. 1–13. doi: 10.1007/s12518-018-0222-6.

Aparna *et al.* (2019) 'Convolutional neural networks based potholes detection using thermal imaging', *Journal of King Saud University - Computer and Information Sciences*. doi: 10.1016/j.jksuci.2019.02.004.

Arastounia, M. (2012) 'Automatic Classification of LiDAR Point Clouds in A Railway Environment', *University of Twente, Netherlands*.

Arastounia, M. (2015) 'Automated recognition of railroad infrastructure in rural areas from LIDAR data', *Remote Sensing*, 7(11), pp. 14916–14938. doi: 10.3390/rs71114916.

Arastounia, M. (2017) 'An Enhanced Algorithm for Concurrent Recognition of Rail Tracks and Power Cables from Terrestrial and Airborne LiDAR Point Clouds', *Infrastructures*. Multidisciplinary Digital Publishing Institute, 2(2), p. 8. doi: 10.3390/infrastructures2020008.

Arastounia, M. and Elberink, S. O. (2016) 'Application of Template Matching for Improving Classification of Urban Railroad Point Clouds'. doi: 10.3390/s16122112.

Arcos-García, A. *et al.* (2017) 'Exploiting synergies of mobile mapping sensors and deep learning for traffic sign recognition systems', *Expert Systems with Applications*, 89, pp. 286–295. doi: 10.1016/j.eswa.2017.07.042.

Arias, P. *et al.* (2015) 'Simple Approaches To Improve the Automatic Inventory of Zebra Crossing From Mls Data', *ISPRS - International Archives of the Photogrammetry, Remote Sensing and Spatial Information Sciences*, XL-3/W3, pp. 103–108. doi: 10.5194/isprsarchives-XL-3-W3-103-2015.

Armesto-González, J. *et al.* (2010) 'Terrestrial laser scanning intensity data applied to damage detection for historical buildings', *Journal of Archaeological Science*. Elsevier Ltd, 37(12), pp. 3037–3047. doi: 10.1016/j.jas.2010.06.031.

Beger, R. *et al.* (2011) 'Data fusion of extremely high resolution aerial imagery and LiDAR data for automated railroad centre line reconstruction', *ISPRS Journal of Photogrammetry and Remote Sensing*. International Society for Photogrammetry and Remote Sensing, Inc. (ISPRS), 66(6 SUPPL.), pp. S40–S51. doi: 10.1016/j.isprsjprs.2011.09.012.

Beraldin, J. A. *et al.* (2000) 'Real world modelling through high resolution digital 3D imaging of objects and structures', *ISPRS Journal of Photogrammetry and Remote Sensing*, 55(4), pp. 230–250. doi: 10.1016/S0924-2716(00)00013-7.

Besl, P. J. and McKay, N. D. (1992) 'A Method for Registration of 3-D Shapes', *IEEE Transactions on Pattern Analysis and Machine Intelligence*. doi: 10.1109/34.121791.

Blug, A. *et al.* (2004) 'Fast fiber coupled clearance profile scanner using real time 3D data processing with automatic rail detection', in *IEEE Intelligent Vehicles Symposium, 2004*. IEEE, pp. 658–663. doi: 10.1109/ivs.2004.1336462.

Bovenga, F. *et al.* (2012) 'Using C/X-band SAR interferometry and GNSS measurements for the Assisi landslide analysis', *nternational Journal of Remote Sensing*, 34(11), pp. 4083–4104. doi: 10.1080/01431161.2013.772310.

Cabo, C. *et al.* (2014) 'An algorithm for automatic detection of pole-like street furniture objects from Mobile Laser Scanner point clouds', *ISPRS Journal of Photogrammetry and Remote Sensing*. International Society for Photogrammetry and Remote Sensing, Inc. (ISPRS), 87, pp. 47–56. doi: 10.1016/j.isprsjprs.2013.10.008.

Cabo, C. *et al.* (2016) 'An algorithm for automatic road asphalt edge delineation from mobile laser scanner data using the line clouds concept', *Remote Sensing*. doi: 10.3390/rs8090740.

Chasmer, L. *et al.* (2006) 'Examining the Influence of Changing Laser Pulse Repetition Frequencies on Conifer Forest Canopy Returns', 72(12), pp. 1359–1367.

Che, E., Jung, J. and Olsen, M. J. (2019) 'Object recognition, segmentation, and classification of mobile laser scanning point clouds: A state of the art review', *Sensors (Switzerland)*, 19(4). doi: 10.3390/s19040810.

Che, E. and Olsen, M. J. (2017) 'Fast ground filtering for TLS data via Scanline Density Analysis', *ISPRS Journal of Photogrammetry and Remote Sensing*. doi: 10.1016/j.isprsjprs.2017.05.006.

Chen, P. *et al.* (2017) 'A rail wear measurement method based on structured light scanning', in Bernstein, A. V., Olaru, A., and Zhou, J. (eds) *2016 International Conference on Robotics and Machine Vision*, p. 102530J. doi: 10.1117/12.2266469.

Chen, X. *et al.* (2016) 'A feasibility study on use of generic mobile laser scanning system', in *The International Archives of the Photogrammetry, Remote Sensing and Spatial Information Sciences*, pp. 545–549. doi: 10.5194/isprsarchives-XLI-B1-545-2016.

Cheng, L. *et al.* (2014) 'Extraction of Urban Power Lines from Vehicle-Borne LiDAR Data', *Remote Sensing*. doi: 10.3390/rs6043302.

Closas, P., Fernández-Prades, C. and Fernández-Rubio, J. A. (2009) 'A Bayesian approach to multipath mitigation in GNSS receivers', *IEEE Journal on Selected Topics in Signal Processing*, 3(4), pp. 695–706. doi: 10.1109/JSTSP.2009.2023831.

Collin, B., Carreaud, P. and Lançon, H. (2016) 'High Efficiency Techniques for the Assessment of Railways Infrastructures and Buildings', in *Transportation Research Procedia*, pp. 1865–1874. doi: 10.1016/j.trpro.2016.05.153.

Conforti, D. and Zampa, F. (2012) 'LYNX Mobile Mapper for surveying city centers and highways', *ISPRS - International Archives of the Photogrammetry, Remote Sensing and Spatial Information Sciences*, XXXVIII-5/, pp. 219–222. doi: 10.5194/isprsarchives-XXXVIII-5-W16-219-2011.

Dai, F. *et al.* (2012) 'Comparison of Image-Based and Time-of-Flight-Based Technologies for Three-Dimensional Reconstruction of Infrastructure', *Journal of Construction Engineering and Management*, 139(1), pp. 69–79. doi: 10.1061/(asce)co.1943-7862.0000565.

Dana, P. H. (1997) 'Global Positioning System (GPS) Time Dissemination for Real-Time Applications', *Real-Time Systems*, 12(1), pp. 9–40. doi: 10.1023/A:1007906014916.

Díaz-Vilariño, L. *et al.* (2016) 'Automatic classification of urban pavements using mobile LiDAR data and roughness descriptors', *Construction and Building Materials*. doi: 10.1016/j.conbuildmat.2015.10.199.

Ding, L. *et al.* (2019) 'Improved road marking detection and recognition', in *Proceedings - 2018 15th International Symposium on Pervasive Systems, Algorithms and Networks, I-SPAN 2018*. doi: 10.1109/I-SPAN.2018.00047.

Douillard, B. *et al.* (2011) 'On the segmentation of 3D lidar point clouds', *Proceedings - IEEE International Conference on Robotics and Automation*, pp. 2798–2805. doi: 10.1109/ICRA.2011.5979818.

Elberink, S. and Khoshelham, K. (2015) 'Automatic Extraction of Railroad Centerlines from Mobile Laser Scanning Data', *Remote Sensing*. Multidisciplinary Digital Publishing Institute, 7(5), pp. 5565–5583. doi: 10.3390/rs70505565.

Ellum, C. and El-sheimy, N. (2000) 'The development of a backpack mobile mapping system', *Archives*, XXXIII, pp. 184–191.

Falamarzi, A., Moridpour, S. and Nazem, M. (2019) 'A Review on Existing Sensors and Devices for Inspecting Railway Infrastructure', *Jurnal Kejuruteraan*, 31(1), pp. 1–10. doi: 10.17576/jkukm-2019-31(1)-01.

Fan, H., Yao, W. and Tang, L. (2014) 'Identifying man-made objects along urban

road corridors from mobile lidar data', *IEEE Geoscience and Remote Sensing Letters*. doi: 10.1109/LGRS.2013.2283090.

Filgueira, A. *et al.* (2017) 'Quantifying the influence of rain in LiDAR performance', *Measurement: Journal of the International Measurement Confederation*. Elsevier Ltd, 95, pp. 143–148. doi: 10.1016/j.measurement.2016.10.009.

Fischler, M. A. and Bolles, R. C. (1981) 'Random sample consensus: a paradigm for model fitting with applications to image analysis and automated cartography', *Communications of the ACM*. doi: 10.1145/358669.358692.

Fu, L., Chang, S. and Liu, C. (2018) 'Automatic measuring method of catenary geometric parameters based on laser scanning and imaging', in Zhu, J. et al. (eds) *2017 International Conference on Optical Instruments and Technology: Optoelectronic Measurement Technology and Systems*. SPIE, p. 75. doi: 10.1117/12.2295340.

Gavilán, M. *et al.* (2011) 'Adaptive Road Crack Detection System by Pavement Classification', *Sensors*, 11(10), pp. 9628–9657. doi: 10.3390/s111009628.

Géron, A. (no date) *Hands-On Machine Learning with Scikit-Learn*.

Golparvar-Fard, M. *et al.* (2011) 'Evaluation of image-based modeling and laser scanning accuracy for emerging automated performance monitoring techniques', *Automation in Construction*. Elsevier B.V., 20(8), pp. 1143–1155. doi: 10.1016/j.autcon.2011.04.016.

Golparvar-Fard, M., Peña-Mora, F. and Savarese, S. (2009) 'D 4 AR – A 4-Dimensional augmented reality model for automating construction progress data collection , processing and communication', 14(June), pp. 129–153.

Guan, H., Yu, Y., *et al.* (2014) 'Automated extraction of manhole covers using mobile LiDAR data', *Remote Sensing Letters*, (December). doi: 10.1080/2150704X.2014.994716.

Guan, H., Li, J., *et al.* (2014) 'Using mobile laser scanning data for automated extraction of road markings', *ISPRS Journal of Photogrammetry and Remote Sensing*. International Society for Photogrammetry and Remote Sensing, Inc. (ISPRS), 87, pp. 93–107. doi: 10.1016/j.isprsjprs.2013.11.005.

Guan, H., Yu, Y., Ji, Z., *et al.* (2015) 'Deep learning-based tree classification using mobile LiDAR data', *Remote Sensing Letters*. doi: 10.1080/2150704X.2015.1088668.

Guan, H., Li, J., Yu, Y., *et al.* (2015) 'Iterative tensor voting for pavement crack extraction using mobile laser scanning data', *IEEE Transactions on Geoscience and Remote Sensing*. IEEE, 53(3), pp. 1527–1537. doi: 10.1109/TGRS.2014.2344714.

Guan, H., Li, J., Member, S., *et al.* (2015) 'Using Mobile LiDAR Data for Rapidly Updating Road Markings', *IEEE Transactions on Intelligent Transportation Systems*, pp. 1–10.

Guan, H., Yu, Y., *et al.* (2016) 'Pole-Like Road Object Detection in Mobile LiDAR Data via Supervoxel and Bag-of-Contextual-Visual-Words Representation', *IEEE Geoscience and Remote Sensing Letters*. doi:

10.1109/LGRS.2016.2521684.

Guan, H., Li, J., *et al.* (2016) 'Use of mobile LiDAR in road information inventory: A review', *International Journal of Image and Data Fusion*. doi: 10.1080/19479832.2016.1188860.

Guan, H. *et al.* (2018) 'Robust Traffic-Sign Detection and Classification Using Mobile LiDAR Data with Digital Images', *IEEE Journal of Selected Topics in Applied Earth Observations and Remote Sensing*. doi: 10.1109/JSTARS.2018.2810143.

Gudigar, A. *et al.* (2019) 'An efficient traffic sign recognition based on graph embedding features', *Neural Computing and Applications*. doi: 10.1007/s00521-017-3063-z.

Guo, B. *et al.* (2016) 'An Improved Method for Power-Line Reconstruction from Point Cloud Data', *Remote Sensing*, 8(1), p. 36. doi: 10.3390/rs8010036.

Guo, J., Tsai, M.-J. and Han, J.-Y. (2015) 'Automatic reconstruction of road surface features by using terrestrial mobile lidar', *Automation in Construction*. Elsevier B.V., 58, pp. 165–175. doi: 10.1016/j.autcon.2015.07.017.

Haas, R. *et al.* (2009) 'Measurable Performance Indicators for Roads: Canadian and International Practice', *Annual Conference of the Transportation Association of Canada*. Available at: http://conf.tac-atc.ca/english/resourcecentre/readingroom/conference/conf2009/pdf/Haas.pdf.

Hackel, T. *et al.* (2015) 'Track detection in 3D laser scanning data of railway infrastructure', in *2015 IEEE International Instrumentation and Measurement Technology Conference (I2MTC) Proceedings*. IEEE, pp. 693–698. doi: 10.1109/I2MTC.2015.7151352.

Hakkert, A.S, Gitelman, V. and Vis, M. A. (2007) 'Institutional Repository Road Safety Performance Indicators : Theory . Deliverable D3 . 6 of the EU FP6 project SafetyNet .', p. 166.

Hata, A. Y., Osorio, F. S. and Wolf, D. F. (2014) 'Robust curb detection and vehicle localization in urban environments', *IEEE Intelligent Vehicles Symposium, Proceedings*. IEEE, (Iv), pp. 1257–1262. doi: 10.1109/IVS.2014.6856405.

Hickman, G. D. and Hogg, J. E. (1969) 'Application of an airborne pulsed laser for near shore bathymetric measurements', *Remote Sensing of Environment*, 1(1), pp. 47–58. doi: 10.1016/S0034-4257(69)90088-1.

Huang, P. *et al.* (2015) 'Extraction of street trees from mobile laser scanning point clouds based on subdivided dimensional features', in *International Geoscience and Remote Sensing Symposium (IGARSS)*. doi: 10.1109/IGARSS.2015.7325824.

Huang, P. *et al.* (2017) 'Traffic Sign Occlusion Detection Using Mobile Laser Scanning Point Clouds', *IEEE Transactions on Intelligent Transportation Systems*, 18(9), pp. 2364–2376.

Ibrahim, S. and Lichti, D. (2012) 'Curb-based street floor extraction from mobile terrestrial lidar point cloud', *ISPRS - International Archives of the*

Photogrammetry, Remote Sensing and Spatial Information Sciences. doi: 10.5194/isprsarchives-xxxix-b5-193-2012.

Ingensand, H. (2006) 'Metrological aspects in terrestrial laser-scanning technology', *3rd IAG / 12th FIG Symposium*.

Jaakkola, A. *et al.* (2008) 'Retrieval algorithms for road surface modelling using laser- based mobile mapping', *Sensors*, 8(9), pp. 5238–5249. doi: 10.3390/s8095238.

Jain, A. *et al.* (2019) 'A Novel Genetically Optimized Convolutional Neural Network for Traffic Sign Recognition: A New Benchmark on Belgium and Chinese Traffic Sign Datasets', *Neural Processing Letters*. doi: 10.1007/s11063-019-09991-x.

Jeon, W. G. and Choi, B. G. (2013) 'A Study on the Automatic Detection of Railroad Power Lines Using LiDAR Data and RANSAC Algorithm', *Journal of the Korean Society of Surveying, Geodesy, Photogrammetry and Cartography*, 31(4), pp. 331–339. doi: 10.7848/ksgpc.2013.31.4.331.

Jia, H. *et al.* (2018) 'Biologically Visual Perceptual Model and Discriminative Model for Road Markings Detection and Recognition', *Mathematical Problems in Engineering*. doi: 10.1155/2018/6062081.

Jung, J. *et al.* (2016) 'Multi-Range Conditional Random Field for Classifying Railway Electrification System Objects Using Mobile Laser Scanning Data', *Remote Sensing*, 8(12), p. 1008. doi: 10.3390/rs8121008.

Jung, J. *et al.* (2019) 'Efficient and robust lane marking extraction from mobile lidar point clouds', *ISPRS Journal of Photogrammetry and Remote Sensing*. doi: 10.1016/j.isprsjprs.2018.11.012.

Kais, M. *et al.* (2005) 'Development of loosely-coupled FOG/DGPS and FOG/RTK systems for ADAS and a methodology to assess their real-time performances', *IEEE Intelligent Vehicles Symposium, Proceedings*, 2005(4), pp. 358–363. doi: 10.1109/IVS.2005.1505129.

Kao, W.-W. (2010) 'Integration of GPS and Dead-Reckoning Navigation Systems', *SAE Technical Paper Series*. IEEE, 1. doi: 10.4271/912808.

Karagiannis, G., Olsen, S. and Pedersen, K. (2020) 'Deep Learning for Detection of Railway Signs and Signals', in. Springer, Cham, pp. 1–15. doi: 10.1007/978-3-030-17795-9_1.

Kashani, A. G. *et al.* (2015) 'A review of LIDAR radiometric processing: From ad hoc intensity correction to rigorous radiometric calibration', *Sensors (Switzerland)*, 15(11), pp. 28099–28128. doi: 10.3390/s151128099.

Kavanagh, M. (2007) 'Gyroscopes for Orientation and Inertial Navigation Systems', *Kig*, pp. 254–270.

Kim, H., Liu, B. and Myung, H. (2017) 'Road-feature extraction using point cloud and 3D LiDAR sensor for vehicle localization', *2017 14th International Conference on Ubiquitous Robots and Ambient Intelligence, URAI 2017*, 2, pp. 891–892. doi: 10.1109/URAI.2017.7992858.

Kiziltas, S. *et al.* (2008) 'Technological assessment and process implications of

field data capture technologies for construction and facility/infrastructure management', *Electronic Journal of Information Technology in Construction*, 13(April), pp. 134–154.

Kobler, A. *et al.* (2007) 'Repetitive interpolation: A robust algorithm for DTM generation from Aerial Laser Scanner Data in forested terrain', *Remote Sensing of Environment*, 108(1), pp. 9–23. doi: 10.1016/j.rse.2006.10.013.

Kukko, A. *et al.* (2012) 'Multiplatform mobile laser scanning: Usability and performance', *Sensors (Switzerland)*, 12(9), pp. 11712–11733. doi: 10.3390/s120911712.

Kumar, B. *et al.* (2019) 'A multi-faceted CNN architecture for automatic classification of mobile LiDAR data and an algorithm to reproduce point cloud samples for enhanced training', *ISPRS Journal of Photogrammetry and Remote Sensing*. doi: 10.1016/j.isprsjprs.2018.11.006.

Kumar, P. *et al.* (2013) 'An automated algorithm for extracting road edges from terrestrial mobile LiDAR data', *ISPRS Journal of Photogrammetry and Remote Sensing*. International Society for Photogrammetry and Remote Sensing, Inc. (ISPRS), 85(2013), pp. 44–55. doi: 10.1016/j.isprsjprs.2013.08.003.

Kumar, P., Lewis, P. and McCarthy, T. (2017) 'The Potential of Active Contour Models in Extracting Road Edges from Mobile Laser Scanning Data', *Infrastructures*, 2(3), p. 9. doi: 10.3390/infrastructures2030009.

Kwoczynska, B., Sagan, W. and Dziura, K. (2016) 'Elaboration and Modeling of the Railway Infrastructure Using Data from Airborne and Mobile Laser Scanning', *Proceedings - 2016 Baltic Geodetic Congress (Geomatics), BGC Geomatics 2016*, pp. 106–115. doi: 10.1109/BGC.Geomatics.2016.28.

Langley, R. B. (1999) 'Gpsworld.May99', (May).

Leslar, M., Perry, G. and McNease, K. (2010) 'Using mobile lidar to survey a railway line for asset inventory', in *American Society for Photogrammetry and Remote Sensing Annual Conference 2010: Opportunities for Emerging Geospatial Technologies*. San Diego: American Society for Photogrammetry & Remote Sensing, pp. 526–533.

Li, J. *et al.* (2017) 'Deep Neural Network for Structural Prediction and Lane Detection in Traffic Scene', *IEEE Transactions on Neural Networks and Learning Systems*. doi: 10.1109/TNNLS.2016.2522428.

Li, L. *et al.* (2016) 'A dual growing method for the automatic extraction of individual trees from mobile laser scanning data', *ISPRS Journal of Photogrammetry and Remote Sensing*. doi: 10.1016/j.isprsjprs.2016.07.009.

Li, L., Li, Y. and Li, D. (2016) 'A method based on an adaptive radius cylinder model for detecting pole-like objects in mobile laser scanning data', *Remote Sensing Letters*. Taylor & Francis, 7(3), pp. 249–258. doi: 10.1080/2150704X.2015.1126377.

Link, L. E. and Collins, J. G. (1981) 'Airborne laser systems use in terrain mapping', in *Proceedings of the 15th International Symposium on Remote Sensing of Environment*, pp. 95–110.

Lohr, U. (1998) 'Digital elevation models by laser scanning', *Photogrammetric Record*, 16(91), pp. 105–109. doi: Doi 10.1111/0031-868x.00117.

Lou, Y. *et al.* (2018) 'A Fast Algorithm for Rail Extraction Using Mobile Laser Scanning Data', *Remote Sensing*, 10(12), p. 1998. doi: 10.3390/rs10121998.

Luo, C., Jwa, Y. and Sohn, G. (2014) 'Context based multiple railway object recognition from mobile laser scanning data', *International Geoscience and Remote Sensing Symposium (IGARSS)*. IEEE, pp. 3602–3605. doi: 10.1109/IGARSS.2014.6947262.

Luo, Z. *et al.* (2019) 'Learning high-level features by fusing multi-view representation of MLS point clouds for 3D object recognition in road environments', *ISPRS Journal of Photogrammetry and Remote Sensing*. doi: 10.1016/j.isprsjprs.2019.01.024.

Ma, L. *et al.* (2018) 'Mobile laser scanned point-clouds for road object detection and extraction: A review', *Remote Sensing*, 10(10), pp. 1–33. doi: 10.3390/rs10101531.

Ma, L. *et al.* (2019) 'Generation of Horizontally Curved Driving Lines in HD Maps Using Mobile Laser Scanning Point Clouds', *IEEE Journal of Selected Topics in Applied Earth Observations and Remote Sensing*. IEEE, PP, pp. 1–15. doi: 10.1109/jstars.2019.2904514.

Marmo, R., Lombardi, L. and Gagliardi, N. (2008) 'Railway sign detection and classification', in. doi: 10.1109/itsc.2006.1707412.

Massimi, V. (2018) 'Rheticus: Satellite-based Information Services for Utilities', *Geomedia Journal*, 3.

Massimi, V., Forenza, G. and Alisiconi, A. (2018) *Monitoring the health of water and sewerage networks - The Ever Growing use of Copernicus across Europe's regions*.

Meng, X., Wang, H. and Liu, B. (2017) 'A Robust Vehicle Localization Approach Based on GNSS/IMU/DMI/LiDAR Sensor Fusion for Autonomous Vehicles.', *Sensors (Basel, Switzerland)*. Multidisciplinary Digital Publishing Institute (MDPI), 17(9). doi: 10.3390/s17092140.

Mikrut, S. *et al.* (2016) 'Mobile Laser Scanning Systems for Measuring the Clearance Gauge of Railways: State of Play, Testing and Outlook', *Sensors*, 16(5), p. 683. doi: 10.3390/s16050683.

Minbashi, N. *et al.* (2016) 'Turnout Degradation Modelling Using New Inspection Technologies: A Literature Review', *Lecture Notes in Mechanical Engineering*. doi: 10.1007/978-3-319-23597-4_5.

Moosmann, F. and Stiller, C. (2011) 'Velodyne SLAM', *IEEE Intelligent Vehicles Symposium, Proceedings*. IEEE, (Iv), pp. 393–398. doi: 10.1109/IVS.2011.5940396.

Neubert, M. *et al.* (2012) 'Extraction of Railroad Objects From Very High Resolution Helicopter-Borne Lidar and Ortho-Image Data', *Commission VI, WG VI/4*.

Niina, Y. *et al.* (2018) 'Automatic rail extraction and celarance check with a point

cloud captured by MLS in a Railway', in *International Archives of the Photogrammetry, Remote Sensing and Spatial Information Sciences - ISPRS Archives*, pp. 767–771. doi: 10.5194/isprs-archives-XLII-2-767-2018.

Nutricato, R. *et al.* (2017) 'C/X-band SAR interferometry applied to ground monitoring: examples and new potentials', in *Proc. SPIE 8891, SAR image Analysis, Modeling and Techniques XIII*. doi: 10.1117/12.2029096.

Olsen, M. J. *et al.* (2010) 'terrestrial Laser Scanned-Based Structural Damage Assessment'.

Park, H. S. *et al.* (2007) 'A new approach for health monitoring of structures: Terrestrial laser scanning', *Computer-Aided Civil and Infrastructure Engineering*, 22(1), pp. 19–30. doi: 10.1111/j.1467-8667.2006.00466.x.

Pastucha, E. (2016) 'Catenary System Detection, Localization and Classification Using Mobile Scanning Data', *Remote Sensing*, 8(10), p. 801. doi: 10.3390/rs8100801.

Petit, G., Arias, F. and Panfilo, G. (2015) 'International atomic time: Status and future challenges', *Comptes Rendus Physique*. Elsevier Masson SAS, 16(5), pp. 480–488. doi: 10.1016/j.crhy.2015.03.002.

Pu, S. *et al.* (2011) 'Recognizing basic structures from mobile laser scanning data for road inventory studies', *ISPRS Journal of Photogrammetry and Remote Sensing*. International Society for Photogrammetry and Remote Sensing, Inc. (ISPRS), 66(6 SUPPL.), pp. S28–S39. doi: 10.1016/j.isprsjprs.2011.08.006.

Puente, I. *et al.* (2012) 'Land-Based Mobile Laser Scanning Systems: a Review', *ISPRS - International Archives of the Photogrammetry, Remote Sensing and Spatial Information Sciences*, XXXVIII-5/(August), pp. 163–168. doi: 10.5194/isprsarchives-xxxviii-5-w12-163-2011.

Puente, Iván *et al.* (2013) 'Accuracy verification of the Lynx Mobile Mapper system', *Optics & Laser Technology*, 45(1), pp. 578–586. doi: 10.1016/j.optlastec.2012.05.029.

Puente, I., González-Jorge, H., Riveiro, B., *et al.* (2013) 'Accuracy verification of the Lynx Mobile Mapper system', *Optics and Laser Technology*, 45(1), pp. 578–586. doi: 10.1016/j.optlastec.2012.05.029.

Puente, I., González-Jorge, H., Martínez-Sánchez, J., *et al.* (2013) 'Review of mobile mapping and surveying technologies', *Measurement: Journal of the International Measurement Confederation*, 46(7), pp. 2127–2145. doi: 10.1016/j.measurement.2013.03.006.

Qi, C. R. *et al.* (2016) 'PointNet: Deep Learning on Point Sets for 3D Classification and Segmentation', pp. 601–610. doi: 10.1109/3DV.2016.68.

Qi, C. R. *et al.* (2017) 'PointNet++: Deep Hierarchical Feature Learning on Point Sets in a Metric Space'. Available at: http://arxiv.org/abs/1706.02413.

Quality specifications for roadway bridges, standardization at a European level (no date).

Riveiro, B. *et al.* (2015) 'Automatic detection of zebra crossings from mobile LiDAR

data', *Optics and Laser Technology*. doi: 10.1016/j.optlastec.2015.01.011.

Riveiro, Belén *et al.* (2016) 'Automatic Segmentation and Shape-Based Classification of Retro-Reflective Traffic Signs from Mobile LiDAR Data', *IEEE Journal of Selected Topics in Applied Earth Observations and Remote Sensing*, 9(1), pp. 295–303. doi: 10.1109/JSTARS.2015.2461680.

Riveiro, B *et al.* (2016) 'Laser Scanning Technology: Fundamentals, Principles and Applications in Infrastructure', *Non-Destructive Techniques for the Evaluation of Structures and Infrastructure*, pp. 7–33. doi: 10.1201/b19024-4.

Riveiro, B., Conde, B. and Arias, P. (2015) 'Laser Scanning for the Evaluation of Historic Structures', in *Handbook of Research on Seismic Assessment and Rehabilitation of Historic Structures*, pp. 213–256. doi: 10.4018/978-1-4666-8286-3.

Rizaldy, A. *et al.* (2018) 'Ground and multi-class classification of Airborne Laser Scanner point clouds using Fully Convolutional Networks', *Remote Sensing*, 10(11). doi: 10.3390/rs10111723.

Rodríguez-Cuenca, B. *et al.* (2015a) 'An approach to detect and delineate street curbs from MLS 3D point cloud data', *Automation in Construction*, 51(C), pp. 103–112. doi: 10.1016/j.autcon.2014.12.009.

Rodríguez-Cuenca, B. *et al.* (2015b) 'Automatic detection and classification of pole-like objects in urban point cloud data using an anomaly detection algorithm', *Remote Sensing*. doi: 10.3390/rs71012680.

Rodríguez-Cuenca, B. *et al.* (2016) 'Morphological Operations to Extract Urban Curbs in 3D MLS Point Clouds', *ISPRS International Journal of Geo-Information*. doi: 10.3390/ijgi5060093.

Sadeghi, J. *et al.* (2019) 'Development of railway ballast geometry index using automated measurement system', *Measurement*, 138, pp. 132–142. doi: 10.1016/j.measurement.2019.01.092.

Sánchez-Rodríguez, A. *et al.* (2018) 'Automated detection and decomposition of railway tunnels from Mobile Laser Scanning Datasets', *Automation in Construction*, 96(April), pp. 171–179. doi: 10.1016/j.autcon.2018.09.014.

Serna, A. and Marcotegui, B. (2013) 'Urban accessibility diagnosis from mobile laser scanning data', *ISPRS Journal of Photogrammetry and Remote Sensing*, 84, pp. 23–32. doi: 10.1016/j.isprsjprs.2013.07.001.

Serna, A. and Marcotegui, B. (2014) 'Detection, segmentation and classification of 3D urban objects using mathematical morphology and supervised learning', *ISPRS Journal of Photogrammetry and Remote Sensing*, 93, pp. 243–255. doi: 10.1016/j.isprsjprs.2014.03.015.

Seshia, A. A., Howe, R. T. and Montaguet, S. (2002) 'An integrated microelectromechanical resonant output - gyroscope', pp. 722–726.

Sithole, G. (2001) 'Filtering of Laser Altimetry Data Using a Slope Adaptive Filter', *International Archives of Photogrammetry, Remote Sensing and Spatial Information Sciences*, XXXIV(34(3/W4)), pp. 203–210. Available at:

http://www.isprs.org/proceedings/xxxiv/3-w4/pdf/Sithole.pdf.

Soilán, M. *et al.* (2016a) 'Automatic road sign inventory using mobile mapping systems', *International Archives of the Photogrammetry, Remote Sensing and Spatial Information Sciences - ISPRS Archives*, 41(July), pp. 717–723. doi: 10.5194/isprsarchives-XLI-B3-717-2016.

Soilán, M. *et al.* (2016b) 'Traffic sign detection in MLS acquired point clouds for geometric and image-based semantic inventory', *ISPRS Journal of Photogrammetry and Remote Sensing*, 114, pp. 92–101. doi: 10.1016/j.isprsjprs.2016.01.019.

Soilán, M. *et al.* (2017) 'Segmentation and classification of road markings using MLS data', *ISPRS Journal of Photogrammetry and Remote Sensing*, 123, pp. 94–103. doi: 10.1016/j.isprsjprs.2016.11.011.

Soilán, M. *et al.* (2018) 'Safety assessment on pedestrian crossing environments using MLS data', *Accident Analysis and Prevention*, 111. doi: 10.1016/j.aap.2017.12.009.

Soni, A., Robson, S. and Gleeson, B. (2014) 'Extracting rail track geometry from static terrestrial laser scans for monitoring purposes', in *International Archives of the Photogrammetry, Remote Sensing and Spatial Information Sciences - ISPRS Archives*, pp. 553–557. doi: 10.5194/isprsarchives-XL-5-553-2014.

Stein, D. (2018) 'Mobile laser scanning based determination of railway network topology and branching direction on turnouts'. doi: 10.5445/ksp/1000077900.

Stein, D., Spindler, M. and Lauer, M. (2016) 'Model-based rail detection in mobile laser scanning data', *IEEE Intelligent Vehicles Symposium, Proceedings*. IEEE, 2016-Augus(Iv), pp. 654–661. doi: 10.1109/IVS.2016.7535457.

Stenström, C., Parida, A. and Galar, D. (2012) 'Performance Indicators of Railway Infrastructure', *International Journal of Railway Technology*, 1(3), pp. 1–18. doi: 10.4203/ijrt.1.3.1.

Su, H. *et al.* (2018) 'SPLATNet: Sparse Lattice Networks for Point Cloud Processing', in *Proceedings of the IEEE Computer Society Conference on Computer Vision and Pattern Recognition*. doi: 10.1109/CVPR.2018.00268.

Tan, M. *et al.* (2016) 'Weakly Supervised Metric Learning for Traffic Sign Recognition in a LIDAR-Equipped Vehicle', *IEEE Transactions on Intelligent Transportation Systems*. IEEE, 17(5), pp. 1415–1427. doi: 10.1109/TITS.2015.2506182.

Tao, C. V (2000) 'Mobile mapping technology for road network data acquisition', *Journal of Geospatial Engineering*, 2(2), pp. 1–14.

Tatarchenko, M., Dosovitskiy, A. and Brox, T. (2017) 'Octree Generating Networks: Efficient Convolutional Architectures for High-resolution 3D Outputs'. Available at: http://arxiv.org/abs/1703.09438.

Teledyne Optech (2019). Available at: https://www.teledyneoptech.com/en/home/ (Accessed: 28 June 2019).

Teo, T. A. and Chiu, C. M. (2015) 'Pole-Like Road Object Detection from Mobile Lidar System Using a Coarse-to-Fine Approach', *IEEE Journal of Selected Topics in Applied Earth Observations and Remote Sensing*. doi: 10.1109/JSTARS.2015.2467160.

Tian, Y. *et al.* (2018) 'Lane marking detection via deep convolutional neural network', *Neurocomputing*. doi: 10.1016/j.neucom.2017.09.098.

Venmans, A. A. M., Van De Ven, R. and Kollen, J. (2016) 'Rapid and Non-intrusive Measurements of Moisture in Road Constructions Using Passive Microwave Radiometry and GPR - Full Scale Test', in *Procedia Engineering*. doi: 10.1016/j.proeng.2016.06.111.

Wagner, W. *et al.* (2004) 'From single-pulse to full-waveform airborne laser scanners: potential and practical challenges', *International Archives of Photogrammetry, Remote Sensing and Spatial Information Sciences*, XXXV(Part B/3), pp. 201–206.

Wagner, W. *et al.* (2006) 'Gaussian decomposition and calibration of a novel small-footprint full-waveform digitising airborne laser scanner', *ISPRS Journal of Photogrammetry and Remote Sensing*, 60(2), pp. 100–112. doi: 10.1016/j.isprsjprs.2005.12.001.

Wang, H., Wang, C., *et al.* (2015) '3-D Point Cloud Object Detection Based on Supervoxel Neighborhood With Hough Forest Framework', *IEEE Journal of Selected Topics in Applied Earth Observations and Remote Sensing*. doi: 10.1109/JSTARS.2015.2394803.

Wang, H., Luo, H., *et al.* (2015) 'Road Boundaries Detection Based on Local Normal Saliency From Mobile Laser Scanning Data', 12(10), pp. 2085–2089.

Wang, J., Lindenbergh, R. and Menenti, M. (2017) 'SigVox – A 3D feature matching algorithm for automatic street object recognition in mobile laser scanning point clouds', *ISPRS Journal of Photogrammetry and Remote Sensing*. doi: 10.1016/j.isprsjprs.2017.03.012.

Wang, Y. *et al.* (2018) 'A Hierarchical unsupervised method for power line classification from airborne LiDAR data', *International Journal of Digital Earth*, July, pp. 1–17. doi: 10.1080/17538947.2018.1503740.

Wehr, A. and Lohr, U. (1999) 'Airborne laser scanning - An introduction and overview', *ISPRS Journal of Photogrammetry and Remote Sensing*, 54(2–3), pp. 68–82. doi: 10.1016/S0924-2716(99)00011-8.

Weinmann, Martin *et al.* (2017) 'A classification-segmentation framework for the detection of individual trees in dense MMS point cloud data acquired in urban areas', *Remote Sensing*. doi: 10.3390/rs903277.

Welch, G., Bishop, G. and Hill, C. (1995) 'An Introduction to the Kalman Filter by', pp. 1–16.

Wen, C. *et al.* (2015) 'Spatial-Related Traffic Sign Inspection for Inventory Purposes Using Mobile Laser Scanning Data', *IEEE Transactions on Intelligent Transportation Systems*, 17(1), pp. 27–37. doi: 10.1109/TITS.2015.2418214.

Wen, C. *et al.* (2019) 'A deep learning framework for road marking extraction, classification and completion from mobile laser scanning point clouds', *ISPRS Journal of Photogrammetry and Remote Sensing*. Elsevier, 147(July 2018), pp. 178–192. doi: 10.1016/j.isprsjprs.2018.10.007.

Wu, F. *et al.* (2017) 'Rapid localization and extraction of street light poles in mobile LiDAR point clouds: A supervoxel-based approach', *IEEE Transactions on Intelligent Transportation Systems*. doi: 10.1109/TITS.2016.2565698.

Wujanz, D. *et al.* (2017) 'An intensity-based stochastic model for terrestrial laser scanners', *ISPRS Journal of Photogrammetry and Remote Sensing*. International Society for Photogrammetry and Remote Sensing, Inc. (ISPRS), 125, pp. 146–155. doi: 10.1016/j.isprsjprs.2016.12.006.

Xu, S., Wang, R. and Zheng, H. (2017) 'Road curb extraction from mobile LiDAR point clouds', *IEEE Transactions on Geoscience and Remote Sensing*. IEEE, 55(2), pp. 996–1009. doi: 10.1109/TGRS.2016.2617819.

Xu, Sheng *et al.* (2018) 'Automatic extraction of street trees' nonphotosynthetic components from MLS data', *International Journal of Applied Earth Observation and Geoinformation*. doi: 10.1016/j.jag.2018.02.016.

Yadav, M., Singh, A. K. and Lohani, B. (2017) 'Extraction of road surface from mobile LiDAR data of complex road environment', *International Journal of Remote Sensing*. Taylor & Francis, 38(16), pp. 4645–4672. doi: 10.1080/01431161.2017.1320451.

Yan, L. *et al.* (2016) 'Scan line based road marking extraction from mobile LiDAR point clouds', *Sensors (Switzerland)*, 16(6), pp. 1–21. doi: 10.3390/s16060903.

Yan, L. *et al.* (2017) 'Detection and classification of pole-like road objects from mobile LiDAR data in motorway environment', *Optics and Laser Technology*. doi: 10.1016/j.optlastec.2017.06.015.

Yang, B. and Fang, L. (2014) 'Automated extraction of 3-D railway tracks from mobile laser scanning point clouds', *IEEE Journal of Selected Topics in Applied Earth Observations and Remote Sensing*. IEEE, 7(12), pp. 4750–4761. doi: 10.1109/JSTARS.2014.2312378.

Yang, B., Fang, L. and Li, J. (2013) 'Semi-automated extraction and delineation of 3D roads of street scene from mobile laser scanning point clouds', *ISPRS Journal of Photogrammetry and Remote Sensing*. International Society for Photogrammetry and Remote Sensing, Inc. (ISPRS), 79, pp. 80–93. doi: 10.1016/j.isprsjprs.2013.01.016.

Ye, C. *et al.* (2019) 'Semi-Automated Generation of Road Transition Lines Using Mobile Laser Scanning Data', *IEEE Transactions on Intelligent Transportation Systems*. IEEE, PP, pp. 1–14. doi: 10.1109/TITS.2019.2904735.

Ying Zhou *et al.* (2014) 'A Fast and Accurate Segmentation Method for Ordered LiDAR Point Cloud of Large-Scale Scenes', *IEEE Geoscience and Remote Sensing Letters*. IEEE, 11(11), pp. 1981–1985. doi: 10.1109/lgrs.2014.2316009.

Yoo, H. J. *et al.* (2010) 'Analysis and Improvement of Laser Terrestrial',

International Archives of Photogrammetry Remote Sensing and Spatial Information Sciences, XXXVIII(1), pp. 633–638.

Yu, Y. *et al.* (2014) '3D crack skeleton extraction from mobile LiDAR point clouds', *International Geoscience and Remote Sensing Symposium (IGARSS)*, pp. 914–917. doi: 10.1109/IGARSS.2014.6946574.

Yu, Y., Li, J., Guan, H., Jia, F., *et al.* (2015) 'Learning Hierarchical Features for Automated Extraction of Road Markings From 3-D Mobile LiDAR Point Clouds', *IEEE Journal of Selected Topics in Applied Earth Observations and Remote Sensing*, 8(2), pp. 709–726.

Yu, Y., Li, J., Guan, H., Wang, C., *et al.* (2015) 'Semiautomated Extraction of Street Light Poles From Mobile LiDAR Point-Clouds', *IEEE Transactions on Geoscience and Remote Sensing*, 53(3), pp. 1374–1386. doi: 10.1109/TGRS.2014.2338915.

Yu, Y., Li, J., Wen, C., *et al.* (2016) 'Bag-of-visual-phrases and hierarchical deep models for traffic sign detection and recognition in mobile laser scanning data', *ISPRS Journal of Photogrammetry and Remote Sensing*. International Society for Photogrammetry and Remote Sensing, Inc. (ISPRS), 113, pp. 106–123. doi: 10.1016/j.isprsjprs.2016.01.005.

Yu, Y., Li, J., Guan, H., *et al.* (2016) 'Bag of contextual-visual words for road scene object detection from mobile laser scanning data', *IEEE Transactions on Intelligent Transportation Systems*. doi: 10.1109/TITS.2016.2550798.

Yu, Y., Guan, H. and Ji, Z. (2015) 'Automated Detection of Urban Road Manhole Covers Using Mobile Laser Scanning Data', *IEEE Transactions on Intelligent Transportation Systems*. doi: 10.1109/TITS.2015.2413812.

Zai, D. *et al.* (2018) '3-D Road Boundary Extraction from Mobile Laser Scanning Data via Supervoxels and Graph Cuts', *IEEE Transactions on Intelligent Transportation Systems*. doi: 10.1109/TITS.2017.2701403.

Zhang, S. *et al.* (2016) 'Automatic railway power line extraction using mobile laser scanning data', in *International Archives of the Photogrammetry, Remote Sensing and Spatial Information Sciences - ISPRS Archives*, pp. 615–619. doi: 10.5194/isprsarchives-XLI-B5-615-2016.

Zhao, H. (2017) *Recognizing Features in Mobile Laser Scanning Point Clouds Towards 3D High-definition Road Maps for Autonomous Vehicles*.

Zhu, L. *et al.* (2011) 'Photorealistic building reconstruction from mobile laser scanning data', *Remote Sensing*, 3(7), pp. 1406–1426. doi: 10.3390/rs3071406.

Zhu, L. and Hyyppa, J. (2014) 'The Use of Airborne and Mobile Laser Scanning for Modeling Railway Environments in 3D', *Remote Sensing*, 6(4), pp. 3075–3100. doi: 10.3390/rs6043075.

Zou, X. *et al.* (2017) 'Tree Classification in Complex Forest Point Clouds Based on Deep Learning', *IEEE Geoscience and Remote Sensing Letters*. doi: 10.1109/LGRS.2017.2764938.

SAFEWAY

GIS-BASED INFRASTRUCTURE MANAGEMENT SYSTEM FOR OPTIMIZED RESPONSE TO EXTREME EVENTS OF TERRESTRIAL TRANSPORT NETWORKS

Grant Agreement No. 769255

Data Acquisition Report - Appendices

WP 3 MULTI-SCALE INFRASTRUCTURE MODELLING & MONITORING

Deliverable ID	**D3.1**
Deliverable name	**Data acquisition report**
Lead partner	PLANETEK ITALIA
Contributors	UNIVERSITY OF VIGO

PUBLIC

Appendix 1. Tables

Table 10: SAR satellite missions and main parameters

Satellite Mission	Wave-Length (cm)	Life Status	Resolution Az./Range (m)	Repeat Cycle (days)	Swath Width (km)	Max. Vel. (cm/year)	Incident Angle (degree)
			L Band				
J-ERS	23.5	1992_1998	18	44	75	48.7	35
ALOS PALSAR	23.6	2006÷2011	≈5/(7÷88)	46	40÷70	46.8	8÷60
ALOS-2	22.9	2014	1/3 (3÷10)/(3÷10) 100/100	14	25 (Spot) 50÷70 (Strip) 350 (Scan)	149.2	8÷70
SAOCOM * (2 Sat)	23.5	2018	(10÷50)/(10÷50)	8,16	20÷150	268 134	20÷50
Tandem-L * (2 Sat)	23.6	2023	≈ (7÷10)/(7÷10)	8,16	350	268 134	30÷50
NISAR * (L & S)	24 & 12	2021	6.4/(2÷6) (L) 6.9/(2÷30) (S)	12	>240 Km	180 (L) 90 (S)	33÷47
			C Band				
ERS-1/2	5.6	1992÷2001	≈6/24	35	100	14.6	23

Satellite Mission	Wave-Length (cm)	Life Status	Resolution Az./Range (m)	Repeat Cycle (days)	Swath Width (km)	Max. Vel. (cm/year)	Incident Angle (degree)
ENVISAT	5.6	2003÷2010	≈6/24	35	100	14.6	19÷44
RADARSAT-1	5.5	1995÷2013	≈ (8÷30)/(8÷30)	24	45 (fine) 100 (Strip) 200 (Scan)	20.4	20_50
RADARSAT-2	5.5	2007	≈3/3 ≈8/8 ≈26/25	24	10 (Spot) 40 (Strip) 200 (Scan)	20.4	20÷50
Sentinel-1	5.6	2014	20/5	6, 12	250	85 42.5	30÷46
Gaofen-3	5.6	2016	≈1/1 ≈25/25	29	10 (Spot) 130 (Strip)	17.6	20÷50
RADARSAT Constellation Mission * (3 Sat)	5.5	2018	(3÷50)/(3÷50)	4÷12	30÷350	42÷125	20÷55
			X Band				
COSMO-SkyMED (4 Sat)	3.1	2007	1.0/1.0 ≈2.5/2.5 ≈30/30	2, 4, 8, 16	10 (Spot) 40 (Strip) 200 (Scan)	17.7 35.4 70.7 141.4	20÷60

Satellite Mission	Wave-Length (cm)	Life Status	Resolution Az./Range (m)	Repeat Cycle (days)	Swath Width (km)	Max. Vel. (cm/year)	Incident Angle (degree)
TerraSAR-X	3.1	2007	1.0/1.0 ≈3.3/2.8 ≈20/20	11	10 (Spot) 30 (Strip) 100 (Scan)	25.7	20÷55
KOMPSAT-5	3.2	2013	3/3 1/1	28	5 (Spot) 30 (Strip)	10.4	20_45
COSMO-SkyMED-SG* **(2 Sat)**	3.1	2020	(1÷3)/(1÷3)	8, 16	10÷40	17.7 35.4	20÷60
TerraSAR-X-NG * **(constel. with PAZ)**	3.1	2020	(0.25÷30)/(0.25÷30)	11	5÷20 (Spot) 10÷24 (Strip) 50÷400 (TOPS)	25.7	20÷50
PAZ **(constel. with TerraSAR-X)**	3.1	2018	(1÷6)/(1÷18)	11	10 (Spot) 30 (Strip) 100 (Scan)	25.7	20÷50

Table 11: Network assets and assessment capabilities of the proposed technologies

Asset		Technologies	General Description
BRIDGE			
BRIDGE		OS RS LS PHTGR	
Type of bridge		LS PHTGR	- *Arch* - *Flat Soffit* - *Both*
Material of construction		LS PHTGR	
Type of road under		Uncertain	
Signalization		MLS, TLS PHTGRM	Location, condition, reading
Road vertical alignment		LS	
Lightning		TLS, MLS THRMGR~Semi PHTGRM~Semi	Street lighting and traffic light control – Presence/absence
Identification plates		Uncertain (TLS, MLS; PHTGRM)	Location
Measured headroom		TLS, MLS PHTGRM	
Collision protection beams		LS PHTGRM	Number, Location, Condition
Supports		TLS, MLS PHTGRM~Semi	Condition (Piers, column…)
Deck	**Geometrical characteristics**	LS PHTGRM	- *Nº decks, Space between two supports, Nº spans, Width perpendicular to the parapets, Lengths, Maximum soffit height* - *Some pathologies*
	Health Monitoring	LS~Semi PHTGRM~Semi	

Asset	Technologies	General Description
Road above – Surface condition	RS Uncertain	
Vegetation	OS LS PHTGRM	Presence/absence
Health Monitoring (General)	Uncertain (LS~Semi)	*Some pathologies*
Metal inspection	Uncertain	*Some pathologies*
Masonry inspection	Uncertain	*Some pathologies*
Timber inspection	Uncertain	*Some pathologies*
Parapets, vehicle safety fences and handrails	TLS, MLS PHTGRM	Presence/absence, Minimum height, Defects and damage
UNDERLINE BRIDGE		
Health monitoring	RS LS THRMGR PHTGR	*- Some pathologies* *- Not all technologies available are good for every damage*
Position of tracks relative to the bridge	LS PHTGR	
Flood	RS LS~Semi PHTGR~Semi	
OVERLINE BRIDGE		
Health Monitoring	LS THRMGR PHTGR	*- Some pathologies* *- Not all technologies available are good for every damage*
CULVERT		
Geometrical characteristics	OS ~Semi TLS, MLS PHTGR	Dimensions, Distances to track

Asset		Technologies	General Description
Geometrical Inspection		OS ~Semi TLS, MLS PHTGR	
Watercourse		RS OS Uncertain (LS~Semi; PHTGR~Semi)	Functionality, Scours
Trash screen		TLS, MLS PHTGR~Semi	- *Presence/ Absence* - *Blockage*
Bedstones, bearings, trestles, etc.		LS PHTGR	Settlement
Arch barrel - Inspection		LS THRMGR PHTGR	
River bank	**Geometrical characteristics**	OS ~Semi LS PHTGR	- *Position, form* - *Erosion*
	Health Monitoring	OS ~Semi LS PHTGR~Semi	
RETAINING WALLS			
Dimensions		OS ~Semi LS PHTGR	
Position of tracks relative to the retaining walls		LS PHTGR	
Health monitoring		RS ~Semi LS THRMGR PHTGR	- *Some pathologies* - *Not all technologies available are good for every damage*

Asset	Technologies	General Description
Basket	TLS, MLS~Semi THRMGR~Semi PHTGR~Semi	Corrosion
Gabions	OS RS LS PHTGR~Semi	Overturning, sliding
Parapets, Handrails or Vehicle Safety Fences	TLS, MLS~Semi PHTGR~Semi	Condition
Road	Uncertain (PHTGR~Semi)	Cracks
TUNNELS		
Cracks	RS Uncertain (PHTGR~Semi)	Movements of the ground above the tunnel may be measured by means or RS
Water ingress	TLS, MLS THRMGR PHTGR~Semi	
Concrete and Masonry inspection	TLS, MLS PHTGR	
Masonry inspection	TLS, MLS PHTGR	
Metal inspection	TLS, MLS THRMGR PHTGR	
Concrete and Metal	TLS, MLS PHTGR	

Table 12. Legend for assessment capability tables

*General information, not component details	
A	Automatic
M	Semiautomatic
N	Not detectable
?	Not Applicable

- **PILOT 1 (PORTUGAL)**

Table 13. Road bridge assessment capabilities for the different data acquisition technologies (Pilot 1 – Portugal)

Component	Element	Type	Detection of elements					Features to be inspected	Extract information* / Detect changes				
			TLS	MLS	ALS	THRMGR	PHTGRM		TLS	MLS	ALS	THRMGR	PHTGRM
Wall	Wall	Wing wall	A	A	A	N	M	Superficial damage (porosity, spalling)	M	M	N	M	M
		Parallel to the road						Bulging	A	A	N	N	M
		Wings						Debris, waste, graffiti	A	A	N	N	M
		Spandrel wall						Cracks	N	N	N	N	M
		Retaining wall						Fractures	M	M	N	N	M
	Foundation	Continuous plinth	N	N	N	N	N	Corrosion (exposed rebars)	M	M	N	M	M
		Piles						Blistering	N	N	N	N	N
		Soil preparation						Water penetration	A	A	N	A	M
		Slab						Dimensions (height to contain embankments)	A	A	N	N	M
		Beams						Deflection, twisting	A	A	N	N	N
		Micro-piles						Vegetation	A	A	M	N	M
Embankment	Slope	On corner	A	A	A	A	A	Vegetation	A	A	A	N	A
		Parallel to the road						Cracks	N	N	N	N	M
		Under the structure						Fractures	M	M	N	N	M

Component	Element	Type	Detection of elements					Features to be inspected	Extract information* / Detect changes				
			TLS	MLS	ALS	THRMGR	PHTGRM		TLS	MLS	ALS	THRMGR	PHTGRM
	Lining	Artificial lining	M	M	M	M	M	Absence, instability of lining	M	M	N	N	M
		Natural lining						Drainage (damage, blockage)	M	M	N	N	N
								Water accumulation	N	N	N	N	N
								Settlement	N	N	N	N	N
Junctions	Foundation	Continuous plinth	N	N	N	N	N	Drainage system	N	N	N	N	M
		Individual plinths						Debris, waste	N	N	N	N	N
		Piles						Cracks	N	N	N	N	N
		Slab						Fractures	M	N	N	N	M
		Beams						Blistering	N	N	N	N	N
		Micro-piles						Corrosion (exposed rebars)	M	N	N	M	M
		Other						Superficial damage (porosity, bulging, spalling)	N	N	N	N	N
	Beam seats	On abutment wall	A	M	N	N	M	Scour	N	N	N	N	N
		On abutment-foundation wall						Settlement	N	N	N	N	N
		On pier											
		Reinforced soil abutment											
		Box-type abutment											

Component	Element	Type	Detection of elements					Features to be inspected	Extract information* / Detect changes				
			TLS	MLS	ALS	THRMGR	PHTGRM		TLS	MLS	ALS	THRMGR	PHTGRM
		(integrates wing walls)											
		Barrel (masonry arch bridge)											
	Pier protections	Around the pier	A	N	N	N	M						
		Downstream											
		Upstream											
Bearings	Bearings	Fixed bearing	M	N	N	N	M	Distortion, twisting	N	N	N	N	N
		Fixed pin bearing						Plinths (fractures, crushing)					
		Fixed pot bearing						Joint misalignment					
		Unidirectional sliding bearing						Corrosion					
		Unidirectional pot bearing						Cracks, fractures					
		Unidirectional roller bearing						Crashing					
		Unidirectional pin-roller bearing						Debris, waste					
		Bidirectional elastomeric bearing						Blockage of joint movement					
		Bidirectional pot bearing											
		Anti-seismic											
Support (substructure)	Supports	Pier	A	A	M	N	M	Cracks	N	N	N	N	M
		Pier/pier cap						Fractures	M	M	N	N	M
		Transversal beam on pier						Spalling	M	M	N	M	M

Component	Element	Type	Detection of elements					Features to be inspected	Extract information* / Detect changes				
			TLS	MLS	ALS	THRMGR	PHTGRM		TLS	MLS	ALS	THRMGR	PHTGRM
		Continuous wall						Corrosion (Exposed rebars)	M	M	N	N	M
		Barrel (masonry arch bridge)						Unfilled holes	M	M	N	N	M
	Foundation	Continuous plinth	N	N	N	N	N	Porosity	N	N	N	N	N
		Individual plinths)						Scour	A	M	N	N	M
		Piles						Water penetration	A	A	N	A	M
		Micro-piles						Graffiti, poster	A	A	N	N	M
		Slab						Settlement	N	N	N	N	N
		Beams						Broaden junctions	N	N	N	N	N
	Protection	Around the pier	A	N	N	N	M	Loss of material	M	M	N	N	M
		Upstream/Downstream						Vegetation	A	A	M	N	M
		Cutwater						Efflorescence	A	A	N	M	M
Deck	Towers	Towers	A	A	A	N	M	Spalling	M	M	N	M	M
	Supportive elements (superstructure)	Truss (lower deck)	A	A	M	N	M	Cracks	N	N	N	N	M
		Truss (upper deck)						Fractures	M	M	N	N	M
		Truss (intermediate deck)						Distortion	A	A	N	N	N
		Upper braced frame						Corrosion (exposed rebars)	M	M	N	M	M
		Lower braced frame						Superficial damage (porosity, roughness)	M	M	N	M	M

Component	Element	Type	Detection of elements					Features to be inspected	Extract information* / Detect changes				
			TLS	MLS	ALS	THRMGR	PHTGRM		TLS	MLS	ALS	THRMGR	PHTGRM
		Transversal braced frame						Water penetration	A	A	N	A	M
		Lower arch						Drainpipe position	M	M	N	N	M
		Upper arch						Holes	M	M	N	N	M
		Cable-stayed bridge superstructure						Corrosion (exposed rebars)	M	M	N	N	M
		Tied-arch bridge superstructure						Broaden junctions	N	N	N	N	N
		Suspension bridge superstructure						Efflorescenc e	A	A	N	M	M
		Lower arch (open spandrel)											
	Deck	Deck slab	A	A	N	N	M						
		Ribbed slab											
		Slab (cemented in-situ)											
		Slad (cemented in-situ) with beams (prefabricated)											
		Box-girder section (cemented in-situ)											
		Box-girder section (prefabricated)											
		Vault (tunnel)											
		Arch											
		Solid slab											
		Slab (prefabricated) with beams (cemented in-situ)											

Component	Element	Type	Detection of elements					Features to be inspected	Extract information* / Detect changes				
			TLS	MLS	ALS	THRMGR	PHTGRM		TLS	MLS	ALS	THRMGR	PHTGRM
		Slab with beams (both prefabricated)											
		Other											
Ledge	Ledge	Prefabricated	A	A	N	N	M	Spalling	M	M	N	M	M
		Made in-situ						Fractures	M	M	N	N	M
								Vegetation	A	A	M	N	M
								Loss of material	M	M	N	N	M
								Location and attachment	M	M	N	N	M
								Water penetration	A	A	N	A	M
Barrier/fence	Barrier/fence	Prefabricated	A	A	N	N	M	Deformation (due to car crashes)	A	A	M	N	M
		Made in-situ						Paint peeling	N	N	N	N	M
		Other						Assembling elements	N	N	N	N	N
	Barrier ends	Prefabricated	A	A	N	N	M	Attachment to the structure	M	M	N	N	M
		Made in-situ						Expansion joints	A	A	N	N	M
		Other						Spalling (concrete)	M	M	N	M	M
								Cracks (concrete)	N	N	N	N	M
								Fractures (concrete)	M	M	N	N	M
Guardrail	Lateral/central guardrail	W type	A	A	N	N	M	Deformation (due to car crashes)	A	A	M	N	M

Component	Element	Type	Detection of elements					Features to be inspected	Extract information* / Detect changes				
			TLS	MLS	ALS	THRMGR	PHTGRM		TLS	MLS	ALS	THRMGR	PHTGRM
		Double W type						Absence of elements (dampers)	M	M	N	N	M
		"Skirt" type (steel flat screen)						Assembling	N	N	N	N	N
		Double metallic beam						Corrosion	M	M	N	M	M
		"New Jersey" type						Expansion joints	A	A	N	N	M
		Other						Spalling (concrete)	M	M	N	M	M
	Lateral/central curbs	"Trief" type	A	A	M	N	M	Cracks (concrete)	N	N	N	N	M
		Median curb						Fractures (concrete)	M	M	N	N	M
		Other						Misalignments	A	A	M	N	N
Walkway	Covering/overlay	Accessible (Public)	A	A	A	A	A	Cracks	N	N	N	N	M
		Non-accessible (Maintenance)						Fractures	M	M	N	N	M
	Infill	Accessible (Public)	N	N	N	N	N	Spalling	M	M	N	M	M
		Non-accessible (Maintenance)						Absence of lining sections	M	M	N	N	M
								Settlement	N	N	N	N	N
								Expansion joints (and protective covers)	A	A	N	N	M
								Debris, waste	N	N	N	N	N
								Corrosion (exposed rebars)	M	M	N	M	M
Pavement	Pavement	Bridge	A	A	A	M	A	Spalling	M	M	N	M	M

Component	Element	Type	Detection of elements					Features to be inspected	Extract information* / Detect changes				
			TLS	MLS	ALS	THRMGR	PHTGRM		TLS	MLS	ALS	THRMGR	PHTGRM
		Tunnel						Cracks	N	N	N	N	M
								Fractures	M	M	N	N	M
								Holes	M	M	N	N	M
								Roughness, adherence	N	N	N	N	M
								Bulging	A	A	N	N	M
								Drainage	M	M	N	N	M
								Settlement	N	N	N	N	N
								Debris, waste	N	N	N	N	N
Drainage	Drainage	Canal (ground level)	A	A	A	N	M	Location	M	M	N	N	M
		Sink						Rainwater drainage	M	M	N	N	M
		Ditch						Elements linkage to culverts	N	N	N	N	N
		Deck piping						Cracks, fractures	N	N	N	N	N
		Canal (on top of a wall)						Debris, waste	N	N	N	N	N
		Canal (on the slope of an embankment)						Blockage	M	M	N	N	M
		Culverts						Sediments in culverts	M	M	N	N	M
								Protective covers	A	A	M	N	M
								Grooves in slopes	A	A	M	N	M
								Leakage	N	N	N	N	N
		Fixed	A	A	N	M	M	Unevenness	A	A	N	N	N

Component	Element	Type	Detection of elements					Features to be inspected	Extract information* / Detect changes				
			TLS	MLS	ALS	THRMGR	PHTGRM		TLS	MLS	ALS	THRMGR	PHTGRM
Expansion joints	Expansion joints	Movable						Distortion, misalignment	A	A	N	N	N
		Other						Broken or unattached sections	A	A	N	N	M
								Corrosion	M	M	N	M	M
								Debris, waste	N	N	N	N	N
								Filling material	N	N	N	N	N

- **PILOT 2 (SPAIN)**

Table 14: Subdimension: Monitoring – Remote Sensing (Pilot 2 – Spain)

Component	Subcomponent	Detection (of elements)					Extract information* / Detect changes				
		TLS	MLS	ALS	THRMGR	PHTGRM	TLS	MLS	ALS	THRMGR	PHTGRM
Structures	Underpass / Overpass	A	A	A	?	A	A	A	M	?	N
	Tunnel	A	A	N		N	A	A	N		N
	Viaduct	A	A	A		A	A	M	A		M
Slope of embankment	Cut slope	A	A	A	?	A	A	A	A	?	A
	Embankment	A	M	A		A	A	M	A		A
	Tunnel entrance, cut and cover	A	A	A		A	A	A	N		N
Culverts	Drains	A	A	N	?	M	A	A	N	?	M
	Culverts	A	M	N		M	A	M	N		M
Protection elements	Handrail	A	A	N	?	M	A	A	N	?	M
	Anti-climb fencing	A	A	N		M	A	A	N		M
Fencing	Posts	A	A	N	?	M	A	A	N	?	N
	Gates	A	A	N		M	A	A	N		M
	Wire netting	A	A	N		M	A	A	N		M
Vegetation	Land cleaning	A	A	A	?	A	A	A	A	?	A
	Tree felling	A	A	A		A	A	A	A		A
Track	Rail track	A	A	M	?	A	A	A	N	?	N
	Fish plate joint	A	M	N		N	M	M	N		N
	Railway sleeper	A	A	N		M	A	M	N		N
	Ballast	A	A	A		A	A	A	M		M
	Railroad switch	A	A	N		N	A	A	N		N
	Expansion joint	A	N	N		N	M	N	N		N

- **Pilot 3 (United Kingdom)**

Table 15: Subdimension: Monitoring – Remote Sensing: Terrestrial. Bridges – General (Pilot 3 –Uk)

Description	Component	Damage / Measurements	Detection (of elements)					Extract information* / Detect changes				
			TLS	MLS	ALS	THRMGR	PHTGRM	TLS	MLS	ALS	THRMGR	PHTGRM
Bridge type	-	-Arch -Flat soffit -Both	A	A	A	N	A	A	A	A	N	A
Material of construction	-	-Brick -Stone -Concrete -Wrought iron -Cast iron -Steel	?					A	A	A	N	A
Road under	-	Type	A	A	A	N	A	A	A	A	N	A
		Recent resurfacing						N	N	N	N	M
Signalization	-	Condition	A	A	N	N	A	A	A	N	N	A
		Speed Limit						N	N	N	N	A
		Headroom (Permitted vehicle height)						N	N	N	N	A
		Weight restriction						N	N	N	N	A
		Conflict between mandatory (roundel) and warning (triangular) signs						N	N	N	N	M
		Chevron						A	A	N	N	A
		Hazard warnings (arch)						N	N	N	N	N
		Road traffic signs illuminated?						N	N	N	N	M
		Are there any distracting adverts adjacent to the bridge?						N	N	N	N	M

Description	Component	Damage / Measurements	Detection (of elements)					Extract information* / Detect changes				
			TLS	MLS	ALS	THRMGR	PHTGRM	TLS	MLS	ALS	THRMGR	PHTGRM
Road	-	Vertical alignment	A	A	A	N	A	A	A	A	N	N
Lightning (Street lighting and traffic light control)	-	Presence / Absence	A	A	N	A	A	A	A	N	M	A
Identification plates (road and track level)	-	Plates erected?	A	A	N	A	A	A	A	N	N	A
		Clean?						A	A	N	N	A
		Telephone number on?						N	N	N	N	N
-	-	Measured headroom	A	A	N	N	A	A	A	N	N	A
Collision protection beams	-	Number	M	M	M	N	M	M	M	M	N	M
		Location						A	A	A	N	A
		Condition						M	M	M	N	M
Supports	-Pier / Trestle -Column / Cylinder	Condition	A	A	A	N	A	A	A	N	N	M
Deck	-	Number of decks	A	A	A	N	A	A	A	A	N	A
	Span	Space between two supports						A	A	A	N	A
		Number of spans						A	A	A	N	A
		Width perpendicular to the parapets						A	A	A	N	A
		Lengths: -Parallel to parapets -Perpendicular to abutments						A	A	A	N	A
		Maximum soffit height						A	A	A	N	A
	-End support -Intermediate supports	Spalling						M	M	N	M	M
		Corrosion						M	M	N	M	M
		Timber deterioration						M	M	N	N	M
Road above	-	Surface condition	A	A	A	N	A	N	N	N	N	N
Vegetation	-	Presence / absence	A	A	A	N	A	A	A	A	N	A
General	-	Cracking	?	?	?	?	?	N	N	N	N	M

Description	Component	Damage / Measurements	Detection (of elements)					Extract information* / Detect changes				
			TLS	MLS	ALS	THRMGR	PHTGRM	TLS	MLS	ALS	THRMGR	PHTGRM
	-	Spalling						M	M	N	M	M
	-	Bulging						M	M	M	N	M
	-	Fire damage						N	N	N	N	N
Metal	-	Corrosion	?	?	?	?	?	M	M	N	M	M
	-	Loss of section						N	N	N	N	N
	-	Tears						N	N	N	N	N
	-	Fracture						M	M	N	N	M
	-	Cracked welds						N	N	N	N	N
	-	Buckling						A	A	A	N	M
	-	Permanent distortion						A	A	A	N	A
	-	Displacement						A	A	A	N	A
	-	Abrasion						M	M	N	M	M
	-	Flaking or blistering						N	N	N	N	M
	-	Loss of coating to parent metal						N	N	N	N	M
	-	Impact						N	N	N	N	N
Masonry	-	Loss of material	?	?	?	?	?	M	M	M	N	M
	-	Weathering						N	N	N	N	M
	-	Deformation (Bulging, distortion, tilting)						A	A	A	N	A
	-	Cracking						N	N	N	N	M
	-	Loosening and/or wedging						A	A	N	N	A
	-	Spalling						M	M	N	M	M
Timber	-	Wetness	?	?	?	?	?	A	A	N	M	A
	-	Splits/shakes						N	N	N	M	M
	-	Corrosion of bolts, screws…						M	M	N	M	M
	-	Missing bolts, screws…						M	M	N	N	M
	-	Surface softening/fire damage						N	N	N	N	M

Description	Component	Damage / Measurements	Detection (of elements)					Extract information* / Detect changes				
			TLS	MLS	ALS	THRMGR	PHTGRM	TLS	MLS	ALS	THRMGR	PHTGRM
	-	Loss						M	M	N	N	M
	-	Permanent displacement						A	A	A	N	A
Parapets, vehicle safety fences and handrails	-	Presence/Absence	A	A	N	N	A	A	A	N	N	A
	-	Minimum height of the parapets						A	A	N	N	A
	-	Defects and damage						M	M	N	N	M

Table 16: Subdimension: Monitoring – Remote Sensing: Terrestrial. Underline Bridge (Pilot 3 –Uk)

Description	Component	Damage / Measurements	Detection (of elements)					Extract information* / Detect changes				
			TLS	MLS	ALS	THRMGR	PHTGRM	TLS	MLS	ALS	THRMGR	PHTGRM
Masonry arch bridge	Spandrel wall	Separation	A	A	A	N	A	A	A	A	N	A
	Ring	Separation	A	A	N	N	A	A	A	N	N	A
	-	Bulging	?					M	M	N	N	M
	-	Water penetration						A	A	N	M	M
	-	Dropped stones/bricks						M	M	N	N	M
	-	Spalling						M	M	N	M	M
	-	Cracking						N	N	N	N	M
	-	Evidence of bridge strike						N	N	N	N	N
Observations under moving loads	-	Abnormal movement or evidence of settlement	?					M	M	M	N	M
	-	Deflection, lateral sway, twisting, looseness or vibration						A	A	A	N	A
	-	Separation or differential vertical or horizontal movements of parts of a Bridge						A	A	N	N	A
	-	Lifting and "hammering" of a girder off its bearings						M	M	N	N	M
Railway track	-	Lateral and vertical position of the tracks relative to the bridge	A	A	A	N	A	A	A	A	N	A
Bridges over watercourses	-	Changes in the watercourse regime (flood)	A	A	A	N	M	M	M	M	N	M
Survey of river bed	-	Bed levels around piers, abutments and at sections across the river	M	M	M	N	M	N	N	N	N	N

Table 17: Subdimension: Monitoring – Remote Sensing: Terrestrial. Overline Bridge (Pilot 3 –Uk)

Description	Component	Damage / Measurements	Detection (of elements)					Extract information* / Detect changes				
			TLS	MLS	ALS	THRMGR	PHTGRM	TLS	MLS	ALS	THRMGR	PHTGRM
Footbridges	Stairs, treads, risers, landings, stringers and balustrades	Condition	A	A	A	N	M	A	A	A	N	M
	-	Glazing and cladding	M	M	M	N	M	N	N	N	N	N
	Canopies and their supporting elements	Condition	A	A	A	N	M	A	A	A	N	N
	Lift shafts and escalator supports	Condition	N	N	N	N	N	N	N	N	N	N
Fatigue susceptible elements	-	Cracking	?					N	N	N	N	M
	-	Water seepage						A	A	N	M	M

Table 18: Subdimension: Monitoring – Remote Sensing: Terrestrial. Culverts (Pilot 3 –Uk)

Description	Component	Damage / Measurements	Detection (of elements)					Extract information* / Detect changes				
			TLS	MLS	ALS	THRMGR	PHTGRM	TLS	MLS	ALS	THRMGR	PHTGRM
General	Culvert	Dimensions	A	A	N	N	M	A	A	N	N	A
		Distances to track						A	A	N	N	A
		Deflection, lateral sway, twisting, looseness or vibration						A	A	N	N	M
		Separation or differential vertical or horizontal movement of parts						A	A	N	N	M
		Lifting, and "hammering" of a girder off its bearings						M	M	N	N	M
	Watercourse	Functionality	A	A	A	N	M	M	M	N	N	M
		Depth of water (water level)						N	N	N	N	N
		Scours						M	M	M	N	M
	-	Approach ditch functionality	?	?	?	?	?	A	A	N	N	N
	Silt	Depth	N	N	N	N	N	N	N	N	N	N
	Trash screen	Presence/ Absence	A	A	N	N	M	A	A	N	N	M
		Blockage						A	A	N	N	M
	-	Lack of air flow	?	?	?	?	?	N	N	N	N	N
	-	Biological / toxic Hazard / fumes	?	?	?	?	?	N	N	N	N	N
	-	Confined spaces	?	?	?	?	?	N	N	N	N	N
	Services in culvert	Do they prevent or restrict examination?	N	N	N	N	N	N	N	N	N	N
	Bed stones, bearings, trestles, etc.	Settlement	A	A	A	N	M	A	A	A	N	A

Description	Component	Damage / Measurements	Detection (of elements)					Extract information* / Detect changes				
			TLS	MLS	ALS	THRMGR	PHTGRM	TLS	MLS	ALS	THRMGR	PHTGRM
Masonry culvert	Arch barrel	Separation from spandrel wall / headwall	A	A	N	N	A	A	A	N	N	A
		Ring separation or drumminess						A	A	N	N	A
		Bulging						M	M	N	N	M
		Dropped stones or bricks						M	M	N	N	M
		Spalling						M	M	N	M	M
		Cracks						N	N	N	N	M
River bank	-	Position	M	M	M	N	M	A	A	A	N	A
	-	Form						M	M	M	N	M
	-	Condition						N	N	N	N	N
	-	Erosion						M	M	M	N	M

Table 19: Subdimension: Monitoring – Remote Sensing: Terrestrial. Retaining Walls (Pilot 3 –Uk)

Description	Component	Damage / Measurements	Detection (of elements)					Extract information* / Detect changes				
			TLS	MLS	ALS	THRMGR	PHTGRM	TLS	MLS	ALS	THRMGR	PHTGRM
Retaining wall	-	Dimensions	A	A	A	N	A	A	A	A	N	A
	-	Position of the tracks relative to the retaining wall						A	A	A	N	A
	-	Damage in movement joints						M	M	N	N	M
	-	Displacement of one part of a RW relative to another						A	A	A	N	A
	-	Percloration of water through a joint						N	N	N	M	M
	-	Loss or deterioration of filler or sealant						N	N	N	N	N
	-	Corrosion of steel piles						M	M	N	M	M
	-	Overturning/sliding forward of the wall						A	A	N	N	M
	-	Changes in alignment						A	A	A	N	A
	-	Loss of material						M	M	N	N	M
	-	Deformation						A	A	A	N	A
	-	Cracking						N	N	N	N	M
	-	Wedging						A	A	N	N	A
-	Basket	Corrosion	M	M	M	N	M	M	M	N	M	M
		Spilling of infill						N	N	N	N	N
-	Gabions	Overturning	M	M	M	N	M	A	A	A	N	M
		Sliding						A	A	A	N	M
		Bearing failure						N	N	N	N	N
-	Parapets, Handrails or Vehicle Safety Fences	Condition	A	A	N	N	A	M	M	N	N	M
-	Road	Cracks	A	A	A	N	A	N	N	N	N	M

Table 20: Subdimension: Monitoring – Remote Sensing: Terrestrial. Tunnels (Pilot 3 –Uk)

Description	Component	Damage / Measurements	Detection (of elements)					Extract information* / Detect changes				
			TLS	MLS	ALS	THRMGR	PHTGRM	TLS	MLS	ALS	THRMGR	PHTGRM
General	-	Crack	?	?	?	?	?	N	N	N	N	M
		Water ingress						A	A	N	A	M
Concrete and Masonry	-	Spalling						M	M	N	M	M
		Hollow/drummy						M	M	N	N	M
		Bulging						M	M	N	N	M
Masonry	-	Brick/stone open joints						A	A	N	N	A
		Loss of bricks/stones						M	M	N	N	M
		Missing bricks/stones						M	M	N	N	M
Metal	-	Corrosion/Loss of section						M	M	N	M	M
		Distortion, displacement						A	A	N	N	A
Concrete and Metal	-	Stepped segment/ring						M	M	N	N	M
		Loose fixings						M	M	N	N	M

Table 21: Subdimension: Monitoring – Remote Sensing: Terrestrial. Coastal, Estuarine and River Defences (Pilot 3 –Uk)

Description	Component	Damage / Measurements	Detection (of elements)					Extract information* / Detect changes				
			TLS	MLS	ALS	THRMGR	PHTGRM	TLS	MLS	ALS	THRMGR	PHTGRM
-	Track	Misalignment, heave or subsidence	A	A	A	N	A	A	A	A	N	M
-	Ballast	Loss of ballast	A	A	A	N	A	M	M	M	N	M
-	Structure, parapets, wave return walls and adjacent ground and buildings	Crack	A	A	A	N	A	N	N	N	N	M
-	-	Leakage or seepage	?					A	A	N	M	M
		Flooding	A	A	A	N	A	M	M	M	N	M
		Voids	A	A	A	N	M	M	M	M	N	M
		Scour / undermining of the toe	A	A	A	N	M	M	M	M	N	M
		Tilting	?					A	A	N	N	A
		Sliding	M	M	M	N	M	A	A	N	N	M
Defence	-	Beach or foreshore level	M	M	M	M	M	M	M	M	N	M
	Groynes and Breakwaters	Condition	A	A	A	N	A	M	M	N	N	M
	Rock armour, concrete revetments, rip-rap, gabions…	Condition	M	M	M	N	M	M	M	N	N	N
		Position	A	A	A	N	A	M	M	M	N	M